Università degli Studi di Ferrara

DOTTORATO DI RICERCA IN
"BIOCHIMICA, BIOLOGIA MOLECOLARE E
BIOTECNOLOGIE"

CICLO XXIV

COORDINATORE Prof. Francesco Bernardi

Cell encapsulation systems based on hybrid hydrogels

Settore Scientifico Disciplinare BIO/10

Dottorando   **Tutore**

Dott. Mazzitelli Stefania   Prof. Gambari Roberto

                                                       Cotutore

                                           Prof. Claudio Nastruzzi

Anni 2009/2011

TABLE OF CONTENTS

PREFACE

This PhD thesis was focused on the production and characterization of encapsulation systems for cell therapy and tissue engineering applications. The structure of the work is organized in four main chapters: (i) the general characteristics of hydrogel based devices for cell encapsulation, (ii) the description of the experimental encapsulation procedures for microcapsular devices for the embedding of different cell types, (iii) the design of new strategies for engineered and or fibrous scaffolds and finally (iv) the main conclusion gathered by the entire experimental results of the research project.

In detail, chapter 1 presents an overview of commonly applied biomaterials, as well as the characteristics of optimal encapsulation systems for in vivo application. In particular hydrogels performances are discussed analysing advantages and disadvantages for cell therapy applications. Chapter 2 and 3 are devoted to the description of different fabrication techniques to process hydrogels containing different cell types into scaffolds.

Each chapter refers to one or more journal articles dealing with the experiments performed to produce the encapsulation devices. Particularly, chapter 2 is related to papers on various procedures for microcapsule production, while chapter 3 is relative to contributions about new scaffolds in form of engineered microcapsules or multifunctional microfibres.

The scientific work presented in the current PhD thesis program has benefced of the skilled collaboration of researchers and scientific Institutions:

1. Prof. S.F. Badylak, MacGowan Institue for Regenerative Medicine, University of Pittsburgh, Pittsburgh, PA, USA
2. Prof. X. Zhang, Engineering and the Environment, University of Southampton, Southampton, UK
3. Biomaterials Group, King's College, London, UK
4. Prof. C. Nastruzzi, Dipartimento di Scienze farmaceutiche, Università degli

Studi di Ferrara, Ferrara, Italy

5. Prof. R. Piva, Dipartimento di Biochimica e Biologia Molecolare, Università di Ferrara, Ferrara, Italy

6. Prof. E. Becchetti, Dr. G. Luca, Dr. M. Calvitti, Dr. F. Mancuso, Dipartimento di Medicina Sperimentale e Scienze Biochimiche, Università degli Studi di Perugia, Perugia, Italy.

ACKNOWLEDGMENTS

The important thing is not stop questioning.
AlbertEinstein

Foremost, I would like to express my sincere gratitude to Prof. Claudio Nastruzzi. During more than seven years of knowing him, he showed me science in its full depth and taught me how to appreciate the good scientific work. His knowledge with his originality has triggered and nourished my intellectual maturity that I will benefit from, for a long time to come.

I am deeply grateful to my supervisor, Professor Roberto Gambari for his important support throughout this work.

I owe my gratitude to Professor S.F. Badylak of the McGowan Institute of Regenerative Medicine who gave me the opportunity to work with him and to join his group in Pittsburgh.

All the work would not have been possible without the guidance of several colleagues who in one way or another contributed and extended their valuable assistance in the preparation and completion of this study. First of all, the researchers from the University of Perugia (G. Luca, F. Mancuso, M. Calvitti) that introduced me to cell work and gave me extraordinary experiences through out the work. Moreover all the colleagues from the groups of Prof. Gambari and Prof. Piva, University of Ferrara, who helped me with my experimental project.

During the thesis I had the opportunity to work at the Biomaterials Group of the King's college in London and at the School of Engineering Sciences of the University of Southampton, where I met and collaborated with people for whom I have great regards (Prof. S. Deb, Prof. L. Di Silvio, Prof. X. Zhang, Obi, Cristian, Daniel, Emanuele, Dario).

Special thanks to my colleagues and most of all friends Lorenzo and Stefano, with whom not only I had many productive scientific discussions but also chats in front many beers.

From the non-scientific side, individual acknowledgments are also owed to my childhood friends in Tropea (Lucia, Gemma, Rosaria, Francesca), my friends in Perugia (Mino, Cinzia, Pasquale, Kasia, Nicoletta) and the new ones in Ferrara (Emilia, Elena, Francesca). They provided me unflinching friendship, making me always smile and enjoy the life.

My parents, brother and my sister-in-law deserve special mention for their inseparable support and encouragement. My Father, Pino, in the first place is the person who put the fundament of my learning character and my Mother, Luciana, is the one who raised me with care and love.

And last but not least I wish to extend my thanks to Giusa and Federico. The first one for always letting me know that I can count on her even when far away form each other and for the good advice, even if never follow them. The second one for the special person he is and for having come along at the right time, supporting me with an incredible amount of patience.

CHAPTER 1

Bioencapsulation for cell therapy:
general considerations

1.1. Introduction

Millions of surgical procedures are performed each year to replace or reconstruct damaged tissue resulting from chronic/degenerative diseases, injury, congenital malformations and cancer. Unfortunately, there is a wide gap between the demand for organs and replacement tissue and patients actually receiving transplants. The cellular therapy and tissue engineering based protocols offer a potential solution to the shortage of organ donors and the problems relating with the repair of damaged tissues (i.e. risk of graft failure) [1]. Cellular therapy is indeed a novel technology based on the use of cells to treat a wide range of human diseases by replacing damaged cells or tissues.

These approaches are based on the administration/transplant of living cells to specific body sites, where cells can exert therapeutic effects through: (a) the repair/replacement of damaged tissue/organs or (b) the production/release of specific bioactive molecules (e.g. enzymes, growth factors and antibodies) [2].

Recently, cells have been increasingly exploited as alternative controlled drug delivery vehicles. Cells can indeed act as drug depots enabling the delivery of "de novo" produced therapeutic products with site specificity over an extended time period, providing the possibility to treat various diseases that cannot be cured with currently available therapeutic protocols [3].

In this respect, different cell types (primary, stem and bioengineered cells) have been considered as potential therapeutic tools and tested in preclinical and clinical studies for the treatment of many pathologies, such as diabetes, anemia, hemophilia, bone defects and cancer [4-6].

For instance, biomolecules secreted by cells may be delivered continuously such as an angiogenesis inhibitor to a tumor [7], or in response to a physiologic signal, such as insulin to glucose for the treatment of diabetes [8]. Erythropoietin cell production in response to oxygen delivery can found application for the treatment of anemia [9]. A selected protein may also be expressed and produced by the cell implant after genetic modification, such as the coagulation factors VIII and IX for the treatment of hemophilia A and B. Moreover, stem cells can secrete a diverse array of growth factors, including vascular endothelial growth factor (VEGF) and nerve growth factor, which are used to treat ischemia and neuronal damage, respectively [10,11].

Over the years, two conceptually different strategies to deliver cells into diseased tissue have been developed: the first approach consists of the injection of free autologous, allogenic or xenogenic cells, the second one is based on cells seeded or embedded in scaffold; notably, the latter approach finds applications both in vitro (basic and applied research) and in vivo (reconstructive medicine) [12].
Unfortunately, the use of free cells, in spite of the superior handling, holds the major drawback to elicit the host immune rejection. Furthermore, transplanted cells not protected from external mechanical loadings or not surrounded by the proper microenvironment may rapidly lose their viability and functionality. Therefore, an increasing number of natural and synthetic structures have been developed as potential immunoisolating scaffold for cell embedding [13].
Cell immunoisolation into scaffolds represents the major advance in cell based therapy since it avoids constraints associated with cell sources, making allogenic and xenogenic cells a good alternative to the limited autologous donors.

A cellular based therapy requires the combined use of suitable scaffolds and selected cell populations to create biocompatible devices that once transplanted, can immunoisolate the cells from the host's immune system,

possibly eliminating or reducing the requirement for immunosuppressant systemic drug administration (Fig. 1). Non-specific suppression of the immune system may lead to a variety of unwanted complications in patients, including infections and failure of tumor surveillance [14].

A key role in preserving cell functions is played by the biomaterial used to produce the cellular scaffolds suitable for implanting cells into the host in order to regenerate a tissue or to obtain a long-term systemic delivery of biomolecules.
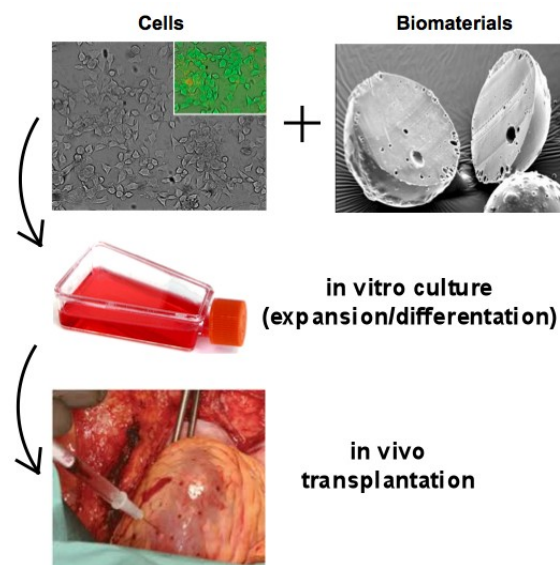
Fig. 1. Schematic representation of a system for cell therapy protocols based on cells and biomaterials.

Cells can be adequately combined with biomaterials following two main approaches. On the one hand, cells are isolated from the host's body by a microcapsular structure allowing exchange of nutrients; on the other one, cells can be seeded onto a preformed scaffold, that is generally implanted into the host after a given cultivation time.

The concept of cell immunoisolation was initially described by Chang in 1960s and since then, various biomaterials have been proposed to embed cells in immunoisolating microenvironments, manly in form of microcapsules, creating a semi-permeable membrane/barriers that control the outward and inward diffusion of gases (oxygen and carbon dioxide), metabolic and therapeutic molecules.

Irrespectively of the strategy employed, the success of any bioencapsulation approach is mostly related to the properties of the biomaterial, that should be biocompatible, easy to sterilize and biodegradable over an appropriate length of time into products metabolized or excreted by the recipient without inducing adverse inflammatory responses.

Ideally, the selected biomaterials should be reproducibly processed into a desired shape and structure (i.e. spherical or tubular configurations), maintained even after the in vivo implantation.

Moreover, an immunoisolation biomaterial must provide a structured protective environment with tissue-specific mechanical properties and porous niche for cells capable of delivering potentially therapeutic factors.

Finally, the biomaterial should offer an appropriate regulation of cell behaviour including adhesion, proliferation, migration and differentiation. When in vivo implanted, the biomaterials must provide temporary mechanical support sufficient to withstand forces exerted by the surrounding tissue.

It is important to underline that the different, and in a certain sense opposite biomaterial characteristics, are provided by a very limited number of materials. In this respect, hydrogel forming biomaterials occupy a prominent position, thanks to their special physical properties and feasibility for cell encapsulation procedures. Hydrogels provide a highly controlled, synthetic 3D environment that is structurally and biomechanically similar to native extracellular matrix (ECM) topology and provides a rich ligand landscape to influence cell behaviour [15].

1.2. Hydrogels

Hydrogels represent an important class of biomaterials for biotechnology and biomedical applications, since they exhibit excellent biocompatibility with minimal inflammatory responses and tissue damage. By definition, the hydrogel structure is constituted of a polymeric network with three-dimensional configuration capable of imbibing high amounts of water or

biological fluids. The high water affinity is attributed to the presence of hydrophilic groups such as –OH, –CONH$_2$– and –SO$_3$H, in the polymers forming hydrogels, that create a hydrated network with different degrees (sometimes, more than 90% of water by weight), depending on the nature of the aqueous environment and the polymer chemical composition. The polymeric network is usually cross-linked by different modalities, including covalent bonds, hydrogen binding, van der Waals interactions, or physical entanglements. Hydrogels are extremely suitable for a variety of applications in the pharmaceutical and medical industry since they hold a number of appealing features [16]. Thanks to the presence of large amounts of water, hydrogels resemble certain native tissues; their framework presents a defined pore size allowing the diffusion of water/metabolites and exchange of nutrients/wastes, but strictly avoiding the overall migration or leakage of individual cells. Moreover, hydrogels can be easily fabricated into different shapes and sizes, from nano-scale particles to centimetre long sheets. In conclusion, the embedding of cells on hydrogels is very suitable for in situ cell delivery and cell therapy as demonstrated by numerous articles having as topic the regeneration of cartilage, cornea, nerve and liver [17].

Classification of hydrogels can be made according to various criteria including: the material used for their preparation, the preparation method, the overall charge and the mechanical characteristics.

With respect to materials, hydrogels can be obtained by natural or synthetic polymers. To the first class belongs polysaccharides (e.g. agarose, alginate) and proteins (e.g. collagen and gelatin); to the other one poly(ethylene glycol) (PEG), poly(vinyl alcohol) (PVA), poly-lactic-co-glycolic acid (PLGA) and poly (hydroxylethyl methacrylate) (PHEMA) [18].

Concerns regarding synthetic polymers inducing non-physiologic cellular responses have caused a shift of interest to using more natural materials, such as stand-alone products, chemically derived, physically derived, or extracellular matrix-derived materials.

The advantage of employing some natural biomaterials, such as collagen, fibrin, hyaluronan (HA), gelatin is their ability to mimic certain features of

native extracellular matrix (especially those of ECM origin), facilitating cell adherence, migration, differentiation. Cells indeed in the body are exposed to a complex milieu regulated by their interactions with other cells, the surrounding cell matrix and soluble factors. A key element of this microenvironment is the three dimensional (3D) architecture of the extracellular matrix. By removing the cells from this microenvironment many cell types quickly loose their function. Therefore, the ability to resemble the in vivo microenvironment of cells outside the body could be a potentially powerful tool.

In table 1 and in the following sections are briefly described some example of natural polymer usually employed for the preparation of hydrogels that have found a large number of applications in cell based protocols.

Table 1. Natural biomaterials used for cell based therapy and tissue engineering applications.

Biomaterials	Source	Chemical composition	Gelation method	Mechanism of degradation
Collagen	animal/human	protein	neutralization	Enzymatic
Gelatin	animal/human	protein	thermal	Enzymatic
Hyaluronan	animal/human	protein	chemical crosslinking	Enzymatic
Agarose	seaweed	polysaccharide	thermal	Non-degradable
Alginate	seaweed	polysaccharide	inotropic cross-linking	Ion exchange

1.2.1. Collagen

Collagen is the major structural component of mammalian connective tissue and has been used in cell immobilization due to its biocompatibility, biodegradability, abundance in nature and the ability to bind cells. The main sources of collagen are generally represented by cartilage, tendon, skin, bone, cartilage and ligament, where it is present in high concentrations. Collagen can be readily processed into different shaped scaffold including porous sponges, fibres, films, membranes and injectable cell immobilization carriers, since the gelation process occurs without chemicals modifications [19]. However, to improve the mechanical properties of scaffolded gels

different methods have been proposed such as crosslinking by chemicals, UV, temperature or polymeric agents. Collagen plays an important in regulating essential cellular events, such as proliferation, migration and differentiation via cell–matrix interaction and via integrin binding. Its natural ability to bind cells makes it a promising material for controlling cellular distribution within immunoisolated systems and its enzymatic degradation can provide appropriate degradation kinetics for tissue regeneration in microporous scaffolds. Moreover, collagen contains cell-adhesion domain sequences (e.g. RGD) that exhibit specific cellular interactions that can help to retain the phenotype and activity of many types of cells, including fibroblasts and chondrocytes.

Collagen has been extensively used to produce scaffold for many biomedical/regenerative applications, nevertheless it still has some constrains mainly related to the presence of antigenic components associated to the collagen molecules that can evoke host immunoreactions [20].

1.2.2. Gelatin

Gelatin is a naturally derived protein from collagen via a partial hydrolysis of the native collagen. During the manufacturing of gelatin, raw animal material is treated with dilute acid or alkali, resulting in partial cleavage of the crosslinks. Moreover, gelatin is a product of the meat-processing industry and it is a readily and economically available material, which has been used for decades in the food and pharmaceutical industries [21]. At a temperature of about 40°C, gelatin aqueous solutions are in the sol state and form physical thermoreversible gels after cooling. During the gelation process, the chains undergo a conformational disorder-order transition and tend to recover the original collagen triple-helix structure.

It is widely used for its non-toxicity, non-irritant and biodegradable properties and its mild gelling process that makes it is an attractive candidate as starting material for preparing hydrogels for drug delivery systems (i.e. hard and soft capsules, microspheres) and tissue engineering approaches (i.e. vascular

prostheses and wound dressing). As a biomaterial, gelatin displays several advantages: it is a natural polymer that has not shown antigenicity, it is completely resorbable in vivo and the presence of the large number of functional groups in the side chain offers the possibility to bind and release growth factors or incorporate proteins that can influence cell adhesion and growth in a controlled manner [22].

Compared to collagen, gelatin does not express antigenicity in physiological conditions, due to the denaturing process, and it is much cheaper and easier to obtain in concentrate solutions. Conversely, gelatin based hydrogels exhibits poor mechanical properties that can be overcame only via chemically cross-linking with various bifunctional agents, including glutaraldehyde or water-soluble carbodiimide that unfortunately reduce the initial high gelatin gel biocompatibility [23].

1.2.3. Hyaluronic acid

Hyaluronic acid (HA) is a nonsulphated glycosaminoglycan, composed of alternating units of D-glucuronic acid and D-N-acetylglucosamine, linked together via alternating β-1,4 and β-1,3 glycosidic bonds. HA is one of the major components of the extracellular matrix of skin, cartilage and the vitreous humor.

It plays a vital role in maintaining tissue integrity, as well as in facilitating adhesion and differentiation of cells during inflammation, wound repair, and embryonic development. Covalently cross-linked HA hydrogels can be formed by means of multiple chemical modifications. Hyaluronan is highly non- antigenic and non-immunogenic, owing to its high structural homology across species, and poor interaction with blood components [24].

A variety of commercially available preparations of HA derivatives and cross-linked HA materials have been developed for the production of drug delivery systems (microspheres, liposomes, fibres) or hydrogel-based scaffolds. Application of HA as a cell delivery vehicle has been investigated for cartilage, bone and osteochondral regeneration. Although the main mechanism of HA is unknown, in vivo, in vitro and clinical studies have

demonstrated various physiological effects of exogenous including chondroprotective properties.

Recently, HA has become recognized as an important building block for the creation of new biomaterials for use in cell therapy, three-dimensional (3-D) cell culture and tissue engineering applications. One of the key advantages of using HA gels for tissue engineering is that their degradation can be mediated by hyaluronidase, an enzyme secreted by a various cell types. On the other hand, the obtained HA based hydrogels are characterized by a weak mechanical strength resulting in scaffolds difficult to handle or to maintain the characteristics during the sterilization process.

1.2.4. Agarose

Agarose is a natural polysaccharide extracted from the cellular walls of agarophyte seaweed. Agarose gel is formed by cooling aqueous agarose solution, obtained by heating an aqueous suspension of agarose powder, until a clear solution forms. Since agarose gel networks are formed solely through hydrogen bonds without the use of chemicals, they are widely used in molecular biology and in immunoisolation protocols where it has been demonstrated they are well accepted following implantation [25]. The gelation mechanism is indeed governed completely by hydrogen bonding between agarose molecules and the resulting gel network is stabilized by structured water. In detail, agarose gels are formed when random coils, in a heated sol, become ordered as the sol cools. As cooling progresses, helices are formed which aggregate to form a gel network composed of thick bundles of agarose chains, large pores of water, exhibiting high turbidity and strong elasticity. Due to their soft tissue-like mechanical properties and biocompatibility, agarose gels have been investigated as potential scaffolds for neural [25] and cartilage tissue engineering [26]. The major drawbacks of agarose are the low cell adhesiveness and proliferation, since it does not contain any side groups to bind cell adhesive proteins. Moreover, due to the non-degradable nature of the gel, it has not been widely used in tissue engineering where usually scaffold materials should degrade over time in order to allow space

for accumulation of new tissue. With respect to application of agarose to cell capsulation procedures some important features should be considered. After melting, agarose can be easily transformed into a variety of controlled shapes, including microbeads, by simple and mild temperature reduction (usually below 30°C). In spite this advantageous characteristic, a possible drawback of agarose resides in the slow setting of gels, resulting in the possible cell protrusion from the capsular shell.

1.2.5. Alginate

Alginate is an example of a naturally derived polymer well suited for biomaterial scaffolds in cell-based therapy [27].

Alginates are extracted from three species of brown Algae such as *Laminaria hyperborean*, *Ascophyllum nodosum*, *Macrocystis pyrifera* and generally sold as sodium salt. Alginate is a water-soluble linear polysaccharide and consists of a mixture of β-D-mannuronic acid (M) and α-L-guluronic acid (G) residues. The ratio of M to G blocks can vary significantly depending upon the source of the raw materials used in alginate manufacture. Due to the shape of the monomers and their various ways to link, the geometries of the G-block and M-block regions, are substantially different. In detail, G-blocks have a bucked shape while the M- block tends to be as an extended ribbon (see Fig. 2)
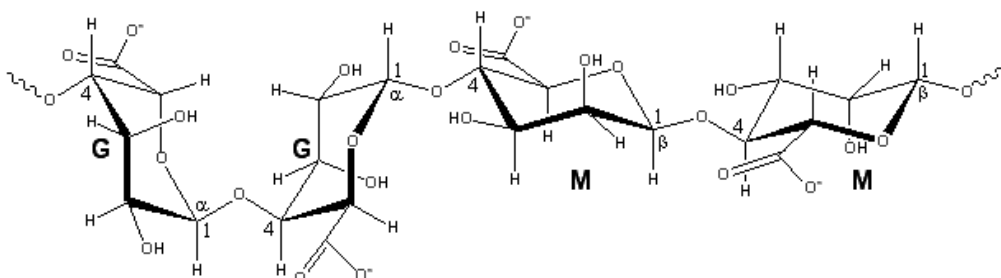
Fig. 2. Chemical structure of alginate constituted of 2 guluronic acid (G) monomers and 2 mannuronic acid (M) monomers, with (1–4) linkages.

Two G-blocks aligned side by side, result in the formation of a hole with specific dimension able to bind selectively divalent ions in a cooperative fashion. On dissolution in an aqueous medium, alginate forms a hydrocolloid, which gels ionotropically following the addition of divalent cations, including Ca^{2+}, Sr^{2+}, or Ba^{2+} (Fig. 3). The most important property of alginate is

indeed this ability to form gels under extremely mild conditions without the use of chemicals or a particular pH.
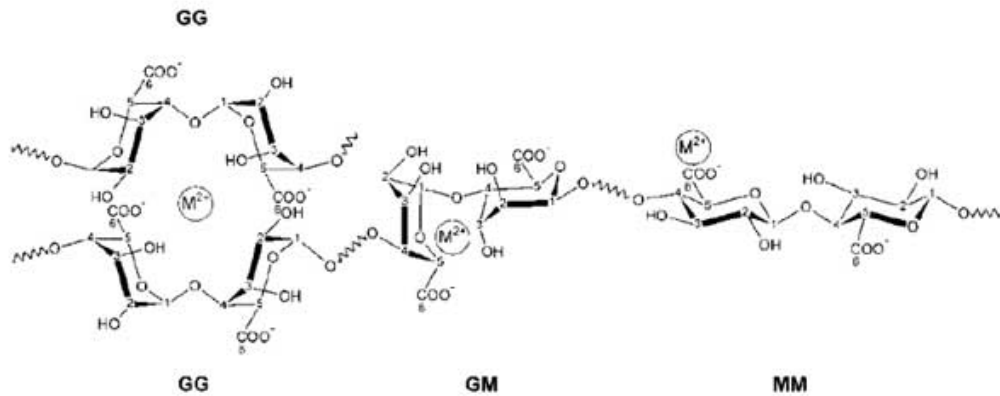
.
Fig. 3. Mechanism of ionotropic gelation of alginate based polymer in the presence of divalent cations (M^{2+}).

The polymer cross-linking occurs following the exchange of sodium ions from the guluronic acids with the divalent cations resulting in a chain-chain association that constitutes the junction zones of the so-called "egg box model" (Fig.4).
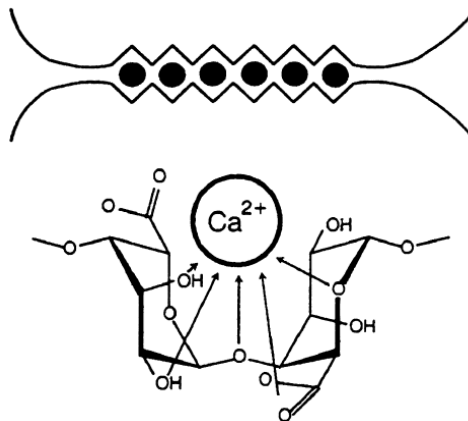
Fig. 4. The egg-box model after binding of divalent cations to homopolymeric G-blocks.

The buckled chain of guluronic acid units is shown as a two-dimensional analogue of a corrugated egg-box with interstices in which the divalent ions may pack and be coordinated. Since hydrogel formation occurs following selectively linkage between the carboxylic moieties on the G blocks of alginate and cations, high ratio of G:M results in stiff gels.

In general, as polysaccharide, alginates are characterized by a polydispersed

molecular weight and, for this reason, the molecular weight is not one unique value.

Polymer molecular weight is important because it determines many physical properties. If molecular weight is too low, the mechanical properties will generally be too low for the polymer material to have any useful practical and commercial applications.

If the Ni is the number and Wi is the weight of polymer molecules having a specific molecular weight Mi, the total number and weight of the polymer is

$$\bar{M}_n = \frac{\sum}{\sum}$$

$$\bar{M}_w = \frac{\sum}{\sum} \qquad \frac{\sum}{\sum}$$

The fraction M_n / M_w is called the polydispersity index and it has been reported to be between 1.4 and 6.0 for alginates, relating to the various purification processes.

The molecular weight distribution has a significant impact on some of the alginate gel properties including biocompatibility, stability, mechanical resistance, permeability, biodegradability and most important the gel formation [28].

Alginate is used extensively in food industry as a thickener, emulsifier and as a stabilizer. Furthermore, being an anionic polymer with carboxyl end groups, it has found application as pharmaceutical excipient to promote the mucoadhesive properties towards mucosal tissues. After the early study of Lim in 1980s, describing the use of alginate for cell microencapsulation, this polymer became the most widely used biomaterial for cell entrapment.

Although the suitability of other natural and synthetic polymers is currently under investigation, none has reached the same level of performance as alginates. For their ability to form gels in very mild conditions, alginate cross-linked with Ca^{2+} or Ba^{2+} ions has been used successfully to encapsulate cells maintaining a good viability and functions also during long-term culture [29]. Among biomaterials, alginate hydrogels are thought to be inert because they

lack native ligands that could allow interaction with mammalian cells, providing numerous advantages for tissue engineering including the possibility of minimally invasive injection of hydrogel/cell microcapsules.

Alginate gels have a defined pore size and a narrow pore-size distribution; in addition, they are mechanical and chemical stabile and contain low amount of toxic, pyrogenic and immunogenic substances.

Unfortunately, all the above features do not pertain at all the commercially available alginates; for biomedical procedures (i.e. cell encapsulation) only ultrapure alginates should be considered.

Alginate has been extensively characterized in terms of purity, biocompatibility and in vivo performances. In fact, as a natural derived material, alginate may contain impurities such as are polyphenols, proteins and lipopolysaccharide (LPS) (endotoxin) that cause a reduction in its biocompatibility. Even commercially available ultrapure alginates have been found to contain residual contaminants that can limit their use for the production of microcapsule. Inflammatory responses due to impurities can influence the performance and function of the devices. For instance, NO, produced form macrophages stimulated by alginate contaminants, thanks to small molecular dimensions can diffuse rapidly through the gel matrix causing severe cytotoxic effects on the encapsulated cells.

In this respect, an efficient purification process, designed to remove contaminants, including potentially immunogenic compounds, represents a mandatory step for tissue engineering application. Nevertheless, it is important that the purification process does not alter the polymer features (especially number and weight average molecular weights) that are critical for the gelation process and therefore the microcapsule formation.

Alginate beads are generally prepared by dripping a sodium alginate solution containing the desired cells into a divalent crosslinking solution such as Ca^{2+}, Sr^{2+}, or Ba^{2+} (gelling bath). Ca^{2+} ions are preferred for gelation of alginate; especially, for the encapsulation procedures, because of the high biocompatibility. After preparation, calcium gelified beads are usually coated by a cationic polyelectrolyte. The coating is performed to slow down the

swelling and in vivo degradation of the microcapsules, however it may cause immunological reactions and fibrotic growth; this latter can subsequently decrease the therapeutic efficacy of the entrapped cells sharply reducing the diffusive properties of the alginate capsule [30].

In this respect, the use of the positively charged polyelectrolytes for the capsular coating (i.e. poly-L-lysine) can induce a more intense overgrowth compared to negative ones. This funding was attributed to activated macrophages that preferentially adhere to positive charged surfaces.

Other cross-linking ions as an alternative for calcium have been used as well as Ba^{2+}. It has been proved that Ba^{2+} ions provide stronger gels [30] allowing the transplantation of microcapsules without the need of coating procedure. As drawback, barium is known to be toxic and concerns have been raised about its use as crosslinking agent. Recent studies have shown that when using low concentrations of barium, short time of gelling incubation and intensive rinsing of the obtained barium beads, no barium leakage from the microcapsules was observed [31]. For this reason, the alginate gelation with barium is preferred since it forms stronger crosslinks with alginate, which results in stronger gels than with calcium.

1.3. Scaffold design and their characteristics

The essential function of a hydrogel based scaffold for cell therapy is to provide a temporary 3D structure for cells. The main criteria for scaffold design include controlled biodegradability, suitable mechanical strength and appropriate surface chemistry. Another important role of the scaffold is its porosity; this property greatly influences indeed the diffusion of nutrients, therapeutic proteins and catabolites.

A large variety of immobilization devices of different geometries have been proposed for cell transplantation purposes and they are generally classified in macrodevices and microdevices (Fig 5) [32].

Macrodevices, usually characterized by dimensions comprised between 0.5-1.5 mm in diameter and 1-10 mm in length are able to entrap thousands to

millions of cells within their wall. The most common geometric configurations for macrodevices are vascular chambers, hollow fibres and flat membranes (sheets). An example of the use of macrodevices for cell transplantation is represented by cells seeded in a special compartment chamber, directly anastomosed to blood vessels, usually as arterio-vein shunts. In this way, the cells are continuously perfused by blood ultrafiltrate, which seemingly facilitated biochemical exchange. The membrane, in contact with the blood stream, is associated with an appropriate molecular weight cut off (commonly below 100 kD) to avoid that immune cells or antibodies would cross the cell containing chamber. However, the requirement of a surgery for implantation and/or retrieval as well as the risk of blood clotting have resulted in the lack of interest for these devices over the last years.
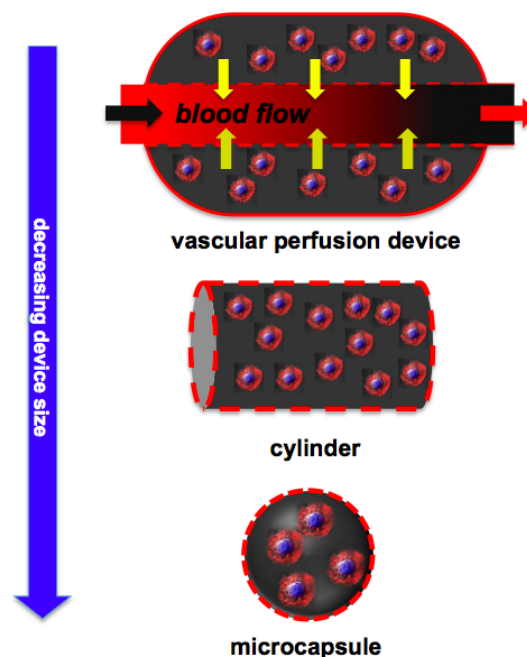
Fig. 5 General scheme of hydrogel based scaffolds suitable for in vivo cells transplantation protocols: vascular chamber, hollow fibre (cylinder) and microcapsule containing embedded cells.

Moreover, the bigger the grafted encapsulated tissue volume, the more frequent is the incidence of adverse side effects in the recipients.

Among microdevices, microcapsules represent the most widely studied immunoisolating systems [33]. In this respect, in the current PhD thesis, a number of new or revisited technologies for the production of

immunoisolating microdevices are investigated and optimized.

The spherical shape of microcapsules is considered advantageous since provide an optimal surface-to-volume ratio for protein and nutrient diffusion, improving the cell viability and functions compared to other scaffold geometries. Furthermore the small microcapsule dimensions, usually with a diameter comprised between 250 to 750 µm, facilitate the implantation in different body sites through small diameter catheters without the need for invasive surgery.
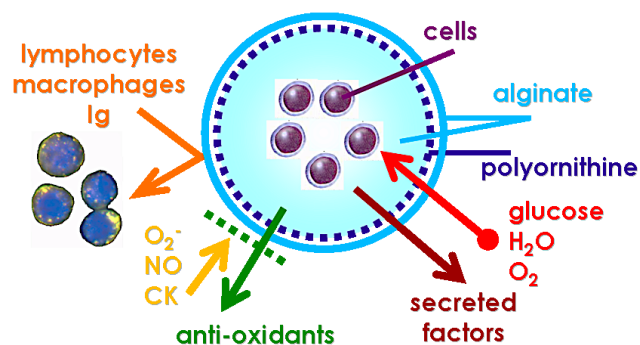

Fig.6. Schematic representation of a microcapsular device for cell encapsulation protocol.

The cell encapsulation in immmunoisolatig microcapsule, schematized in Fig. 6, can result in a number of potential advantages: (a) the physically isolation of cells from the external environment within a 3-D semipermeable membrane barrier, (b) the transplantation of cells without needing of the lifetime systemic administration of immunosuppressive drugs required to prevent the host rejection process, (c) the possibility to co-encapsulate (within the same device) cells from different sources and with distinct characteristics, including genetically engineered cells, (d) compared with encapsulation of proteins, cell immobilization allows a controlled release of produced therapeutic products giving rise to more physiological blood concentrations and (e) in case of mechanical failure of the encapsulation device, the possible toxic effects of a rapid and massive release of the therapeutic products, is avoided compared to macrodevices [34].

Microcapsule surrounding membranes are expected to permit the diffusion of nutrients and molecules such as oxygen and growth factors essential for

cellular metabolism, proliferation, differentiation and morphogenesis, while excluding the entry of all high molecular weight molecules such as immunoglobulins and immune system cells [33].

Microcapsules are generally constituted of hydrogels that offer highly hydrated microenvironment with a high degree of diffusion for low-molecular mass (Mr) biochemical and physical stimuli for cellular processes. Additionally, gels can be prepared by mild and rapid procedures, leading to a uniform distribution of cells into the gel matrix and high biocompatibility associate to minimal host-cell adhesion and protein adsorption phenomena. Nevertheless, the success of therapeutic approaches based on cell encapsulation require a detailed characterization of the biomaterials employed and of the cell–material and material-host tissue interactions, with special regard to the biocompatibility and immunogenicity of the cell-microcapsule assembly.

In conclusion, many requisites have to be considered for the clinical success of microcapsule, including dimensional, mechanical and biocompatibility properties; many of them are below discussed.

1.3.1. Dimensional, permeability and morphological properties

Dimension and morphology represent a critical characteristic that deeply influence many practical aspects related to the microcapsule use, including: cell loading capacity, diffusive properties (later discussed), method of implantation (gauge of the catheter) and finally biocompatibility.

It has been demonstrated that the microcapsule diameter can affect the host immune response, revealing that small dimensions resulted in a cellular reaction.

The success of cell-encapsulating microcapsules is also determined by their abilities to facilitate the transport of biological molecules into and from the encapsulated cells by the microcapsule pores. Extensive efforts are being made to control the pore size in order to prevent the entry of immunogenic molecules and cells. Specifically, the alginate microcapsules calcium cross-linked alginate hydrogel have generally pores ranging from 5 to 20 nm, able

to prevent the diffusion of large molecules, but allowing the diffusion of small ones. As already discussed, the pore size is further controlled by the deposition of polyelectrolyte complex layers on the surface by the exposure of alginate hydrogels to polycations such as poly-L-lysine.

Microcapsular shape also influences the in vivo performances, irregular geometries, such as the presence of fused or partially fused microparticles (a phenomenon usually named as "coalescence") or tear shaped microparticles (phenomenon usually named as "tail") result in the formation of capsular fibrotic overgrowth [35]. Moreover, microcapsular defects, in term of cracks or surface fissures, together with an irregular (rough or waved) surface, often cause a marked immunological in vivo response. Immediately following implantation, the surface of the material is coated with plasma proteins that further direct cellular adhesion and activation. The growth of host cells on the biomaterial device surface is considered to have negative effects because of reduced diffusion of oxygen and nutrients to the encapsulated graft resulting in necrosis of the enveloped cells.

Noteworthy, the surface roughness of the device has recently been described to provoke a strong tissue response in rats when alginate microcapsules were implanted with a strong surface roughness as visualized by atomic force microscopy [30].

1.3.2. Mechanical properties

The mechanical properties of cell-encapsulating microcapsules are highly important to ensure the therapeutic efficacy of transplanted cells. Some hydrogels do not provide an optimal mechanical stiffness (resistance to deformation) and toughness (resistance to fracture) able to structurally protect the embedded cells usually exposed to many different mechanical stresses during the processing, post processing and in vivo implantation procedures.

Cell encapsulation devices may also lose their mechanical and structural integrity, sometimes due to the action of the host immune system. The structural failure is indeed critical when the scaffold is in vivo implanted, in

which high mechanical stress is exerted. In this respect, the mechanical properties are generally studied and determined by specific test such as compression analysis between two flat surfaces resulting in force–displacement and force–time plots by which it is possible to obtain mechanical property parameters. The determination of the mechanical and elastic properties can be used to tune the microcapsule by adjusting the polymer source and concentration, processing methods, formulation and gelling conditions (i.e. the ionic strength of the gelation medium and the type of divalent cations). For example, increasing the polymer and the cross-linking agent concentrations led to an increase of the mechanical stiffness and toughness [30].

1.3.3. Biocompatibility properties

Biocompatibility of the microcapsules and the biomaterial constituents is the most critical issue for their end applications. Microcapsule biocompatibility is usually referred to different specific properties related to the host reaction to the encapsulation device; for instance the potentiality to, in vivo, elicits immune responses [36]. Following the implantation of the cell-encapsulating device, the host immune response is activated by the adsorption of proteins on the surface, which will stimulate the recruitment of immune cells. The immune cells directly destroy the transplanted cells or causes fibrotic overgrowth around the capsule limiting the efflux of nutrients or the bioactive molecules secreted by the entrapped cells. These cascade events are reduced by with the use of biocompatible materials, which present minimal amounts of toxins and prevent protein adsorption.

Other critical issues related to microcapsule performances are the body site and the implantation methods used. Both factors can indeed affect the type and the intensity of host response towards the implanted microcapsules.

1.4. References

[1] A. Atala. Regenerative medicine strategies. J Pediatr Surg, 47(1), 17, 2012.

[2] W.W. Minuth, L. Denk, A. Glashauser. Cell and drug delivery therapeutics for controlled renal parenchyma re generation. Adv Drug Del Rev, 62, 841, 2010.

[3] D. Sheyn, O. Mizrahi, S. Benjamin et al. Genetically modified cells in regenerative medicine and tissue engineering. Adv Drug Del Rev, 62, 683, 2010.

[4] P.Woźniak, M. Bil, J. Ryszkowska et al. Candidate bone-tissue-engineered product based on human-bone-derived cells and polyurethane scaffold. Acta Biomat, 6, 2484, 2010.

[5] Y. Huang, J. Yang, C. Wang et al. Dental Stem Cells and Tooth Banking for Regenerative Medicine. J Experim Clinic Med, 2, 111, 2010.

[6] D. Sheyn, O. Mizrahi, S. Benjamin et al. Genetically modified cells in regenerative medicine and tissue engineering. Adv Drug Del Rev, 62, 683, 2010.

[7] A. M. Davidoff, C. C. Ng, P. Brown et al. Bone marrow-derived cells contribute to tumor neovasculature and when modified to express an angiogenesis inhibitor can restrict tumor growth in mice. Clin Cancer Res, 7, 2870, 2001.

[8] G. Basta, P. Montanucci, G. Luca et al. Long-term metabolic and immunological follow-up of nonimmunosuppressed patients with type 1 diabetes treated with microencapsulated islet allografts: four cases. Diabetes

Care, 34(11), 2406, 2011.

[9] J. Koo, T.M.S. Chang. Secrecation of erythropoietin from microencapsulated rat-kidney cell- Preliminary results. Int Art Org, 16, 557, 1993.

[10] F. Bautz, S. Rafii, L. Kanz, R. Mohle. Expression and secretion of vascular endothelial growth factor-A by cytokine-stimu- lated hematopoietic progenitor cells: Possible role in the hematopoietic microenvironment. Exp Hematol, 28, 700, 2000.

[11] P. Lu, L.L. Jones, E.Y. Snyder et al. Neural stem cells constitutively secrete neurotrophic factors and promote extensive host axonal growth after spinal cord injury. Exp Neurol, 181, 115, 2003.

[12] J. Yang, M. Yamato, K. Nishida et al. Cell delivery in regenerative medicine: the cell sheet engineering approach. J Control Rel, 116(2), 193, 2006.

[13] J. Hubbel. Biomaterials in tissue engineering. Nature Biotech 13, 565, 1995.

[14] J.T. Wilson, E. L. Chaikof. Challenges and emerging technologies in the immunoisolation of cells and tissues. Adv Drug Del Rev, 60, 124, 2008.

[15] B.V. Slaughter, S.S. Khurshid, O.Z. Fisher et al. Hydrogels in Regenerative Medicine. Adv. Mater, 21, 3307, 2009.

[16] A.S. Hoffman. Hydrogels for biomedical applications. Adv Drug Del Rev 54, 3, 2002.

[17] J.L. Drury, D.J. Mooney. Hydrogels for tissue engineering: scaffold

design variables and applications. Biomat, 24, 4337, 2003.

[18] N.A. Peppas, P. Bures, W. Leobandung, H. Ichikawa. Hydrogels in pharmaceutical formulations. Eur J Pharm and Biopharm, 50, 27, 2000.

[19] W. Friess. Collagen–biomaterial for drug delivery. Eur J Pharm Biopharm, 45, 113, 1998.

[20] R.J. Mullins, C. Richards, T. Walker. Allergic reactions to oral, surgical and topical bovine collagen. Anaphylactic risk for surgeons. Austr New Zealand J Ophthalmol, 24(3), 257, 1996.

[21] S. Young, M. Wong, Y. Tabata et al. Gelatin as a delivery vehicle for the controlled release of bioactive molecules. J Control Rel, 109, 256, 2005.

[22] H. Shinmoto, K. Yamagishi, T. Kimura et al. Antigenicity estimation of collagenase-treated gelatins by a novel assay system using human antibodies secreted by B-lymphoblastoid cells. Food Sci Technol Res, 7, 331, 2001.

[23] S.E. Noorjahan, T.P. Sastry. Hydrogels based on physiologically clotted fibrin–gelatin
Composites. J Polymer Science A, 42, 2241, 2004.

[24] J. Necas, L. Bartosikova, P. Brauner et al. Hyaluronic acid (hyaluronan): a review. Veterinarni Medicina, 53, 397, 2008.

[25] S. Stokols, M. H. Tuszynski. Freeze-dried agarose scaffolds with uniaxial channels stimulate and guide linear axonal growth following spinal cord injury. Biomat, 27, 443, 2006.

[26] H.A. Awad, M.Q. Wickham, H. A. Leddy et al. Chondrogenic

differentiation of adipose-derived adult stem cells in agarose, alginate, and gelatin scaffolds. Bioamt, 25, 3211, 2004.

[27] I. Ghidoni, T. Chlapanidas, M. Bucco et al. Alginate cell encapsulation: new advances in reproduction and cartilage regenerative medicine. Cytotech, 59, 49, 2008.

[28] P. De Vos, B.J. De Haan, R. Van Schilfgaarde. Effect of the alginate composition on the biocompatibility of alginate-polylysine microcapsules. Biomat, 18, 273, 1997.

[29] G. Luca, M. Calvitti, C. Nastruzzi et al. Encapsulation, in vitro characterization, and in vivo biocompatibility of Sertoli cells in alginate-based microcapsules. Tissue Eng, 13(3), 641, 2007.

[30] P. de Vos, M.M. Faas, B. Strand et al. Alginate-based microcapsules for immunoisolation of pancreatic islets. Biomaterials, 27, 5603, 2006.

[31] B. Thu, P. Bruheim, T. Espevik et al. Alginate polycation microcapsules. I. Interaction between alginate and polycation. Biomat, 17, 1031, 1996.

[32] E.F. Nafea, A. Marson, L.A. Poole-Warren et al. Immunoisolating semi-permeable membranes for cell encapsulation: focus on hydrogels. J Control Rel 154, 110, 2011.

[33] G.J Lim, S. Zare, M. Van Dyke et al. Cell microencapsulation. Adv Exp Med Biol, 670, 126, 2010.

[34] J.M. Rabanel, X. Banquy, H. Zouaoui et al. Progress technology in microencapsulation methods for cell therapy. Biotechnol Prog, 25, 946, 2009.

[35] S. Mazzitelli, A. Tosi, C. Balestra. Production and characterization of alginate microcapsules produced by a vibrational encapsulation device. J Biomat Appl, 23, 123, 2008.

[36] H. Auchincloss, D.H. Sachs. Xenogeneic transplantation. Annu Rev Immunol, 16, 433, 1998.

CHAPTER 2

Bioencapsulation for cell therapy:
experimental procedures for the production and
characterization of microcapsules

This chapter is extracted from the articles:

2. *"Induction by TNF-α of IL-6 and IL-8 in cystic fibrosis bronchial IB3-1 epithelial cells encapsulated in alginate microbeads"*

M. Borgatti, S. Mazzitelli, G. Breveglieri, R. Gambari and C. Nastruzzi, Journal of Biomedicine and Biotechnology, 2010, Article ID 907964 (Borgatti and Mazzitelli equal contribution).

2. *"Encapsulation of mesenchymal stem cells from Wharton's jelly in alginate microbeads"*

L. Penolazzi, E. Tavanti, R. Vecchiatini, E. Lambertini, F. Vesce, R. Gambari, S. Mazzitelli, F. Mancuso, G. Luca, C. Nastruzzi, R. Piva, Tissue Eng Part C Methods, 2010, 16(1), 141-55.

3. *"Preparation and characterization of polysaccharidic microbeads by a microfluidic technique: application to the encapsulation of Sertoli cells"*

L. Capretto, S. Mazzitelli, G. Luca and C. Nastruzzi, Acta Biomaterialia, 2010, 6(2), 429-35 (Capretto and Mazzitelli equal contribution).

2.1. Cell encapsulation in microparticles: methods of preparation

Although the concept of cell therapy is very appealing, in practice a great deal of technology and know-how is needed for the production of long-term functional cell based devices.

Many types of natural and synthetic polymers have been explored for microencapsulation protocols. As reported in Chapter 1, the capsular material must be biocompatible, mechanically stable and provide an environment assuring the cell survival and the secretion of therapeutic products [1].

As already discussed, alginate is the most used encapsulation polymer for the immunoisolation of allogeneic and xenogeneic cells. Alginate based microcapsules are usually produced by the extrusion of cell containing alginate droplet into a gelling bath, followed by a polycation coating, that assures the control of molecular weight cut-off of the microcapsular structure [2].

The production of alginate microcapsules can be performed by a few alternatives including coaxial bead generator, jetcutter and electrostatic droplet generation technologies (Fig. 1) [3].

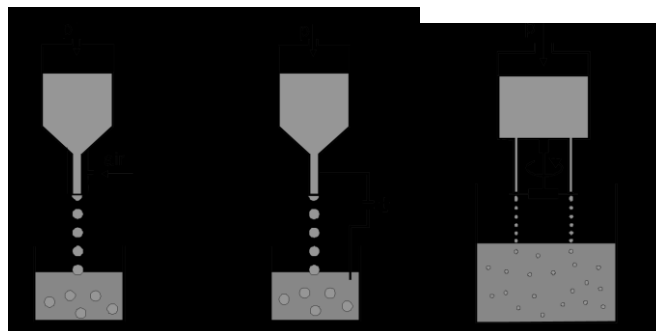Fig. 1. Microcapsule production by coaxial bead generator (left), electrostatic droplet generation (center) and jetcutter technologies (right).

Irrespectively of the preparation strategy, the microcapsule formation consists of three main steps, as below described.

1. The suspension of viable cells in the aqueous colloidal alginate dispersion (the polymer is usually employed at a concentration ranging from 1 to 3 %, w/v).

2. The generation of alginate droplets, representing the precursors of the microcapsules; this step is preferably achieved by a controlled size procedure.

3. The consolidation of the droplets by a gelation process, resulting in the final formation of soft hydrogel based microparticles.

Specifically, the formation of uniform alginate microdroplets (step 2) represents the most critical step of many preparation processes described in the literature.

The underlying principle of the droplet generation is that a liquid, when forced through a nozzle, is extruded initially as individual droplets.

However, with an increasing flow rate, the liquid forms a laminar jet that breaks into small droplets either naturally (by gravity) or with the aid of various means. Generally, the alginate droplet break-off, at the nozzle tip, is achieved by an air-jet directed to the forming droplet, electrostatic forces, a mechanical cutting of the alginate flow or the vibration of the micronozzle. Varying different experimental settings such as the nozzle diameter, the alginate pumping rate and the applied air-flow or electric field, the droplet diameter can be adjusted.

In Fig. 2 are reported the general scheme of the currently employed procedures for the production of alginate microcapsules.

One of the main aim of the PhD thesis was the development of new or more performing encapsulation procedures based on a variety of physical principles and instrumentations, including coaxial bead generator (Fig. 2 A), vibrating-nozzle procedure (Fig. 2 B) and microfluidics. (Fig. 2 C). The studied and well-validated encapsulation procedures were thereafter applied to the entrapment of different cell systems including bronchial epithelial cell line, mesenchymal stem cells and Sertoli cells.
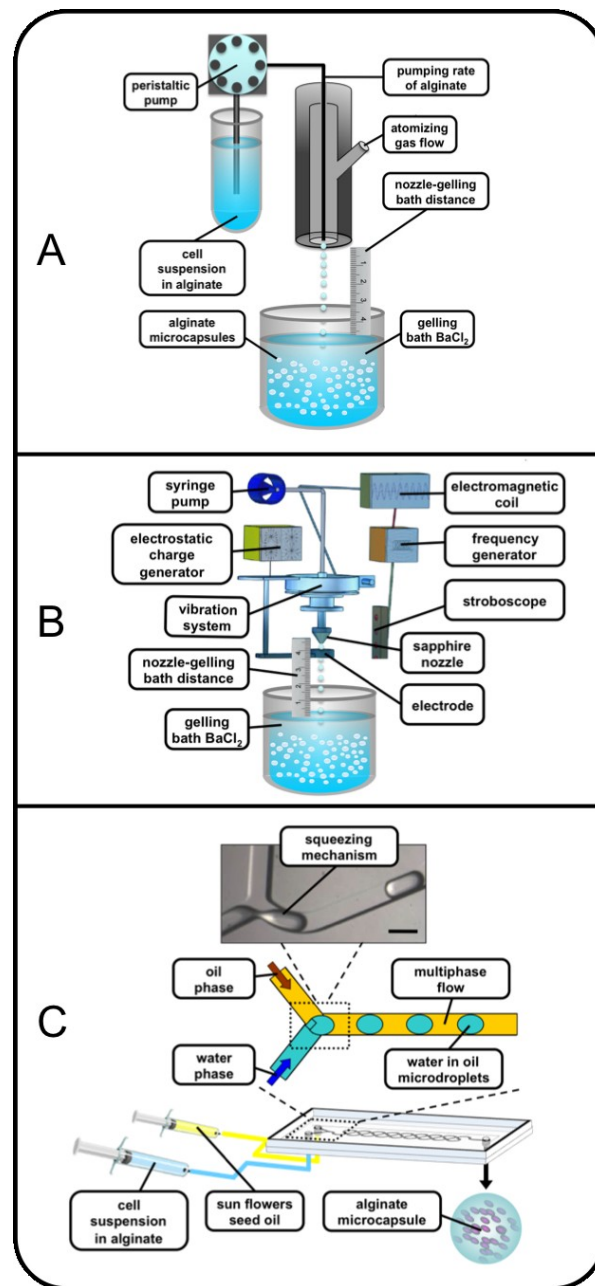
Fig. 2. Schematic representations of different encapsulation protocols: coaxial bead generator (A), vibrating-nozzle procedure (B) and microfluidic based approach (C).

3.2. Cell encapsulation by coaxial bead generator

The encapsulation procedure based on the use of a coaxial bead generator (Fig. 2 A), represents one of the most used instrumentation for the production of polysaccharidic microcapsules, intended for cell encapsulation. Various encapsulation systems are commercially available for the production of

alginate microbeads in a controllable manner (i.e. Coaxial Airflow Induced Dripping VAR J1 from Nisco Engineering Inc, Switzerland, see Fig. 3).

The general principle of the instruments is based on a coaxial air stream that blows polymer droplets from a needle tip into a gelling bath.

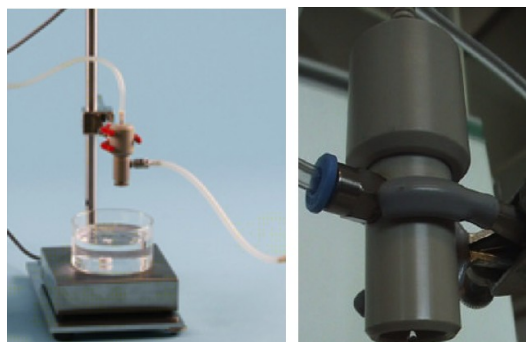Fig. 3. Pictures of the Coaxial Coaxial Airflow Induced Dripping VAR J1 from Nisco Engineering Inc. The instrument is connected with hoses providing alginate solution and air, respectively.

In our laboratory, we have recently designed and produced a new model of coaxial bead generator, named *"gas driven mono-jet device"*. The entire project was developed with the aim to improve some instrumental characteristics and performances of coaxial bead generators on the market available including the connectivity (to alginate-cell suspension and gas/air generator) and the possibility to change the internal diameter of the nozzle, in order to obtain microcapsules with different diameters.
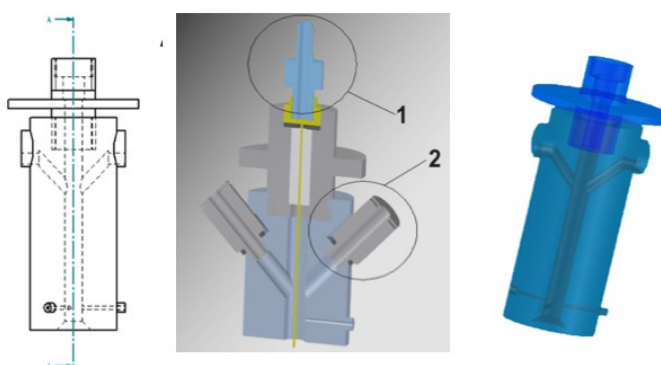

Fig. 4. Schematic and 3-D representation of the gas driven mono-jet device showing the two lateral and top inlets for the alginate feeding (1) and the atomizing gas (2).

In this respect, our device is equipped with two lateral and one top standard rapid connectors based on female luer lock (as air and alginate inlets) and an internal nozzle (commercially available blunt end needles) that is

easily interchangeable, depending on the dimensions of the final droplets required. The complete encapsulation system is composed of a gas driven mono-jet device connected to a precision peristaltic pump (for the alginate feeding) and to a gas flask (usually nitrogen) equipped with a flow meter (providing the gas for the atomization of the alginate). The generated microdroplets are then consolidated to give microparticles by a gelation procedure generally based on calcium or barium ion solutions. Typically, the cell suspension is continuously mixed by a magnetic stirrer to prevent cell clumping, which could lead to inhomogeneous cell distribution within the microparticles.

2.2.1. Application of a coaxial bead generator to IB3-1 cells

Cystic fibrosis (CF) is an autosomal recessive disorder caused by mutations of the CF transmembrane conductance regulator (CFTR) gene, which encodes a transmembrane protein present on a variety of cell types and organelles [4]. The CF lung is characterized by chronic bacterial infection of the airways, thickened airway mucous, and bronchiectasis [5]. The excess of mucus is largely caused by the influx of neutrophils, attracted to the site by the increased expression of chemokines such as interleukin-6 (IL-6) and interleukin-8 (IL-8), by bacterial products and inflammatory cytokines [6]. In particular, IL-8, that is potent chemokine, is induced transcriptionally by a wide variety of stimuli including tumor necrosis factor-alpha (TNF-a), hyperosmotic shock and bacterial [7]. In order to possibly study in detail the mechanism(s) of activation of IL-8 in CF, the IB3-1 cell system has been recently proposed [8]. IB3-1 is a bronchial epithelial cell line, derived from a CF patient with a CFTR genotype of F508del/W1282X, therefore carrying the associated cystic fibrosis mutation. This cell line can be induced to high expression of proinflammatory proteins, following infection with Pseudomonas aeruginosa or by treatment with TNF-a, for at least 24 h. In order to develop a specific system to possibly study the mechanism of bacterial activation of IB3-1 cells as well as the effect of the secreted

chemokines on target cell populations, in co-culture experiments (eg. *Pseudomonas aeruginosa* or polymorphonuclear cells) alginate microcapsules containing IB3-1 cells were produced. The co-culture experiments could be performed in the presence/absence of a semipermeable membrane embedding the IB3-1 cells, representing a physical barrier to cell/cell interactions but allowing the cross-talking among the different cells mediated by soluble factors.

2.2.1.1. Materials and methods

Cell cultures

IB3-1 cells were obtained from LGC Promochem (Teddington, Middlesex, UK) and were grown in LHC-8 basal medium (Biofluids, Rockville, MD, USA), supplemented with 5% FBS in the absence of gentamycin. All culture flasks and plates were coated with a solution containing 35 mg/mL bovine collagen (Becton-Dickinson Italia, Milan, Italy), 1 mg/mL bovine serum albumin (Sigma, St. Louis, MO, USA), and 1mg/mL human fibronectin (Becton-Dickinson).

Encapsulation of IB3-1 cells

Before encapsulation, confluent monolayers of IB3-1 were scraped off by 0.05% trypsin/EDTA (Gibco, Grandisland, NY, USA) (2min), washed with PBS, counted by hemocytometric analysis, and assayed for viability by double staining with propidium iodide (PI) and Calcein-AM (Sigma), following the manufacturer's indications. Briefly, IB3-1 cells were suspended in a 1.5% (w/v) aqueous solution of highly purified sodium alginate (Inotech, Dottikon, Switzerland), further purified by a multistep filtration process, at a concentration of $8–12 \times 10^6$ cells/ml. The resulting cell suspension was continuously aspirated by a syringe pump and extruded through the gas driven mono-jet, developed in our laboratory, under sterile conditions. The generated microdroplets were hardened by an ionotropic gelling process into a 1.2% (w/v) barium chloride solution that resulted in the production of barium alginate microbeads. After 3 min of incubation into the gelling bath,

the microbeads were washed twice with saline and placed in LHC-8 basal medium (Biofluids), supplemented with 5% FBS at 37◦C in an humidified atmosphere of 5% CO_2.

Dimensional and morphological characterization of alginate microbeads

The morphology of barium alginate microbeads was evaluated by optical microscopy and stereomicroscopy (Nikon microscopes, Tokyo, Japan). Microbead size was determined by photomicrograph analyses (Eclipsenet version 1.16.5; Laboratory AU5c Imaging s.r.o. for Nikon B.V.). Samples of 200–400 beads were considered.

Viability determination of encapsulated IB3-1 cells

After encapsulation and after different lengths of time, the viability of IB3-1 cells was analysed by double staining with propidium iodide (PI) and Calcein-AM, following manufacturer's instructions. For the propidium iodide (PI) and Calcein-AM analysis, cells were visualized under a fluorescence microscope (Nikon, Optiphot-2, Nikon Corporation, Japan). Viable cells were stained in green while the dead ones were stained in red.

Experimental Design and Statistical Analysis

To study the effect and the influence of different experimental parameters on the size and size distribution of alginate microbeads, a randomized central compositive face centered design (CCF) consisting of 17 runs was used. The experimental design and the evaluation of the experiments were performed by the PC software MODDE 8.0 (Umetrics AB, Sweden), followed by multiple linear regression (MLR) algorithms. The following experimental parameters ("factors") were considered: the atomizing air flow ("air"), the alginate pumping rate ("pump"), and the distance between the nozzle of gas driven mono-jet device and the surface of the gelling bath ("height").

Treatment of monolayers

IB3-1 cells were seeded at the initial concentration of 30,000 cells/cm^2 and the cell number/ml determined after 3 days of culture. Cell number/ml was determined after trypsin treatment by using a model ZBI Coulter Counter (Coulter Electronics, Hialeah, FL, USA). Treatment of monolayers with 80 ng/ml TNF-α (PeProTech EC, London, UK) was performed on 70% confluent

cells for 24 hours. Treatment of encapsulated cells: equal quantity (20×10^6 cells) of free and encapsulated cells (derived from the same flask, previously cultured for 3 days and successively detached by trypsin) were treated with 80 ng/ml TNF-α for 24 hours.

Cytokine profiles

Cytokines in tissue culture supernatants released from the cells under analysis, were measured by Bio-Plex cytokine assay (Bio-Rad Laboratories, Hercules, CA) [9] as described by the manufacturer. The Bio-Plex cytokine assay is designed for the multiplexed quantitative measurement of multiple cytokines in a single well using as little as 50 µl of sample. In our experiments, the premixed multiplex beads of the Bio-Plex human cytokine 7-plex which included seven cytokines (IL-1rα, IL-6, IL-8, G-CSF, MCP-1 (MCAF), RANTES, VEGF) were used. 50 µl of cytokine standards or samples (supernatants recovered from treated cells) were incubated with 50 µl of anti-cytokine conjugated beads in 96-well filter plates for 30 min at room temperature with shaking. Plates were then washed by vacuum filtration three times with 100 µl of Bio-Plex wash buffer, 25 µl of diluted detection antibody were added, and plates were incubated for 30 min at room temperature with shaking. After three filter washes, 50 µl of streptavidin-phycoerythrin was added, and the plates were incubated for 10 min at room temperature with shaking. Finally, plates were washed by vacuum filtration three times, beads were suspended in Bio-Plex assay buffer, and samples were analysed on a Bio-Rad 96-well plate reader using the Bio-Plex Suspension Array System and Bio-Plex Manager software (Bio-Rad Laboratories, Hercules, CA).

Quantification of IL-8 and IL-6 transcripts

Total RNA was isolated (High Pure RNA isolation kit, Roche), retro transcribed (Promega Corporation, Madison, USA) and the resulting cDNA was quantified by relative quantitative real-time PCR. The sequences of the oligonucleotides used for amplification of IL-8 mRNA were: 5'-GTG CAG TTT TGC CAA GGA GT-3' (forward) and 5'-TTA TGA ATT CTC AGC CCT CTT CAA AAA CTT CTC-3' (reverse); for IL-6 mRNA: 5'-AGG AGA CTT GCC

TGG TGA AA-3' (forward) and 5'-CAG GGG TGG TTA TTG CAT CT-3' (reverse); for GAPDH mRNA: 5'-AAG GTC GGA GTC AAC GGA TTT-3' (forward); 5'-ACT GTG GTC ATG AGT CCT TCC A-3' (reverse). For PCR, 0,5/20 µl aliquots of cDNA were used for each Sybr Green real-time PCR reaction to quantify the relative tissue expression of IL-8 and IL-6 transcripts. Each 25 µl of total reaction volume contained 0.5 µl of cDNA, 10 pmol of primers, 1 x iQ™ SYBR® Green Supermix (Bio-Rad Laboratories, Hercules, CA). Real-time PCR reactions were performed for a total of 40 cycles (denaturation, 95°C for 10 s; annealing, 68°C for 30 s for IL-8, 65°C for 30 s for IL-6; elongation, 72°C for 60 s) using an iCycler IQ® (Bio-Rad Laboratories, Hercules, CA). The relative proportions of each template amplified were determined based on the threshold cycle (Tc) value for each PCR reaction. The ΔΔCt method was used to compare gene expression data. Each sample was quantified in duplicate from at least two independent experiments. Mean ± S.D. values were determined for each fold difference. Amplification of human GAPDH cDNA served as internal standards (housekeeping gene). Duplicate negative controls (no template cDNA) were also run with every experimental plate to assess specificity and indicate potential contamination.

Data Analysis and statistics

Statistical analysis was performed by one-way analysis of variance followed by the Student's t test. A P value <0.05 was considered statistically significant.

2.2.1.2. Results

Release of pro-inflammatory proteins by IB3-1 cells exposed to TNF-α: a Bio-Plex analysis

IB3-1 cystic fibrosis cell monolayers (see Figure 5 A-B) were treated, after 3 days cell culture, for 24 hours in the presence of 80 ng/ml of TNF-α, thereafter, the conditioned media, from treated and control cell populations, were analysed for presence of pro-inflammatory cytokines by
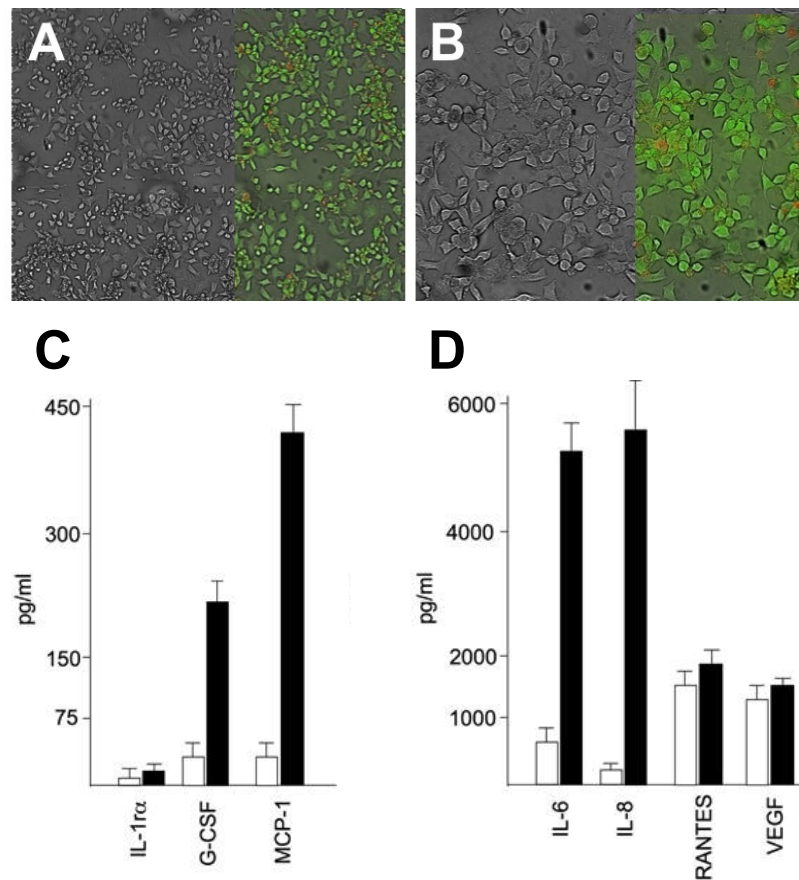
Bio-Plex mediated analysis.

Fig. 5. Morphology (panels A and B) and viability (insets) of IB3-1 cell monolayers, as determinated by bright field and fluorescence photomicrographs. Analysis of the release of pro-inflammatory cytokines by IB3-1 cells, as determinated by Bio-plex analysis (panels C and D). The indicated proteins were analyzed in the IB3-1 cell culture medium, namely: IL-1rα (Interleukin-1 receptor alpha), G-CSF (Granulocyte-colony stimulating factor), MCP-1 (Monocyte chemotactic protein-1), IL-6 (Interleukin 6), IL-8 (interleukin 8), RANTES (Regulated upon activation, normal T cell expressed and secreted), VEGF (Vascular endothelial growth factor). Data are referred to control untreated cells (open bars) and to cells treated for 24 hours with TNF-α (80 ng/ml) (closed bars). Data represent the average of three independent experiments±SD.

Before each induction experiments IB3-1 cell monolayers were assayed by "live/dead cells" test, and in all cases the determinated viability was $\geq$ 90%, as indicated by the fluorescence photomicrographs reported in the insets of Figure 5 A-B.

The Bio–Plex 200 multiplex suspension array represents, in fact, an assay system, employing Luminex xMAP–technology, for the simultaneous detection and quantitation of multiple bioanalytes (proteins, peptides, DNA and RNA) in a single microplate, requiring only very small sample volumes.

A number of proteins were considered in the analysis of IB3-1 medium, namely: IL-1rα, G-CSF, MCP-1, IL-6, IL-8, RANTES and VEGF. The obtained data, reported in Figure 5 (panels C and D), indicate that, apart from RANTES and VEGF (which values are not statistically different in control vs. treated cells), all other proteins are differentially expressed and released in untreated IB3-1 cells and after TNF-α treatment. In particular, IL-6 and IL-8 were present at high concentrations, in the medium of TNF-α treated cells, reaching values of 5.71 and 5.84 ng/mL, respectively.

Encapsulation of IB3-1 in alginate microbeads

IB3-1 were embedded into alginate microbeads by the gas driven mono-jet device for cell encapsulation (see scheme in Figure 6). The encapsulation procedure was relatively simple and consisted of a limited number of steps. In order to achieve complete biocompatibility, essential for mammalian cells, the entire procedure was conducted at room temperature, under physiologic pH and tonicity using a pyrogen-free alginate, purified by a filtration procedure in order to remove possible contaminants.

The hardening of the generated alginate microdroplets was accomplished by an ionic gelation procedure with barium chloride. The resulting barium alginate microbeads were elastic and transparent, thus facilitating the microscopic observation of cell morphology and viability, during the in vitro studies, as evident by the bright field and dark field stereophotomicrographs shown in Figure 7.
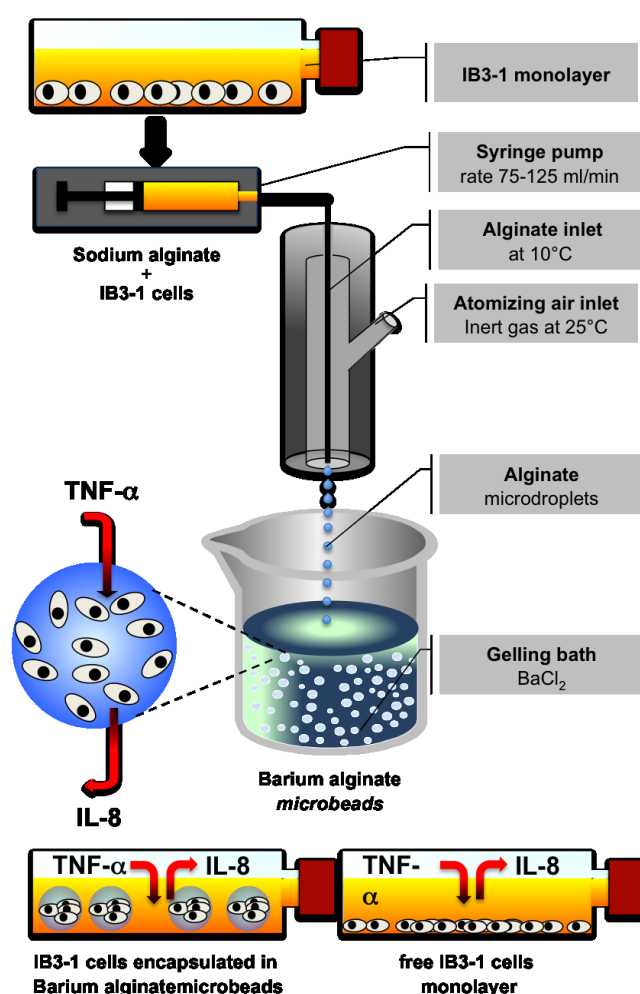
Fig. 6. General scheme of the encapsulation procedure for IB3-1 cells by the gas driven mono-jet device. The lower part of the figure summarizes the procedure for the in vitro experiments with free (right) and encapsulated IB3-1cells (left) treated with TNF-α.

For the screening and optimisation of the experimental parameters, a "design of the experiments" (DoE), was performed, after design by MODDE software. DoE offers a rational approach for experiment-based research by reducing the number of experiments and providing more precise information about the effects of different variables and their possible interactions. The DoE process can help to improve the accuracy with which it is possible to predict operating characteristics of many industrial processes.

A central composite design (one of the most used designs in pharmaceuticals and biological studies) was applied to the optimization of alginate microbeads.
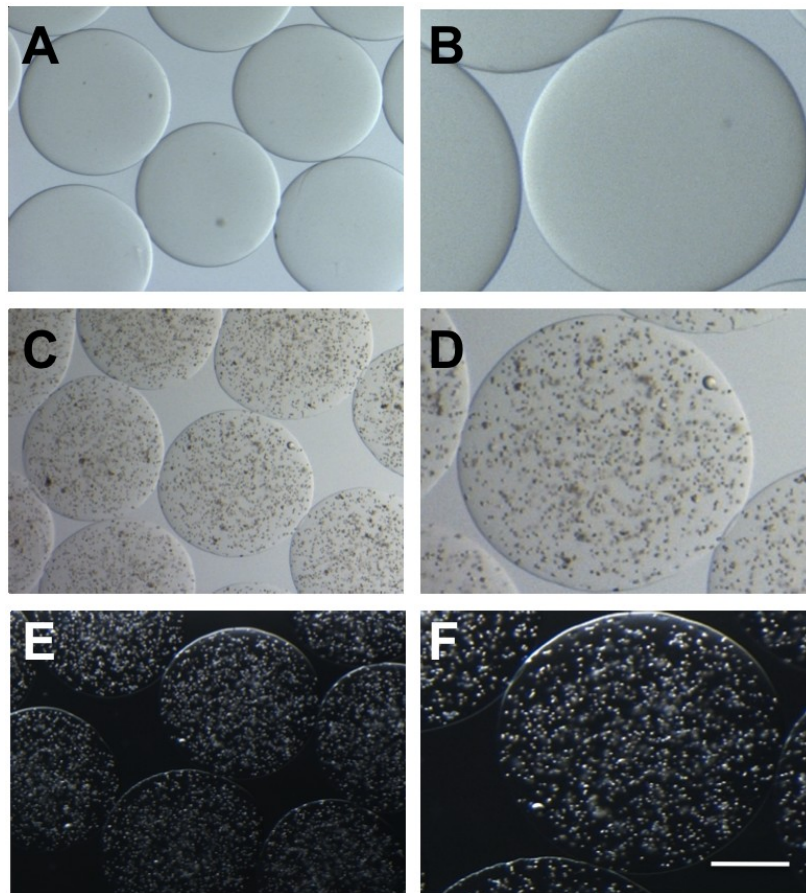
Fig. 7. Bright field (A, B, C, D) and dark field (F) stereophotographs of empty (A,B) and IB3-1 containing (C-F) alginate microbeads. Microbeads were produced by the gas driven mono-jet device. Alginate microbeads were prepared using the experimental parameters reported in Table 1 (batch #15a, b, c). Bar corresponds to 400 (A, B, E) and 250 μm (B, D, F).

This experimental design required 17 experiments (2 k + 2 k + 3, where k is the number of variables) including three center points in order to have an estimation of the experimental error. The high and low values of each variable were defined based on preliminary experiments. The factors/responses and the general results of DoE analysis are reported in Table 1 and Figures 8 and 9, respectively. In particular, in Figure 8 are shown the contour plots, while the response surface plots of the investigated factors are given in Figure 9; the influence of factors on "size" are in panels A-C and on "SD" in panels D-F.

The main observation was that a change in "air" value from a low to a high level (12 to 20 bar) results in a sharp decrease of the microbead "size" while the "SD" response presents a biphasic trend showing a minimum at the

central value for both "air" and "pump". The "height" and "pump" parameters exert an influence at high and low levels causing the increase of the both responses.

Table 1. Experimental design matrix and results of the DoE (design of experiments) approach for alginate microbeads.

Batch #	Factors			Responses	
	Atomizing air (Bar)	Nozzle to gelling bath (cm)	Polymer pumping rate (μm/mL)	Mean diameter (μm)	Standard deviation ($\pm\mu$m)
	"air"	"height"	"pump"	"size"	"SD"
#1	12.0	2.2	75.0	1350.5	63.2
#2	20.0	2.2	75.0	983.1	68.4
#3	12.0	3.0	75.0	1234.1	389.5
#4	20.0	3.0	75.0	917.5	60.5
#5	12.0	2.2	125.0	1177.5	296.5
#6	20.0	2.2	125.0	716.7	99.2
#7	12.0	3.0	125.0	1161.1	83.6
#8	20.0	3.0	125.0	724.8	106.7
#9	12.0	2.6	100.0	1293.6	47.6
#10	20.0	2.6	100.0	835.4	322.3
#11	16.0	2.2	100.0	970.5	54.8
#12	16.0	3.0	100.0	851.6	36.3
#13	16.0	2.6	75.0	920.6	47.2
#14	16.0	2.6	125.0	974.9	58.1
#15a	16.0	2.6	100.0	920.8	43.1
#15b	16.0	2.6	100.0	920.8	43,1
#15c	16.0	2.6	100.0	920.8	43.1

After investigation of the factor influence, the validity and the significance of the model was estimated by analysis of variance (ANOVA). All the data obtained fit well the model determining a good reproducibility of the studied model. We get a large regression coefficient R^2 that is a necessary condition for a validity model with a significant power of prediction of the model Q^2 (data not shown).

Fig. 8. DoE analysis for the production of alginate microbeads containing IB3-1 cells. Contour plots of the responses: "size" (A-C) and "SD" (D-F). The following interactions were reported: "height versus air" (A,D); "pump versus air" (B,E); and "pump versus height" (C,F).
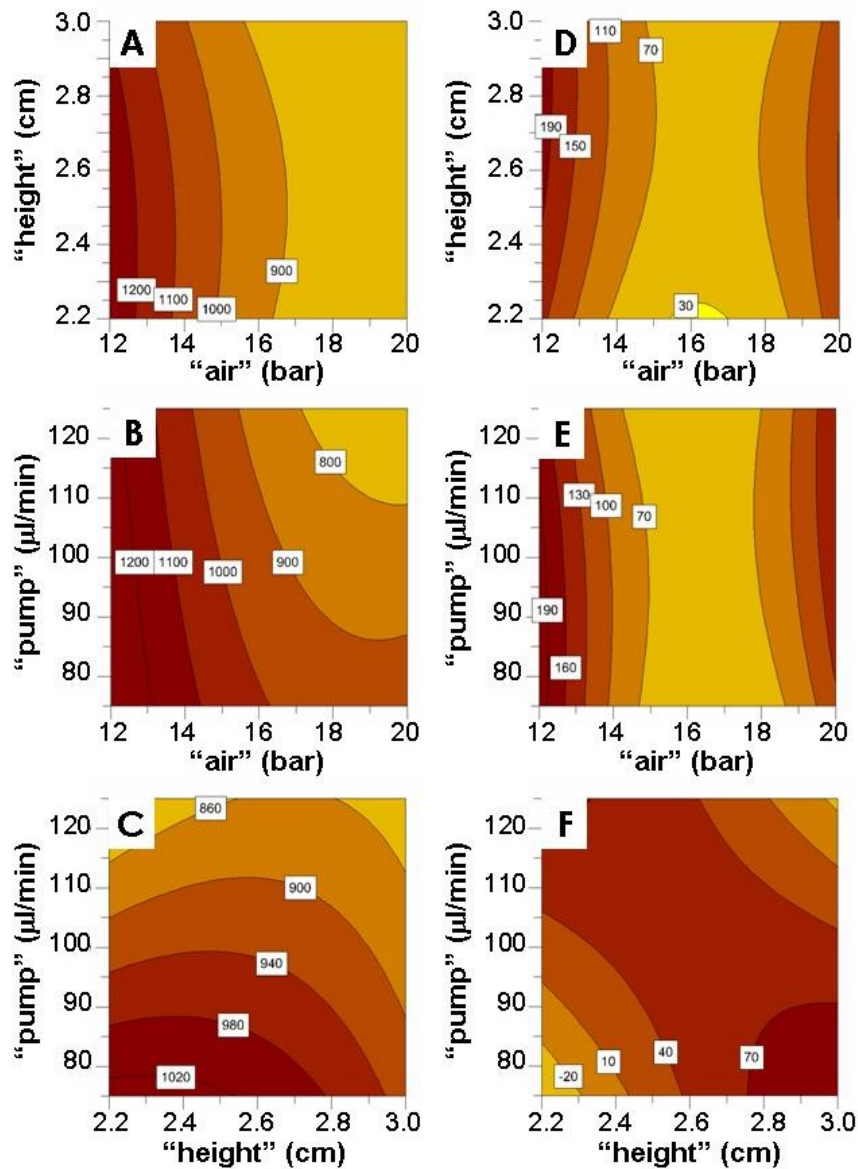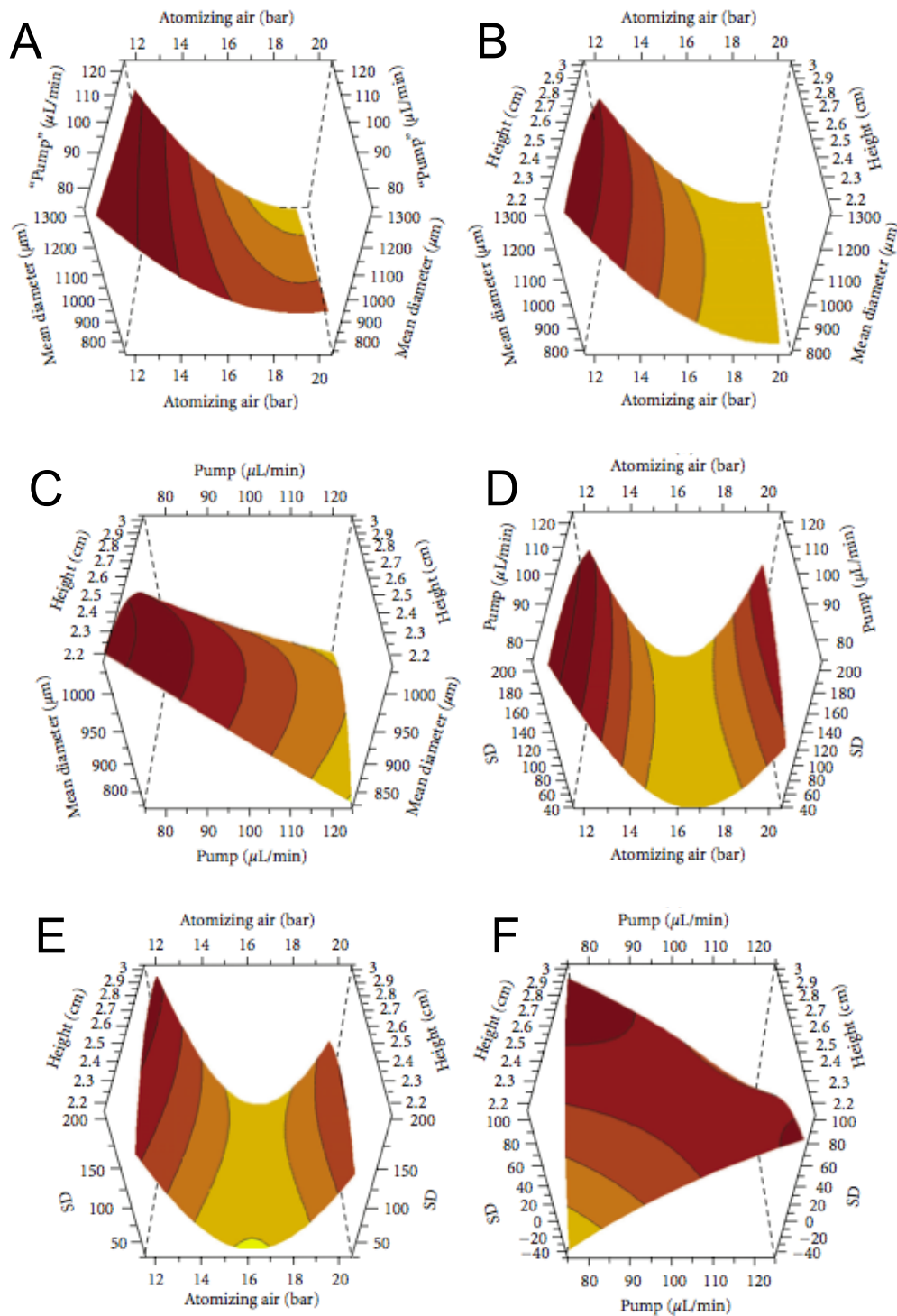
Fig. 9.
DoE analysis for the production of alginate microbeads containing IB3-1 cells. Response surface plots of the responses: "size" (A-C) and "SD" (D-F).

Viability of Encapsulated IB3-1 Cells.

A crucial issue that should be always investigated in the case of embedding/seeding protocols for cell scaffolding concerns the effect of the

encapsulation procedure on viability of cells. For this purpose, the viability of encapsulated cells in alginate beads was determined by the live/dead test. Beads were incubated with Calcein-AM (a marker of living cells; fluorescent signal was monitored using 485 nm excitation wavelength and 530 nm emission wavelength) and with PI (a marker of cell death; excitation, 535nm; emission, >610 nm). The observation of the fluorescent images recorded immediately after the encapsulation procedure at the typical excitation wavelengths (Figure 10) indicated that the cells were highly viable (>95%) after different lengths of culture time (up to 7 days).
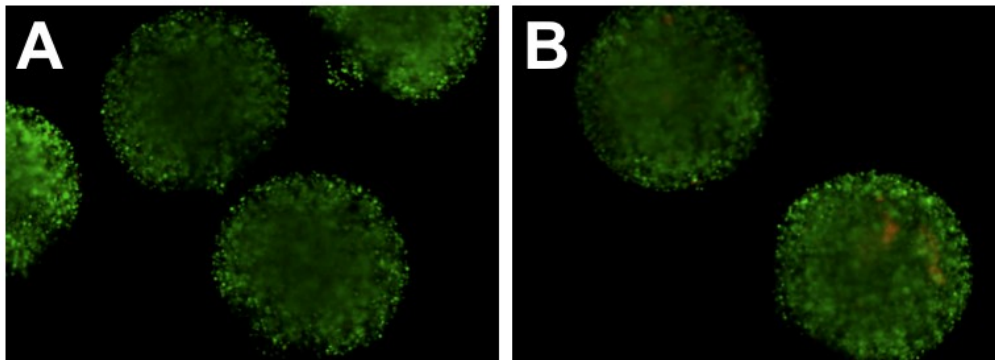

Fig. 10. Fluorescence photomicrographs of alginate microbeads containing IB3-1 cells after 1 (A) and 7 days (C) of cell culture. Fluorescence photomicrographs were taken after double staining with Calcein-AM and propidium bromide.

Increase of Accumulation of IL-8 and IL-6 mRNAs in Encapsulated IB3-1 Cells Treated with TNF-α

Free and encapsulated IB3-1 cystic fibrosis cells were treated for 24 hours in the presence of 80 ng/mL of TNF-α. After this treatment, microcapsules were separated from the culture medium, washed, fused and entrapped cells isolated, washed, and finally lysed for RNA isolation. RT-PCR was performed using primers amplifying IL-8, IL-6, and GAPDH RNA sequences. The results obtained are reported in Figure 11(A), which clearly indicates that encapsulation has only minor effects on IL-8 mRNA accumulation. Consistently, in TNF-α-treated cells (closed bars) the levels of IL-6 and IL- 8 mRNA sequences are higher than those usually found in TNF-α untreated IB3-1 cells (open bars). Moreover, TNF-α induction of IL-6 (Figure 11 A, left side of the panel) and IL-8 (Figure 11 A, right side of the panel) gene

expression is clearly evident, both in free (-) and encapsulated (CAPS) IB3- 1 cells, strongly indicating that (a) TNF-α transfer within the alginate microbeads takes place with high efficiency and (b) its expected effects on gene expression is detectable, mimicking the well-known effect of TNF-α on free IB3-1 cells. In order to determine whether the increases of IL-6 and IL-8 mRNA direct synthesis of the respective proteins and their secretion outside the alginate microbeads, Bio-Plex analysis on the medium was performed.

Increased Release of IL-6 and IL-8 outside the Microcapsules Entrapping IB3-1 Cells Treated with TNF-α

Free and encapsulated IB3-1 cystic fibrosis cells were treated for 24 hours in the presence of 80 ng/mL of TNF-α. After this treatment, microcapsules were separated from the culture medium, which was analysed for content of IL-6 and IL- 8. Figure 11 B shows that minor differences in the amounts of secreted IL-6 and IL-8 protein levels are present when mediums isolated from cultures of free (-) and encapsulated (CAPS) IB3-1 cells are compared. On the contrary, when release by TNF-α-treated cells is compared to that of control IB3-1 cells (compare black to white histograms of Figure 11 B), the levels of IL-6 and IL-8 increase significantly both in free (-) and in encapsulated (CAPS) IB3-1 cells. The TNF-α-mediated fold induction of IL-8 release was found similar in free and encapsulated IB3-1 cells (Figure 11 B, right side of the panel), while in the case of IL-6, the fold increase was more evident in free IB3-1 cells (Figure 11 B, left side of the panel). This observation was reproducibly obtained in several experiments.

2.2.1.3. Discussion

The first aim of the current work was to verify if IB3- 1 cystic fibrosis cells could be encapsulated in alginate microbeads and to test if the immobilized cells could be induced to express proinflammatory genes, after treatment with TNF-α (see the scheme of the experiment shown in Figure 6).
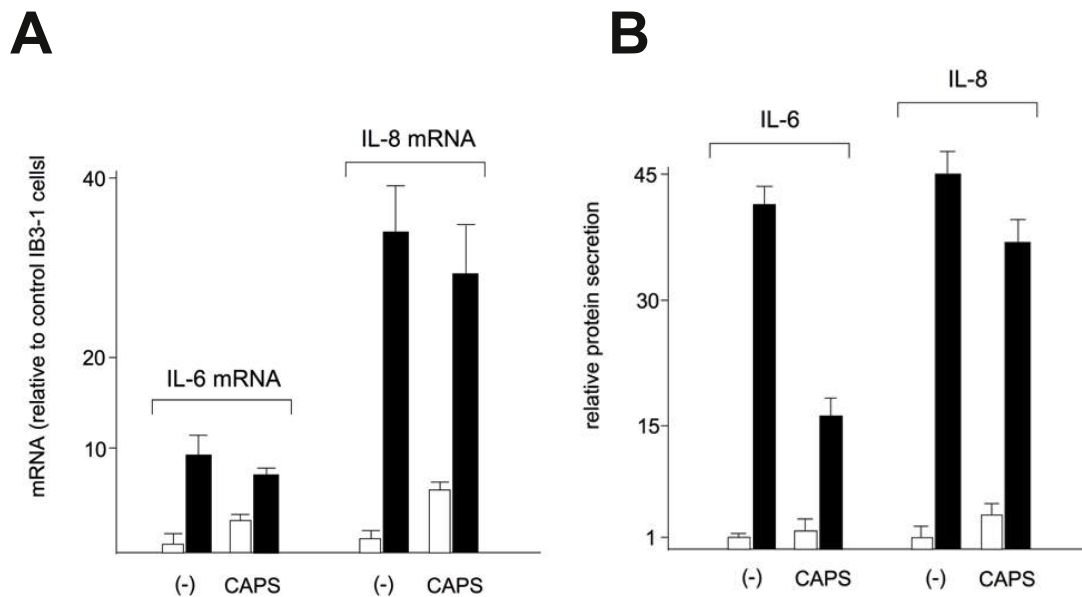
Fig. 11. Analysis of the mRNA levels (A) and release (B) of interleukins 6 and 8 (IL-6, IL-8) by IB3-1 cells. Data are referred to control free cells growing as monolayer (-) and cells encapsulated in alginate microbeads (CAPS). Both free and encapsulated cells were cultured for 24 hours, in the absence (open bars) or in the presence of TNF-α (80 ng/mL) (closed bars). Data represent the average ±SD (N = 3).

In this respect, we demonstrated that IB3-1 cells can be efficiently encapsulated in microbeads that posses a number of specific requisites, such as spherical shape, very narrow size distribution, good mechanical stability, and biocompatibility, assuring cell viability and functions. Furthermore, by this technique, microparticles with different morphological characteristics can be prepared by changing the main experimental parameters, namely: nozzle-to-gelling bath distance, atomizing gas flow, alginate concentration and pumping rate.

The second aim of our experimental strategy was to verify whether TNF-α efficiently induces gene expression alterations in the encapsulated IB3-1 cells. The results obtained by RT-PCR analysis of RNA firmly demonstrate that (a) encapsulation induces only a limited increase of the basal IL-6 and IL-8 mRNA content, whereas (b) TNF- α stimulates a sharp increase of content of IL-6 and IL-8 mRNAs in both free and encapsulated IB3-1 cells. This latter result suggests that TNF-α efficiently diffuses through the alginate microbeads matrix. Therefore, alginate microbeads could be suitably employed in experiments, in which the target cells are grown in a

physically separated, immunoisolated environment, being accessible to externally added soluble proteins possibly causing alterations of gene expression.

However, in order to propose the described system as an experimental model to study cystic fibrosis, further experiments are required to control several unmet issues, including the fact that the encapsulated cells are non adherent, are not polarized and are unable to bind to bacteria (such as *Pseudomonas aeruginosa*) and immune cells inducing responses very different from those of soluble mediators (i.e. TNF-α). These are several parameters playing important roles in modification of gene expression in cystic fibrosis cells [10-11]. In this respect, we like to underline that the alginate-based encapsulation strategy can be further improved. For instance, in our laboratories, experiments in progress are aimed to the production of composites multifunctional microbeads simultaneously containing (a) living cells and (b) an extracellular matrix component, namely, a particulate ECM, that is able to modulate cell adhesion, migration, and polarization. In addition, co-encapsulation of epithelial cells and effector cells is technically feasible and might be explored.

Finally, the third aim of our experimental strategy was to verify whether TNF-α treatment leads to increased production and release of IL-6 and IL-8, confirming the permeability of the alginate microbeads membrane to these proteins. The results obtained firmly demonstrate that IL-6 and IL-8 release outside the microbeads increases in IB3-1 encapsulated cell cultures strongly suggesting that the alginate microbeads membrane is permeable to these proteins. However, while the TNF-α-mediated fold induction of IL-8 release was found similar in free and encapsulated IB3-1 cells, we reproducibly noted that in the case of IL-6 the fold increase was more evident in free cells than that in encapsulated IB3-1 cells. This might be due to a differential intracellular synthesis of IL-6 and IL-8 mRNAs or to a differential permeability of the capsule membranes to IL-6 and IL-8, or both. While additional experiments are required to explain this phenomenon, the possibility that the chemical composition of the microcapsule influences drug release

characteristics has been recently proposed by Jaya et al. and might be used to develop microbeads allowing selective releases [12].

In this respect, the use of cell-based drug delivery has been proposed as a very promising application of encapsulation of cells relevant for production of therapeutic proteins. For instance, erythropoietin-secreting cells immobilized in microcapsules have been described by Murua et al. [13]. The applications in biomedicine of this strategy are very high, in consideration of the importance of erythropoietin for several biological functions, and the pathological conditions due to its disregulation. Similarly, continuous production of IL-12 by microencapsulated engineered cells modified with murine interleukine-12 (mIL-12) gene has been reported by Zheng et al. [14]. The microencapsulated cells have a significant therapeutic effect on experimental colon tumors by activating antitumor immune responses in vivo. These and similar papers support the concept that microencapsulated and genetically engineered cells may be an extremely versatile tool for cellular therapy [15].

In our case, we demonstrate that microencapsulated cells can be induced to produce IL-8 in the presence of high levels of TNF-α. This result allows hypothesizing that the experimental strategy outlined permits the development of a "cell-based microparticle sensor" releasing specific proteins (selective release can be improved by changing the chemical composition of the microcapsules) upon stimulation. This might be of great interest in biomedicine. Bioencapsulation has been indeed shown to be efficacious in mimicking the cell's natural environment and thereby improves the efficiency of production of different metabolites and therapeutic agents, while protecting the cells from larger proteins (e.g., antibodies) and immune cells [15].

2.3. Cell encapsulation by a vibrating-nozzle procedure

In order to produce large amount of alginate based microparticles, the cell embedding was also performed by an alternative procedure, based on the optimization of a vibrating-nozzle encapsulator procedure (EncapBioSystems Inc.), the scheme of which is reported in Fig. 12 [16].
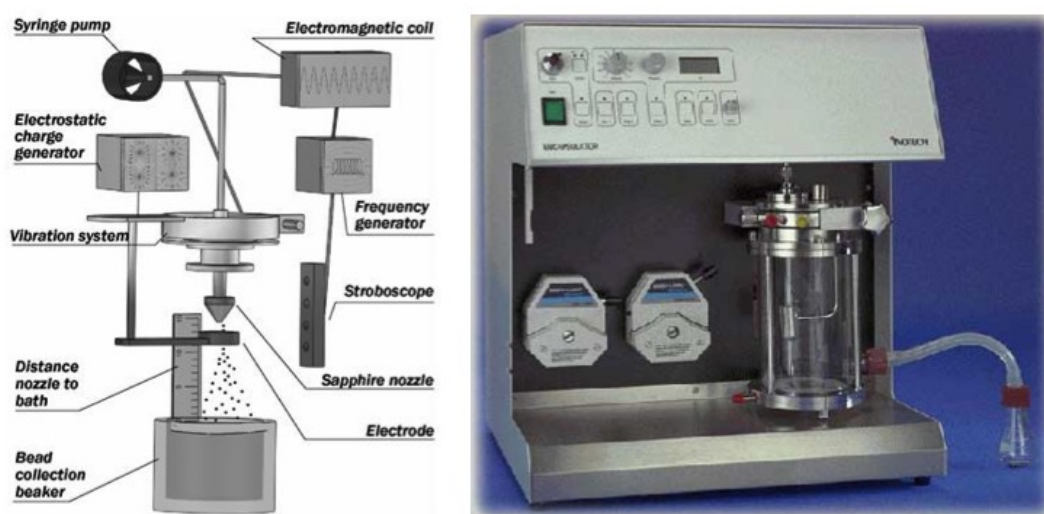

Fig. 12. Schematic representation (left) and photograph (right) of the encapsulation device based on a vibrating nozzle, commercialized by EncapBioSystems Inc.

The Encapsulator from EncapBioSystems Inc. is a vibrating nozzle device capable of producing microcapsules under sterile working conditions. The bead formation is based on the fact that a laminar liquid flow is broken up into equal beads, if it is vibrated at an optimal frequency.

This procedure is carried out by the following steps: 1. the cell to be encapsulated are mixed with the encapsulating polymer (alginate); 2. the alginate/cell suspension is forced into the pulsation chamber (usually by a syringe pump) and then passes through a precisely drilled nozzle (with an internal diameter usually ranging from of 200 to 600 mm); 3. the alginate/cell suspension separates into equal size droplets, that later pass through an electrical field between the nozzle and the electrode resulting in a surface charge. The result is that alginate drops in the liquid jet are highly negatively charged at their surface. As consequence, the charged droplets are deflected

from the vertical resulting in the drops impacting the surface of the gelation solution over a defined area. This device enables the formation of small diameter (<300 mm) beads since the linear velocity of the drops is such that, in the absence of the electrostatic device, the distance between drops is approximately one bead diameter. If all such beads fell vertically, they would impact the hardening solution at the same position and thus impact each other, creating no spherical, coalescent drops. Depending on several variables, 50–3000 beads are generated per second.

2.3.1. Application of a vibrating-nozzle procedure to Mesenchymal stem cells

Mesenchymal stem cells (MSCs), which have largely been investigated, are functionally defined as non-hematopoietic multipotential cells, able to self-renew and to highly proliferate [17].

Many studies suggest that MSCs may differentiate toward cells of different lineages, including chondrocytes, adipocytes, osteocytes, miocytes, neurons, and tenocytes [18-24]. Because of their peculiar characteristics, MSCs are considered to be very important for several applications in the field of regenerative medicine, including the development of cell based therapies and tissue repair procedures [25].

Different adult human tissues have been considered as MSC sources, including bone marrow, trabecular bone, adipose tissue, peripheral blood, synovium, skeletal muscle, dental pulp, and periodontal ligament [26]. Although bone marrow still represents the main and most investigated source of adult MSCs, the isolation and use of these cells still present some drawbacks. For instance, the number of MSCs found in bone marrow decrease progressively starting at age 17, and the harvesting techniques are invasive, often causing severe infections, bleeding, and chronic pain for donors. Looking for alternative MSC sources, fetal tissues, extraembryonic tissues such as placenta, and amniotic fluid, umbilical cord blood and stroma have recently been considered [27-29]. Umbilical cord, due to the unique morphological properties, represents an interesting alternate source for

MSCs, especially if compared to umbilical cord blood. Umbilical cord, usually weighing 40 g and spanning between 60 and 65 cm in length, contains a special primitive connective tissue called Wharton's jelly. This jelly acts as a protective tissue for vessels and contains into its stromal compartment cells with specific mesenchymal characteristics, called Wharton's jelly MSCs (WJMSCs) [30]. Therefore, Wharton's jelly can be an ideal, unique, easily accessible, and uncontroversial source for early MSCs due to the simple collection procedure once umbilical cord is routinely discharged at parturition. It has recently been described that WJMSCs are able to support long-term maintenance of hematopoietic stem cells [31]. In this respect, it is reasonable that WJMSCs, like MSCs collected from other tissues, can release many soluble molecules, including interleukins, chemokines, and many growth factors. The ability to self-renew and to differentiate into several cell types makes the use of MSCs particularly attractive for the development of innovative therapeutic strategies aimed at repairing and replacing damaged tissues and makes them a very promising cell source for tissue engineering applications.

Nevertheless, several factors still hurdle the extensive clinical use of cell-based therapy. The protection of implanted cells from the host's immune response is of primary importance. To solve this problem, WJMSCs human umbilical cord isolated, here presented, were immobilized in barium (Ba)–alginate microbeads by a vibrating nozzle approach. With respect to encapsulation/immobilization procedure for MSCs, Langer and co-workers have reported a methodology to enhance the vascular differentiation of human embryonic stem cells by encapsulating the cells in a bioactive scaffold based on a photopolymerizable dextran hydrogels comprising either insoluble or soluble endothelial growth factors [32]. Moreover, a protocol based on the encapsulation of cells in calcium alginate hydrogels and aimed at maintaining human embryonic stem cell in culture, for a period of up to 260 days, without exposure to animal cells, has recently been published. Finally, alginate beads were also tested to study the chondrogenesis of human MSCs [33].

2.3.1.1. Materials and methods

WJMSCs: isolation procedure and culture conditions

Human umbilical cords (all from natural deliveries) were collected after mothers' consent and approval of the Ethics Committee of the University of Ferrara and S. Anna Hospital. Harvesting procedures of Wharton's jelly from umbilical cord were conducted in full accordance with the Declaration of Helsinki as adopted by the 18th World Medical Assembly in 1964 and successively revised in Edinburgh (2000) and the Good Clinical Practice guidelines. Cords were processed within 4h, and stored at 48C in sterile saline until use. Typically, the cord was rinsed several times with sterile phosphate-buffered saline (PBS) before processing and was cut into pieces (2–4 cm in length). Blood and clots were drained from vessels with PBS to avoid any contamination. Single pieces were dissected, first separating the epithelium of each section along its length, to expose the underlying Wharton's jelly. Later, cord vessels (the two arteries and the vein) were pulled away without opening them. The soft gel tissue was then finely chopped. The same tissue (2–3 mm^2 pieces) was placed directly into a 75-cm^2 flask for culture expansion in 10% fetal calf serum (Euroclone S.p.A., Milan, Italy)–containing Dulbecco's modified Eagle's medium low-glucose medium supplemented with antibiotics (penicillin 100 mg/mL and streptomycin 10 mg/mL) at 37°C in a humidified atmosphere of 5% CO_2. After 5–7 days, the culture medium was removed and thereafter changed twice a week. At a about 70–80% confluence, cells were scraped off by 0.05% trypsin/ethylene diamine tetraacetic acid (EDTA) (Gibco, Grand Island, NE) (2min), washed, counted by hemocytometric analysis, assayed for viability, and thereafter used for further in vitro experiments or for encapsulation procedures.

Flow cytometric analysis

The WJMSCs were analysed for expression of MSC surface marker molecules, by direct immunofluorescent staining, as reported in the literature [34]. Briefly, cell pellets were resuspended in PBS and incubated with

fluorescein iso- thiocyanate (FITC)– or phycoerythrin (PE)–conjugated mouse anti-human antibodies CD45-PE, CD34-FITC, CD90- FITC, CD105-PE, CD44-FITC, and CD29-PE (DakoCytomation; Dako, Denmark) for 15min at 4°C. Monoclonal antibodies with no specificity were used as negative control. Antibody-treated cells were then washed with PBS and spinned down. Cell pellets were resuspended in 400mL of PBS and analyzed by FACS Scan (Becton Dickinson, NJ). For each sample, 20,000 events were acquired and analyzed using the CellQuest software (Becton Dickinson European HQ, Erembodegem Aalst, Belgium).

Encapsulation of WJMSCs

Monodisperse alginate beads containing WJMSCs were prepared using the encapsulation device based on a vibrating nozzle according, to the experimental procedure previously described [16]. The encapsulator is a 2-L glass reaction vessel with stainless steel top and bottom plates. The top plate contains a feed-line connected to a syringe and a vibrating nozzle. A nozzle with an internal diameter of 300 mm was used. The flow of alginate to the nozzle is achieved by a precision syringe pump. The production of WJMSC-filled alginate microcapsules was optimized by changing the following experimental parameters: vibrational frequency (freq), vibrational amplitude (amp), alginate pumping rate (pump), and distance between the nozzle and the surface of the gelling bath (height) (see Table 2). Before encapsulation, WJMSCs were suspended in a 1.5% (w/v) aqueous solution of highly purified sodium alginate (Stern Italia, Milano, Italy) at a concentration of $8–12 \times 10^6$ cells/mL. The generated microdroplets were dropped into an isotonic barium chloride solution (1.2%; w/v); after gelation (3 min), the microbeads were washed twice with saline and cultured in 10% fetal calf serum (Euroclone S.p.A.)–containing Dulbecco's modified Eagle's medium low-glucose medium supplemented with antibiotics (penicillin 100 mg/mL and streptomycin 10 mg/mL) at 37°C in an humidified atmosphere of 5% CO_2. The dimensional analysis, experimental design and statistical analysis were performed as previously reported in paragraph 2.2.1.1.

Table 2. Production of alginate microcapsules by vibrational encapsulation procedure: the investigated experimental parameters and their range of variation.

Parameter	Abbreviation	Meaning	Range
frequency	freq	frequency of the vibration of the nozzle	100.0-140.0 hz
amplitude	amp	amplitude of vibration of the nozzle	1.0-6.0 mm
pump	pump	polymer pumping rate	7.5-9.5 mL/min
height	height	distance from nozzle to surface of gelling bath	100.0-140.0 mm

Viability analysis of WJMSCs

Before and after encapsulation, the viability of the cells was analysed both by colorimetric assay with MTT (thiazolyl blue) and by double staining with propidium iodide (PI) and Calcein-AM according to the manufacturer's instructions. The MTT assay, based on the conversion of the yellow tetrazolium salt MTT to purple formazan crystals by metabolically active cells, provides a quantitative determination of viable cells [35]. After 3, 6, and 9 days of culture 200 mL of MTT was added to each well of beads, and the plate was incubated at 37°C. After 2h the MTT crystals were solubilized with 50% dimethyl formamide; after 24 h spectrophotometric absorbance of each sample was measured at 570 nm. For the PI and Calcein-AM analysis, cells were viewed under a fluorescence microscope (Nikon, Optiphot-2; Nikon Corporation, Tokyo, Japan) using the filter block for fluorescein. Dead cells stained red, while viable ones appeared green.

Induction and evaluation of osteogenic differentiation

For the analysis of osteogenic differentiation, both free WJMSCs (growing in monolayer) and microbead-entrapped cells were incubated in human MSC osteogenic differentiation medium (Lonza, Walkersville, MD) for 21 days. The extracellular matrix composition was analysed by Fourier transform infrared spectroscopy. Cell layers were collected in ammoniated water (50mM ammonium bicarbonate, pH 8.0), lyophilized, and analysed by FT-IR Spectrometer Perkin Elmer, Spectrum 100 (Perkin Elmer, MA, USA). Absorption spectra were collected from 4000 to 600cm^{-1}. After 21 days of incubation in standard and osteogenic conditions, microbeads were assayed for alkaline phosphatase (ALP) activity. Microbeads were incubated at 37°C in a 50 mM

EDTA solution (pH 7.00) for 2 min to dissolve the Ba–alginate microbeads and obtain the free cells. The cells were lysed with 300μL of 0.2% Triton X-100. ALP activity was assayed by measuring, after 30min of incubation at 37°C, the conversion p-nitrophenylphosphate to p-nitrophenol, using an enzyme-linked immunosorbent assay reader at 405 nm wavelength. ALP activity was normalized to total cellular proteins, determined by the Bradford protein assay protocol and expressed as U/mg of protein. One unit was defined as the amount of enzyme that hydrolyzes 1 mmol/min of p-nitrophenylphosphate. For Alizarin Red S staining, free WJMSCs (growing in monolayer) and microbead-entrapped cells were fixed and then stained with 40 mM Alizarin Red S solution (pH 4.2) at room temperature for 10 min. Samples were then rinsed five times with distilled water and washed three times in PBS on an orbital shaker at 40 rpm for 5 min each to reduce nonspecific binding. The stained matrices were microphotographed by an optical microscope (Nikon, Optiphot- 2; Nikon Corporation, Tokyo, Japan). For real-time polymerase chain reaction (PCR) analysis, Ba–alginate microbeads were dissolved as previously reported, and total RNA was isolated from the WJMSC-free cells using Total RNA Isolation system (Promega, WI). Two micrograms of total RNA was reverse transcribed with the Improm-II RT System (Promega). mRNA of target genes was quantified by real-time PCR using the ABI Prism 7700 system and TaqMan probes 50AACCCAGAAG GCACAGACAGAAGCT30 for RUNX-2 (Applied Biosystems, CA). PCR was carried out in a final volume of 25 μL. After 10 min preincubation at 95°C (denaturation) and 1 min at 60°C (annealing/elongation), the mRNA levels were corrected for glyceraldehyde 3-phosphate dehydrogenase mRNA levels (reference gene) and normalized to a calibrator sample (control cells).

Determination of WJMSC secretory pattern by Bio-Plex analysis

After 72 h of in vitro cell culture, the medium from WJMSCs growing as monolayer and embedded in Ba– alginate microbeads was collected and analyzed for a set of selected proteins. To compare and normalize the data of adherent and encapsulated WJMSCs, the microbeads were washed twice

with PBS before the analyses and incubated at 37°C, for 15 min, with 500 μL of 50 mM EDTA (Sigma) in PBS buffer. EDTA was then neutralized with additional 10 mL PBS, and cells were collected by centrifuging at 400 g for 15 min. Pellets obtained from WJMSCs growing as monolayer and embedded in Ba–alginate microbeads were lysed with 50mL buffer (NaCl 150mM; Tris-HCl pH 7.4 20mM; EDTA 1 mM; EGTA 1 mM; Triton X-100 1%; Na_3VO_4 0.1 mM; PMSF 1 mM; PIC 0.1% v/v). About 10 μL of each sample was tested with the Bradford method to determine proteins content. Concentrations of interferon-alpha 2 (IFN-α 2), interleukin-1alpha (IL-1 α), IL-2 receptor α , IL-3, IL-12 (p40), IL-16, IL-18, CTACK, GRO-α , hepatocyte growth factor (HGF), ICAM-1, LIF, MCP3, M-CSF, MIF, MIG, beta- nerve growth factor, stem cell factor, stem cell growth factor- beta (SCGF-β), SDF-1, tumor necrosis factor-beta, TRAIL, and VCAM-1 were simultaneously evaluated using a commercially available multiplex bead–based sandwich immunoassay kit (Human 23-plex; Bio-Rad Laboratories). Bio-Plex analysis was performed following the manufacturer's instructions. About 23 distinct sets of fluorescently dyed beads loaded with capture monoclonal antibodies, specific for each cytokine, were used. Secretion and standard samples (50 μL/well) were incubated with 50μL of premixed bead sets in a prewet 96-well microtiter plate. After incubation and washing, 25μL of fluorescent detection antibody mixture was added and left to react for 30 min under gentle shaking; samples were then washed and resuspended in the assay buffer. Standard calibration curves for each protein were used, ranging from 2 to 32000 pg/mL; the minimum detectable dose was 2 pg/mL. The formation of the different immunocomplexes was measured by the Bio-Plex Protein Array System (Bio-Rad Laboratories). A 50 μL volume sample was withdrawn from each well, and the fluorescent signal of a minimum of 100 beads per region (chemokine/cytokine) was measured. To compare directly secretive con- tent of adherent and encapsulated WJMSCs, all values were normalized with respect to the total protein amount.

Data analysis and statistics. Statistical analysis was performed by one-way

analysis of variance followed by the Student's t-test. A p-value <0.05 was considered statistically significant. Cytokine analysis was performed with Bio-Plex Manager software version 3.0 (Bio-Rad Laboratories). Standard levels between 70% and 130% of the expected values were used. In general, at least five standards were accepted and used to establish standard curves following a five-parameter logistic regression model. Sample concentrations were immediately interpolated from the standard curves. Values were expressed as pg/mL+ standard deviation.

2.3.1.2. Results

Isolation and characterization of WJMSCs

As a source of human MSCs, solely Wharton's jelly was used instead of the whole cord (easier and faster to treat); the choice was made with the aim of isolating a relatively homogeneous cell population, possibly avoiding any epithelial cell contamination. For the isolation of WJMSCs, a slightly modified version of a previously published procedure was used [36]. Can and Karahuseyinoglu have recently reported in a review article (dealing with the umbilical cord stroma as source for stem cells) that a collagenase treatment is critically important, since there is always a risk of over digestion of the cellular external lamina, causing the prevention of cell adhesion to the culture substrate after isolation. In this respect, collagenase, trypsin, and hyal-uronidase treatments were omitted, in agreement with other investigators, observing that skipping the enzymatic digestion treatment favours cell adhesion and viability [37].

When in vitro cultured, the primary cells, isolated from Wharton's jelly, displayed an MSC-like phenotype. After 3 days of culture, the WJMSCs formed adherent colonies, reaching confluence after 10–14 days. High percentage of cells appeared viable, as demonstrated by Calcein-AM stain (Fig. 13 A), and displayed a spindle shape resembling fibroblasts (Fig. 13 B, C). The immunophenotypical profile of WJMSCs was determined by flow cytometric analysis (Fig. 13 D–I). It should be underlined that up to now there

are the MSC-specific markers are unknow. Nevertheless, according to previous studies [38,39], cell surface markers such as CD90 (Thy-1), CD29 (β-1 integrin), CD44 (hyaluronan receptor), and CD105 (SH2, endoglin) were analysed to attribute an MSC-like immunophenotype. Flow cytometry showed that, since first passage, the WJMSCs expressed these markers (Fig. 13 D–G).
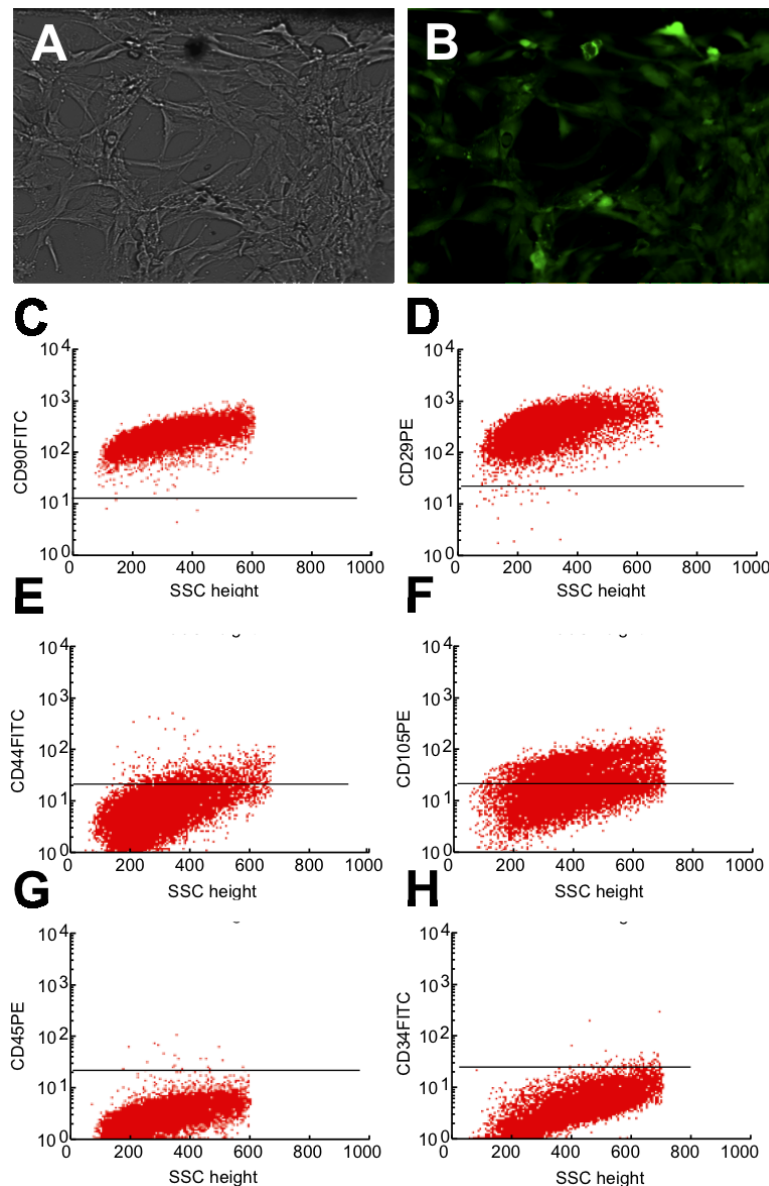

Fig. 13. Phenotype characterization of Wharton's jelly mesenchymal stem cell (WJMSC) monolayers. (A) Representative optical and fluorescence photomicrographs of the WJMSC monolayer after Calcein-AM staining (magnification, 20X). Flow cytometric histograms showing the immunophenotypic characterization of WJMSCs. The experiments were conducted using direct immunofluorescence staining with the indicated fluorescein isothiocyanate (FITC)– or phycoerythrin (PE)–conjugated mouse anti-human antibodies.

The hematopoietic marker CD45 and the hematopoi-etic/endothelial marker CD34 were not detectable in these cells (Fig. 13 H, I), indicating that WJMSCs were not contaminated with cells of hematopoietic or endothelial origin. Rigorous identification of MSCs requires demonstration of their capability to differentiate along specific mesenchymal lineages when induced to do so. In this context, we are interested in demonstrating the ability of WJMSCs to differentiate into osteoblasts. The osteogenic differentiation of expanded WJMSCs was induced by the addition of dexamethasone, b-glycerophosphate, and ascorbate, and was assessed after 21 days by monitoring the production of mineralized extracellular matrix, as a marker for terminally differentiated MSCs into osteoblasts. As shown in Figure 14, we detected the presence of calcium by Alizarin red staining, and the presence of apatite by the Fourier transform infrared spectroscopic assessment of mineral content from the induced WJMSC.
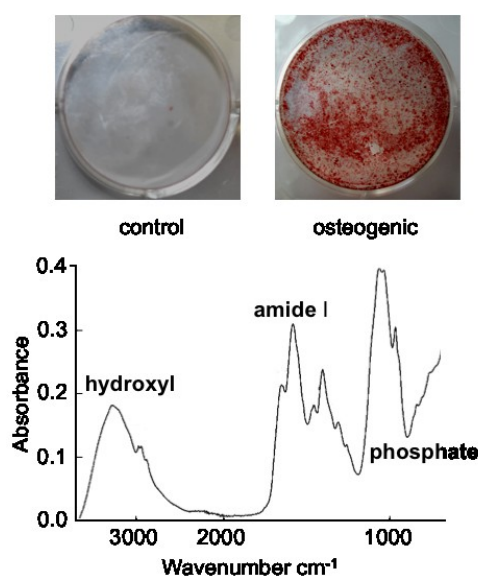

Fig. 14. Alizarin red staining (control WJMSCs, left; differentiated WJMSCs, right) and the Fourier transform infrared (FTIR) spectrum of the mineralized extracellular matrix containing hydroxyapatite matrix formed by WJMSCs after 21 days' culture in osteogenic conditions. The typical spectrum with mineral (phosphate) and matrix (amide I) absorbance is shown.

Encapsulation of WJMSCs in alginate microbeads

WJMSCs were embedded into alginate microbeads by the encapsulation device based on a vibrating-nozzle (see scheme in Fig. 12) under sterile conditions. Firstly, a classical intuitive approach COST (Changing One

Separate factor a Time) was used to define the experimental set up, including the selection of the crucial experimental parameters. The approach was chosen in order to evaluate which factor(s) could mostly affect the morphology of the produced alginate microbeads in terms of general geometry, surface characteristics and dimensions. Following the above procedure, only one experimental parameter was varied at a time (see Table 2), while all the others were maintained constant. Experiments were performed, changing the following parameters: frequency of vibration (freq), amplitude of vibration (amp), polymer pumping rate (pump) and distance between the nozzle and the gelling bath (height) (Fig. 15). The frequency was calculated from knowledge of the alginate solution viscosity for the nozzle diameter used, to obtain the desired microbeads size and morphology (mean diameter comprised between 550 and 650 µm with a spherical shape) [16]. The vibrating frequency of the nozzle was varied from 100.0 to 200.0 Hertz while the rate of polymer pumping was investigated in the range 7.5-9.5 (mL/min) (see Table 3). The investigation of these parameters revealed that increasing both factors led to a decrease of particle size, but if the vibrating frequency was set too high (>200.0 Hertz) a progressive number of coalescences (formation of clusters of microbeads partially fused together) was detectable in the microbead population. The amplitude of the vibration applied to the nozzle (varied in a range from 1.0 to 6.0 mm) had only a slight effect on the microbead characteristics such as size, sphericity and presence of coalescences. On the contrary, the distance between the nozzle and the gelling bath (range 100.0-140.0 mm) had a great effect on the microbead morphology. In fact, a distance of 100.0 or 120.0 mm caused the formation of microbeads with an elliptic shape (formation of tails). Considering the results of this set of experiments (summarized in Table 3), it can be concluded that among the 4 different experimental variables, only the amplitude of the vibration has minor effect on the microbead formation, while all the others exert significant morphological and dimensional changes in the alginate beads.

Table 3. Analysis of the effect of experimental parameters on the characteristics of Wharton's Jelly Mesenchymal Stem Cell–filled alginate microbeads.

Frequency (Hz)	Amplitude (mm)	Pump (mL/min)	Height (mm)	Morphology
Freq				
100	1	8.5	140	wrinkled surface, large number of tails and colascences.
150	1	8.5	140	smooth surface, some tails and colascences
200	1	8.5	140	wrinkled surface and tails and colascences
Amp				
150	1	8.5	140	smooth surface and some tails and colascences
150	3	8.5	140	wrinkled surface and large number of tails and colascences
150	6	8.5	140	wrinkled surface and tails and colascences
Pump				
150	1	7.5	140	wrinkled surface and large number of tails and colascences
150	1	8.5	140	smooth surface and some tails and colascences
150	1	9.5	140	wrinkled surface and tails and colascences
Height				
150	1	8.5	100	irregular shape
150	1	8.5	120	irregular shape
150	1	8.5	140	regular shape and smooth surface , some tails
Selected				
150	1	8.5	140	regular shape and smooth surface

The morphological characteristics of microcapsules were assessed on at least 200 microcapsules/batch, considering the presence of (a) tails, (b) coalescences, and (c) the surface characteristic. All the reported microbeads were prepared with an alginate concentration of 1.5% (w/v). Data represent the average of three independent determinations on different microbead batches.

The microbeads with the best morphology (Fig. 15 A) were produced by the following set up: a frequency of 150 Hz, an amplitude of 1.0 mm, a pump flow rate of 8.5 mL/min and an height of 140.0 mm.
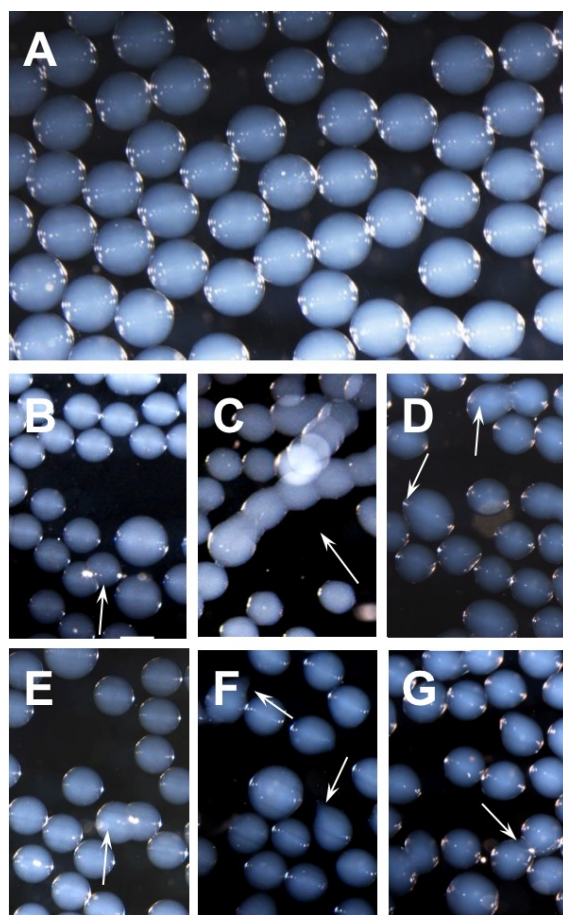
Fig. 15. Optical photomicrographs of empty alginate microbeads prepared by the vibrational encapsulator. Effect of different parameters on microcapsules characteristics. In panel A are depicted the microcapsules prepared using the optimized parameters (see Table 2). Panels B-C effect of the vibrational frequency, B: 100 hz, C: 200 hz; panels D-E: effect of the pump, D: 7.5 mL/min, E: 9.5 mL/min; panels F-G: effect of the height, F: 100 mm, G: 200 mm. Arrows indicate partially fused microcapsules or microcapsules showing tails or irregular morphology.

Effect of alginate concentration on microcapsule characteristics

Once the instrumental set up was achieved, we focused our attention on another important experimental parameter: the concentration of alginate solution. Different percentages were tested, ranging from 0.5 to 3.5% (w/v) and the effect on the production of microbeads was considered as well. At first observation, it should be mentioned that, using the automated vibrating nozzle instrument, we succeeded in obtaining microbeads using alginate concentration up to 2.0% (w/v). On the contrary, using higher concentrations of alginate (>2.0%, w/v), the resulting solution was too viscous to be efficiently converted in microdroplets. Samples of microbeads produced with

an alginate concentration of 0.5, 1.0, 1.5 and 2.0% were analysed for morphology, size and size distribution. Microbeads produced with an alginate concentration comprised between 1.0-2.0% (w/v) were spherical in shape and characterized by a smooth surface. Lowering the alginate concentration down to 0.5% (w/v) caused partial breaking of beads resulting in particles with an irregular shape. This behaviour was attributed to the mechanical stress caused by the landing in the hardening barium chloride solution. Moreover, at the same concentration, some coalescences were detectable. We obtained alginate microbeads with a smaller mean diameter and homogenous dimensional distribution using a polymer concentration of 1.5% (w/v). Increasing the alginate concentration up to 2% (w/v), the size distribution became broader and the mean diameter increased from 630 (in the case of an alginate concentration of 1.5%) to 645 µm (see dimensional distribution plots reported in Fig. 16 A, B). On the other hand, alginate microbeads prepared with lower polymer concentrations (0.5 and 1.0%, w/v) formed some coalescences (see Table 3), although the size distribution remained acceptably narrow.
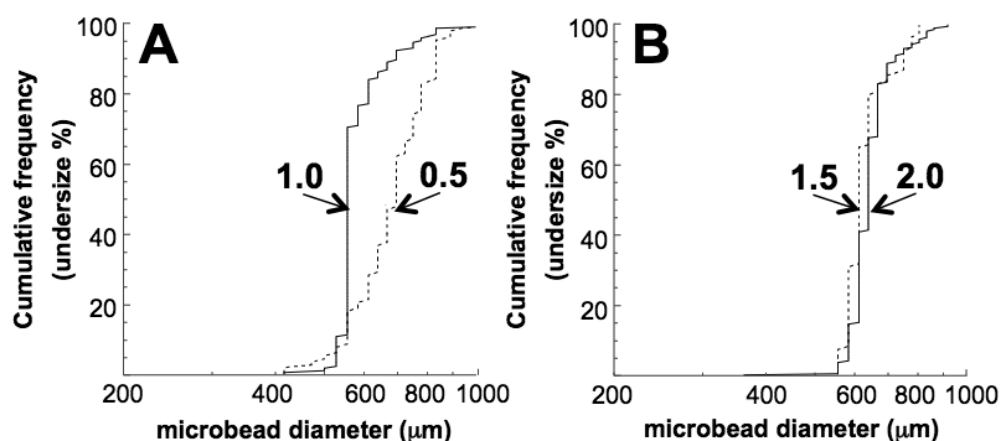

Fig. 16. Cumulative size distribution analysis (A, B) of microbeads prepared using the indicated percentage amounts of alginate. Samples were prepared with the selected experimental parameters reported in the last row of Table 3.

Encapsulation of WJMSCs in alginate microbeads: a DoE approach.

After performing the COST study, a "design of the experiments" (DoE) optimisation and a screening of the experimental parameters were also

conducted (chapter 2.2.1.1.)

The parameters frequency, pump and height were chosen as variables and tested at three levels. Therefore, in our case we selected 14 experiments by a randomized central composite face-centered design (CCF) which requires fewer trials together with three center points in order to have an estimation of the experimental error (Table 4).

Table 4. Experimental design matrix and results of doe (design of experiments) approach for alginate microbeads.

Factors			Responses	
Frequency (Hz)	Pump (mL/min)	Nozzle to bath (mm)	Tails (%)	Coalescences (%)
100.0	7.5	80.0	8.5	9.0
200.0	7.5	80.0	9.0	9.5
100.0	9.5	80.0	7.5	8.0
200.0	9.5	80.0	8.0	8.6
100.0	7.5	160.0	6.4	7.0
200.0	7.5	160.0	6.0	7.8
100.0	9.5	160.0	6.0	7.3
200.0	9.5	160.0	6.1	7.0
100.0	8.5	120.0	6.3	7.1
200.0	8.5	120.0	6.1	7.2
150.0	7.5	120.0	5.8	6.0
150.0	9.5	120.0	6.3	7.0
150.0	8.5	80.0	4.1	4.2
150.0	8.5	160.0	4.0	5.0
150.0	8.5	120.0	3.1	3.3
150.0	8.5	120.0	2.9	4.2
150.0	8.5	120.0	2.1	4.0

Data represent the average of three independent determinations.

By examining the results the main observation was that a change in height value from a low to a high level (80-160 mm) results in an increase of tail formation as well as of coalescences. On the other hand, the freq and pump parameters at high and low levels caused the increase of the both responses (see Table 4).

Three-dimensional graphs of the investigated factors are given in Fig. 17 showing the influence of factors on tails (panels A-C) and coalescences formation (panels D-F). After investigation of the factor influence, the validity and the significance of the model was estimated by analysis of variance (ANOVA). All the data obtained fit well the model determining a good reproducibility of the studied model. We get a large regression coefficient R^2 that is a necessary condition for a validity model with a significant power of prediction of the model Q^2 (see Table 5).

Table 5. Anova Analysis of Variance of the Model for Doe Approach

	N	R^2	R^2Adj	Q^2	SDY	RSD	Model validity	Reproducibility
Coalescences	17	0.88	0.73	0.64	1.96	1.03	0.67	0.93
Tails	17	0.89	0.76	0.61	1.85	0.93	0.66	0.94

N is the number of experiments; R^2 is the percent of the variation of the response explained by the model; R^2 Adj. is the fraction of the variation of the response explained by the model adjusted for the degree of freedom; Q^2 is the percent of the variation of the response predicted by the model.

Viability, proliferation and osteoblastic differentiation of encapsulated WJMSCs.

The viability was assessed by double staining with Calcein-AM (and with propidium iodide, as previously described, indicating that cells were highly viable after the embedding procedure by the vibrational system (see Fig. 18). In order to strengthen these data, the cell viability was determined after different lengths of culture time (up to 9 days) by using two alternative procedures, namely, the double staining with a Calcein-AM cell viability assay kit (Fig. 19 A) and the MTT test (Fig. 19 B). About one hundred alginate beads were incubated with thyazolyl blue, and the presence of formazan salts, marker of the viable cells, was reported in the graph as percentage of viable cells respect to day "0" (rated to 100%). During each day of measurement, we observed a steady but insignificant (p> 0.05) decrease in formazan absorption during the first 10 days.
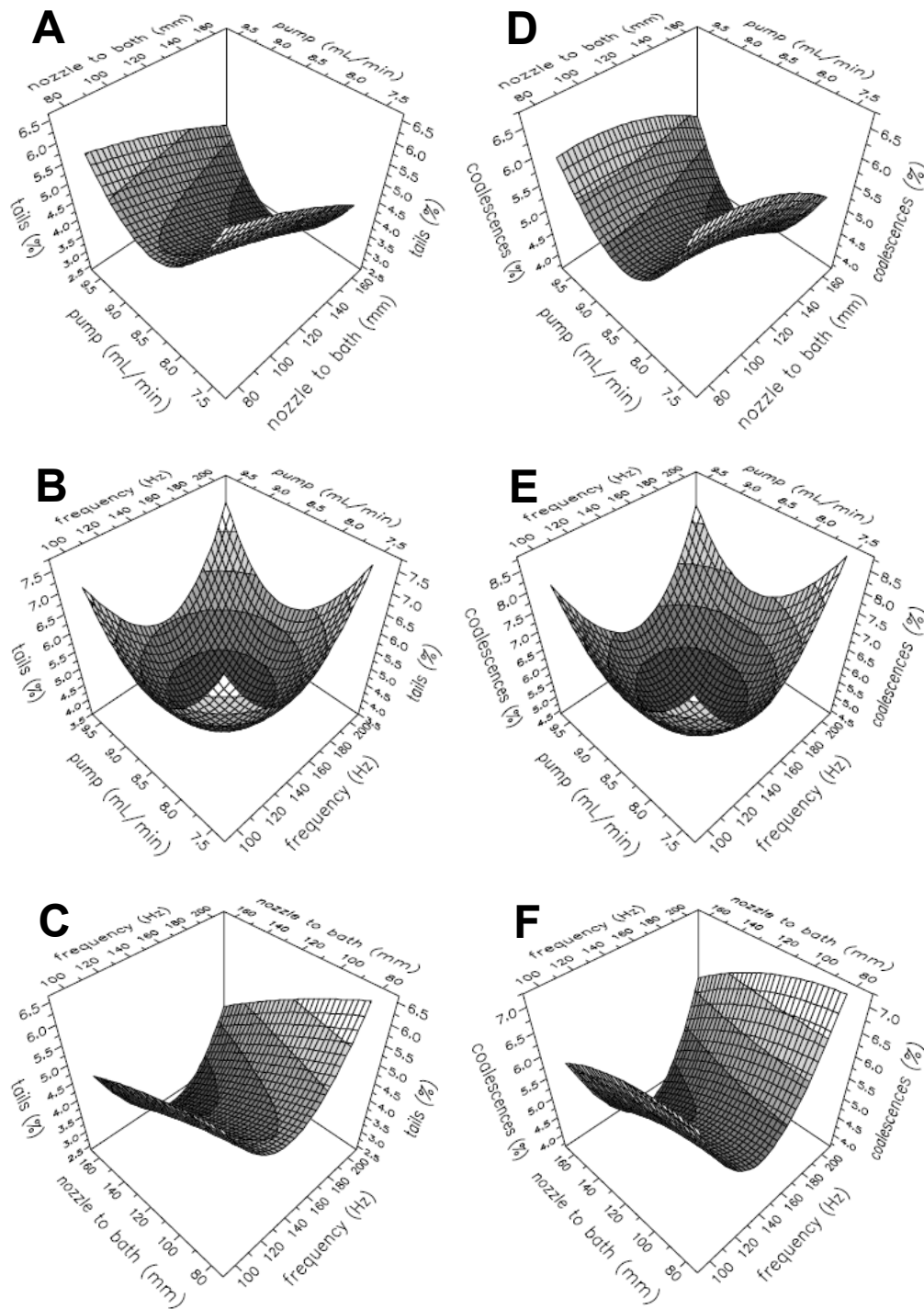
Fig. 17. Design of the experimental analysis for the production of alginate microbeads containing WJMSCs. Response surface plots of the responses: "tails" (A–C) and "coalescences" (D, E). The following interactions were reported: pump and nozzle to bath (A, D); pump and vibrating frequency (B, E); and nozzle to bath and vibrating frequency (C, F).
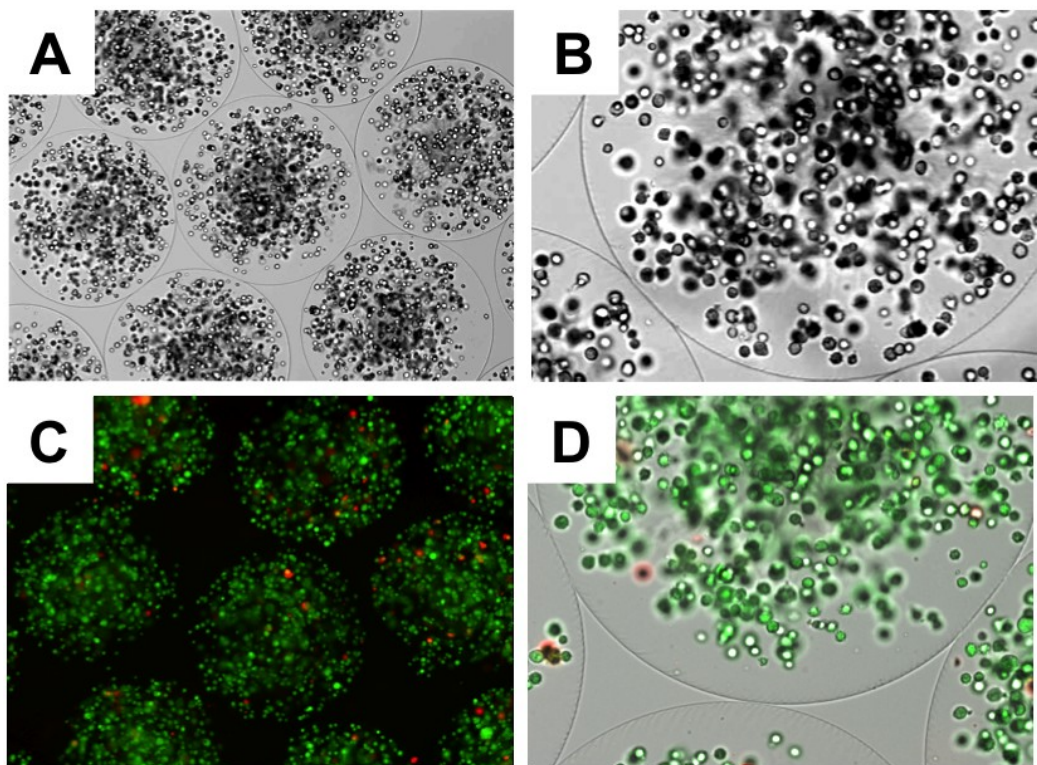
Fig. 18. Optical (A, B) and fluorescence (C, D) photomicrographs of freshly prepared alginate microbeads containing WJMSCs. Bar corresponds to 340 (A, C) and 125 μm (B,D).
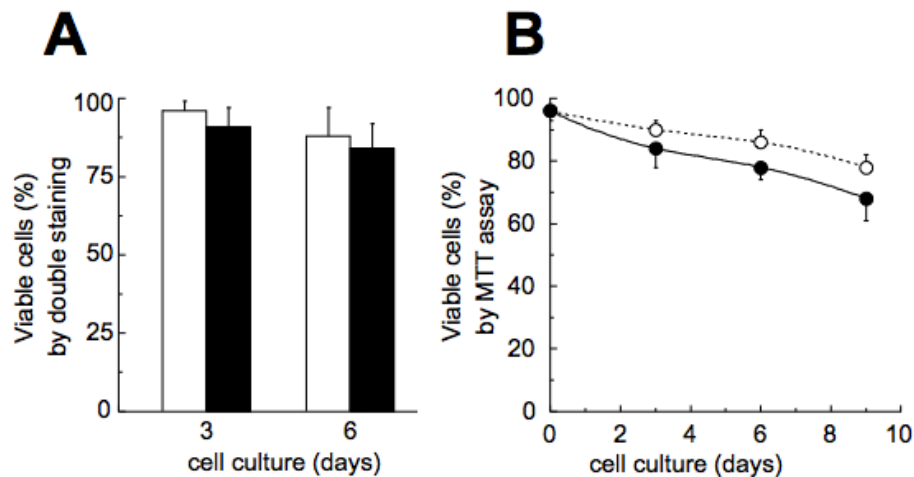

Fig. 19. (A) Histograms reporting the percentage of viable cells (by double staining) determined at days 3 and 6 of cell culture for adherent (gray bars) and encapsulated WJMCs (open bars). (B) Graph reporting the percentage of viable cells (by MTT assay) determined at days 0, 3, 6, and 9 of cell culture for adherent (open circles, dashed line) and encapsulated WJMCs (closed circles, plain line). Values are expressed as percentages of viable cells respect to day 0 (rated to 100%), and represent the mean of three independent samples analyzed in quadruplicate □ standard deviation.

The ability of the WJMSCs entrapped in alginate to differentiate in osteoblasts was assessed at day 21   of   osteogenic   induction

(WJMSCs/alg/ost) by a number of classical criteria (Fig. 20) and compared to WJMSCs entrapped in alginate in absence of osteogenic medium (WJMSCs/alg). The WJMSCs/alg/ost cells showed an appreciable increase of ALP activity, an early marker for osteoblast differentiation, (Fig. 20 A). The WJMSCs/alg/ost cells showed also an increase of the expression of a bone-specific gene such as Runx2 analysed by quantitative RT-PCR (Fig. 20 B). Similarly, mineralization was present in WJMSCs/alg/ost cells (Fig. 20 C). All together, these results suggest that the cells were undergoing osteogenic differentiation despite encapsulation.
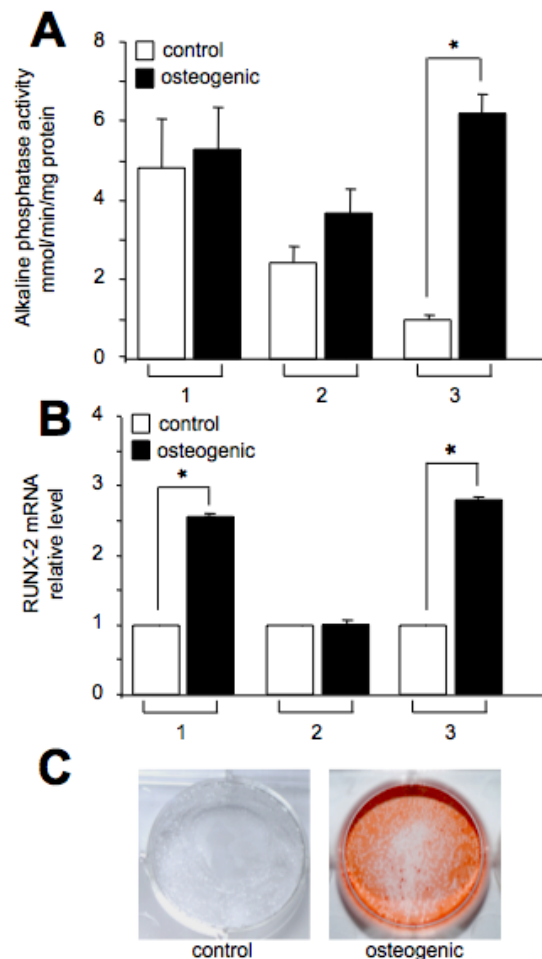

Fig. 20. Osteogenic differentiation of WJMSCs encapsulated in alginate microbeads. WJMSCs from different isolations (samples #1, #2, and #3) were cultured in standard (open bars) and osteogenic conditions (grey bars). After 21 days, alkaline phosphatase activity (A), RUNX-2 mRNA expression (B), and bone matrix deposition (C) were evaluated. Values represent the mean of three different determinations run in triplicate (on different microbead batches) ±standard deviation. *p ≤0.01.

Secretive profile: WJMSCs in alginate beads vs adherent WJMSCs

The secretive profile of both adherent (free) and alginate-encapsulated WJMSCs was analysed by multiplex bead-based sandwich immunoassay (shortly Bio-Plex). As reported in Table 6, the panel of analysed factors includes member of the family of interleukins, chemokines, growth factors and soluble forms of adhesion molecules. It should be underlined that all the proteins analysed have a molecular weight lower than the molecular weight cut off of the microbead membrane. Most of the protein analysed are secreted both by the free and encapsulated cells, even if to a different extent. The levels of IFN-α, IL-2Rα, TRAIL, M-CSF, IL-12, ICAM-1, SCGF-β, CTACK, VCAM, SDF-1α, were higher in the supernatant from free cells. In particular, IFN-α, IL-2Rα, TRAIL, M-CSF, IL-12, ICAM-1, SCGF-β, were significantly higher in the supernatant from free cells (p<0.05). On the contrary, MCP3, GRO-α, MIF and HGF were found more abundantly present in the supernatant from the encapsulated cells. In particular, MCP3 and GRO-α were significantly higher in the supernatant from free cells (p<0.05). Finally, some factors (IL-1α, IL-18, β-NGF, SCF, TNF-β LIF, MIG) were not detectable or detected at very low levels (IL-3, IL-16). Without forcing the speculations on these preliminary data, nevertheless some considerations may be done. The decrease of SCGF-β production by encapsulated WJMSCs may be correlated to their cytostaticity. In fact, SCGF-β is a cytokine of the C-type lectin family acting in hematopoietic stem/progenitor cells to support their proliferation. In addition, an appreciable decrease in the production of factors strictly associated with the immune response including IFN-α (-63%), IL-12 (-60%) was observed in encapsulated cells. IL-3 and IL-16 became undetectable after encapsulation. This should be interpreted as a benefit in consideration of an effective role of alginate in the protection of the cells from the host's immune response. In this respect it should be highlighted that the optimized microbeads have shown an excellent biocompatibility and immunoprotection capabilities, as demonstrated by *in vivo* studies conducted up to 8 months of transplantation in the peritoneal cavity of NOD mice (data not shown). The microbeads hardened with barium

chloride were freely floating in the peritoneal cavity and morphologically intact, with the majority of the microbeads free of fibrotic tissue overgrowth. In addition at 8 months of transplantation, the encapsulated cells were extraordinarily viable.

Table 6. Secretive Profile of Free and Encapsulated Wharton's Jelly Mesenchymal Stem Cells.

Secreted protein	Protein amount (pg/ml/mg ± S.D.)	
	Adherent WJMSCs	Encapsulated WJMSCs
IL-1a	n.d.	n.d.
MIG	n.d.	n.d.
IL-18	n.d.	n.d.
b-NGF	n.d.	n.d.
SCF	n.d.	n.d.
TNF-b	n.d.	n.d.
LIF	n.d.	n.d.
IFN-a	4.83 ± 0.67	1.78 ±0.30
IL-2Ra	1.78 ± 0.73	0.75 ±0.32
CTACK	4.90 ±1.65	1.86 ±0.28
IL-16	0.83 ± 0.36	n.d.
VCAM	1.80 ± 0.40	0.80 ±0.30
IL-3	0.96 ± 0.41	n.d.
TRAIL	6.70 ±1.20	2.60 ±1.40
M-CSF	12.70 ±2.50	3.90 ±0.60
SDF1a	5.80 ±1.50	3.80 ±1.20
IL-12	11.20 ±2.16	4.60 ±0.95
ICAM-1	29.50 ±5.60	13.10 ±3.70
SCGF-β	959.00 ±209.00	289.60 ±98.20
GRO-α	4.20 ±1.70	25.70 ±8.60
MCP3	6.10 ±2.00	19.60 ±5.00
HGF	46.70 ±10.90	78.60 ±18.60
MIF	13.00 ±2.80	13.50 ±3.60

Data represent the average of four independent experiments conducted in triplicate.
WJMSCs, Wharton's jelly mesenchymal stem cells; IL-1□, interleukin- 1alpha; n.d., not detectable; b-NGF, beta-nerve growth factor; SCF, stem cell factor; TNF-b, tumor necrosis factor-beta; IFN-□, interferon- alpha; SCGF-b, stem cell growth factor-beta; HGF, hepatocyte
growth factor.

At the same time, the encapsulation   may   lead   to   modifications   of

WJMSCs, inducing a secretion increase of specific proteins such as GRO-α, MCP3, and HGF. At present, we don't know the correlation between the functionality of encapsulated WJMSCs and the over production of two important chemokines (GRO-α and MCP3) involved in mesenchymal stem cell chemotaxis and a pleyotropic cytokine of mesenchymal origin (HGF, hepatocyte growth factor) promoting migration and survival of MSCs.

The latter (HGF) is one of the factors with therapeutic potential in regenerative medicine greatly studied in the last years and many researchers are looking for the best approach to maintain the therapeutic level of HGF at the repair site for endogenous stem cell recruitment.

2.3.1.3. Discussion

In this work, we present the procedure for the encapsulation of WJMSCs in alginate-based microbeads, and its effects on cell viability and secretive profile analysed by multiplex Bio-Plex technology. This is, to the best of our knowledge, the first report showing the characterization of human WJMSCs in view of their potential use in cell therapy and tissue repair. It is evident from the literature that multipotential MSCs possess a wide therapeutic applicability. Because of their fetal origin WJMSCs have been shown to share both bone marrow MSCs, and embryonic stem cells properties. Up to now, the ability of MSCs to secrete cytokines was determined only by mRNA profile, ELISA or microarray analysis, and the experiments were performed using animal MSCs or human MSCs obtained from other sources, such as adipose tissue, cord blood and bone marrow. Interestingly, our data on the secretion of proteins determined by Bio-Plex suggest that encapsulated WJMSCs maintain a secretive activity. Therefore, it is possible to conclude that alginate doesn't prevent cell functionality, on the contrary, in some cases may promote it. Further studies are required to design and select the appropriate scaffold for specific application of MSCs to the tissue of interest. Nevertheless, our data support the idea that alginate-encapsulated WJMSCs may have an important role for tissue engineering strategies, and may be

useful for improving a regenerative medicine approach for tissue repair based on mesenchymal stem cells. This latter point appears particularly important to the potential application of WJMSCs in clinic; in fact, issues about the safety of free Wharton' jelly derived MSC-based therapy should be considered, including the possibility to produce immunogenic responses or to induce tumor formation.

2.4. Cell encapsulation by microfluidic based approach

Aside the above presented "traditional" bioencapsulation procedures, new techniques are emerging in response to already existing methods, such as microfluidic approaches.

Microfluidics is an emerging and popular technology for a wide range of applications such as chemical synthesis, biochemical assays, drug screening.

Microfluidic devices were conveniently applied as new tools for the formation of multiphasic regimes of flow (constituted of two or more immiscible fluids), later converted, in different ways, in highly monodisperse spherical polymeric microparticles [40]. The procedures allow generating emulsion droplets with the production rates on the order of 1 kg/day, a rate that is sufficient for commercial production. The droplet formation is achieved by two different strategies; namely T-junction chips (squeezing) where the breakup of the flow stream results in a loss of pressure around the emerging drop or Cross-junction chips (flow focusing) where the formation of droplets is due to the viscous forces that extract fluid along the channel (Fig. 21) [41].
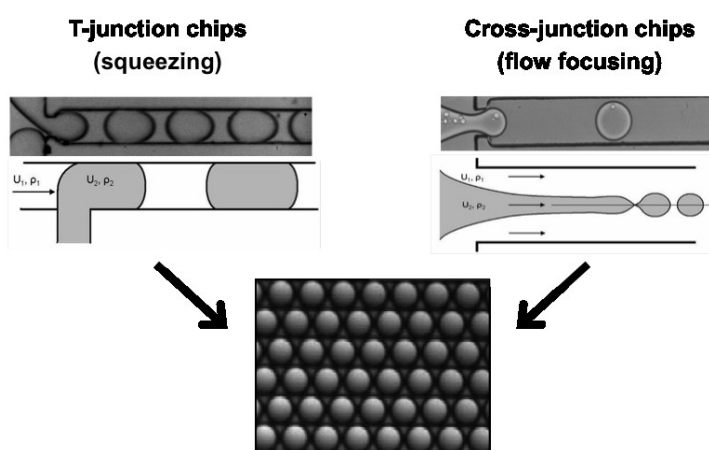

Fig. 21. Droplet formation, within the microfluidic platform, by squeezing and flow focusing mechanisms.

The chemical nature of the droplet phase (disperse phase) determines the next step in which the droplets are transformed into microparticles by a consolidation procedure. Droplets containing monomers can be solidified by

means of thermally initiated or UV-initiated polymerization [42]. Alternatively, droplets of polymer dispersions can be hardened by different procedures including in liquid drying process, [43] interfacial polymerization [44], ionic cross linking [45] or thermal gelation (Fig. 22).

In this respect, we have reported the production of polysaccharidic based microparticles with spherical shape, narrow size distribution and smooth surface combining the microfluidic technology and alternative gelation.
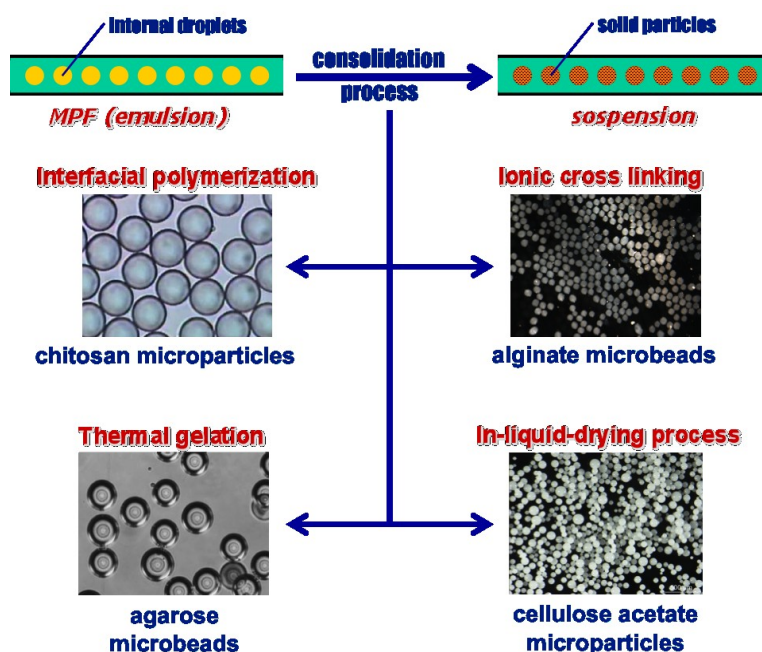

Fig. 22. Schematic representation of the different procedures to consolidate droplets by microfluidic approach.

2.4.1. Application of a microfluidic based approach to Sertoli Cells

Sertoli cells (SCs) have been considered for many years to have only a simple mechanical architectural function in testis. Recently, SCs have been considered as 'nurse' cells because they provide numerous factors required for the development and protection of the maturing germ cells [46]. Adjacent SCs form tight junctions with one another, creating a physical barrier that separates the germ cells localized toward the lumen from the blood supply. This barrier, called blood–testis barrier, allows the SCs to control and regulate the milieu of the developing germ cells and, by the secretion of immunomodulatory factors and nutrients, to create an effective

immune- privileged environment. These unique immune-privileged properties of SCs have led to the idea that SCs could be used for the protection of different cell types in transplantation protocols.

Many papers have described the ability of SC to protect transplanted tissue allografts (mainly pancreatic B-cells) [47] from the immune system, by formation of a testis-like immunoprivileged environment, with no need for prolonged immunosuppression therapy regimens. In particular, it has been demonstrated that in vitro neonatal porcine islet (NPI) maturation/differentiation pathways can significantly be ameliorate by SC-pre-culture, with SC not being included in the graft material. Moreover, when SCs and islets were co-transplanted in non-obese diabetic (NOD) mice (as a model of type 1 diabetes mellitus) the graft survival was significantly prolonged with 40–64% of mice remaining normoglycemic for 60 days after transplantation.

The ability of SCs to protect co-grafted cells is not limited to islets of Langerhans. Recent studies have demonstrated that transplantation of SC can improve the viability/function of both endogenous and co-grafted dopaminergic cells in the brain [48]. Transplantation of allogeneic SC into the rat striatum of animals affected by Parkinson-like symptoms induced, in the plexus of dopaminergic fibres. Finally, a study has demonstrated the ability of Sertoli cells injected into the parenchyma of the spinal cord to protect motor neurons in SOD1 transgenic mice, as animal model of amyotrophic lateral sclerosis [49].

These results have fostered intense study in our laboratory in an attempt to isolate highly purified SCs that were successively encapsulated by a microfluidic approach, in microbeads constituted of alginate and alginate/agarose blends. At the moment, the typical methods of preparing cells containing agarose microbeads are based on the extrusion of a water-in-oil dispersion [50].

To the best of the authors' knowledge, there is only one paper concerning cell-enclosing alginate/agarose microcapsules. Alginate–agarose subsieve-size capsules were produced by a droplet generator-based procedure [51].

The capsules produced, enclosing feline kidney cells, were relatively polydisperse, and the number of enclosed cells/capsule was relatively scarce. This work focuses on two novel features: (a) the new gelation process (ionic plus thermal gelation), which represents the key step to obtaining microbeads; and (b) the production of excellent SC containing microbeads in terms of perfect spherical shape, narrow size distribution and smooth surface.

In conclusion, the present work describes the production and characterization, by a microfluidic approach, of microbeads constituted of alginate and alginate/agarose blends, for the encapsulation Sertoli cells. The general production strategy is based on the formation of water-in-oil multiphase flow by a "Y" junction squeezing mechanism.

2.4.1.1. Materials and Methods

Materials

The polymers used were agarose Type VII (Low Gelling Temperature; appearance: white to off-white powder; solubility: clear to hazy colourless to light yellow solution at 10 mg/ml in water with heat; gel strength; NTL 200 g/cm^2 at 1.0%; gel point 26 to 30°C at 1.5%; electroendosmosis (-mr) NMT 0.1; loss on drying; NMT 10% (Sigma Aldrich, Germany) and sodium alginate IE-1105 (viscosity: 20.0-40.0 CPS, pH: 6.0-8.0 C=1%, H$_2$O) (Inotech Biosystem International, Switzerland). For the gelation of polymers droplets, barium chloride dehydrate (Sigma Aldrich, Germany) was employed. Sunflower seed oil (Collina d'oro, Italy) was used as continuous (external) phase. All other chemicals were from Fluka and were of the highest purity available. For the preparation of microbeads a "Snake mixer slide" chip (Thinxxs, Germany) with squared channels (320x320 μm), was used.

Sertoli cells isolation

SC were isolated from testis of prepubertal neonatal Large-White piglets as previously described [46]. Neonatal pre-pubertal "Large-White" pigs, aging 7-15 days, were used as Sertoli cells donors. The piglets were anesthetized with 0.1 mg/Kg azaperon (Stresnil 40 mg/ml, Janssen, Bruxelles, Belgium)

and 15 mg/Kg ketamine (Imalgene 100 mg/ml, Gellini Farmaceutici, Aprilia, Italy) co-administered intramuscularly. The technical procedure is based on excision of testes; upon removal of their fibrous cap, the testes were finely chopped, to obtain a homogeneous dense tissue. The obtained tissue was enzymatic digested with a 2 mg/ml Collagenase P (Roche Diagnostics, S.p.A., Monza, Italy) solution in HBSS (Sigma Chemical Co, St. Louis, USA) until the separation of seminiferous tubules. The collected tubules were washed twice in HBSS and spinned down at 500 r.p.m. After washing the tubules were incubated with a HBSS solution containing trypsin (2 mg/ml) and DNAse I (Sigma). After the second digestion, the trypsin solution was diluited 1:1 with Hank's + 20% FBS to halt trypsin digestion and washed twice by gravity for 15 min. in order to sediment SC aggregates, while peritubular cells remained in the supernatant and were aspirated off. The tissue pellet was washed twice in Hank's and spinned at 800 rpm for 3 min. The pellet was then resuspended in Hank's, passed through a 500 µM stainless steel mesh, centrifuged at 800 rpm for 5 min and resuspended by pipetting for 7 min. in 1 M glycine, 2 mM EDTA HBSS pH 7,2, in order to eliminate the residual Leydig and peritubular cell. The residual tubules were precipitated for 5 min at 800 rpm, washed twice with HBSS, and finally collected and culture maintained in HAM F12 (Euroclone) supplemented with retinoic acid 0.166 nM (Sigma) and 5 mL/500 ml of insulin-transforming selenium (ITS) (Becton Dickinson #354352), in 95% air/CO_2 at 37°C. Upon 3 days of in vitro culture maintenance, the SC were incubated with 20 mM Tris(hydroxymethyl)aminomethane hydrochloride (TRIS) buffer (Sigma) at pH 7.2, for 5 minutes, in order to eliminate the residual germinal cells. After washing TRIS off, SC were cultured in the same conditions as above reported in 75 cm^2 cell culture flasks.

Microbead preparation

For the injection, into the microfluidic chip, of both dispersed and continuous phases, a syringe pump (KDS Model 100 Series, Kd Scientific) was employed. Polymer dispersions (alginate or alginate/agarose blends) were used as aqueous internal phase (water phase, WP) and slowly injected into a

reagent inlet of the squeezing geometry microchannel. The second immiscible liquid (oil phase, OP) was injected into the other inlet as continuous phase. Polymer dispersion was forced into the OP at the junction of the squeezing channel to form a multiphasic flow (droplets) represented by a w/o emulsion. Finally, the microdroplets were gelled into a $BaCl_2$ solution (1.5%, w/v), in order to produce the final consolidated microbeads (Fig. 23).

Morphological characterization of microbeads

Since an uniform shape and a smooth and regular microbeads membrane are essential to assure the viability of the microencapsulated cells and the biocompatibility of the immobilization device, microparticle morphology, size and size distribution were assessed under inverted phase and stereomicroscopy, by counting at least 300 particles/batches.

Rheological studies

Rheological measurements were carried out by means of a controlled stress rheometer Stresstech HR (Reologica Instruments, AB Milano, Italy) equipped with a cone-plate geometry (diameter of 40 mm and angle 1°). The alginate/agarose gels were characterized by oscillation measurements (oscillation stress sweep at 37°C). The samples were applied to the lower plate to ensure that gel shearing did not occur. The frequency sweep measurements were performed using the frequency range 0.1-10 Hz and the stress value previously determined in the linear viscoelastic region.

Determination of viability and function of encapsulated Sertoli cells

The viability of SC encapsulated in alginate/agarose microbeads was assessed after different lengths of in vitro culture (immediately after microbead preparation and at days 3, 6, 9 and 12) by double staining with ethidium bromide (Sigma) and fluorescein diacetate (FDA, Sigma). Cells were visualized under fluorescence microscope (Nikon, Optiphot-2, Nikon Corporation, Tokyo, Japan) using the filter block for fluorescein. Dead cells were stained in red, while viable cells appeared green. The quantification of the viability of SC encapsulated in alginate/agarose microbeads was determined after dissolution of microbeads by treatment with an EDTA solution (50 mM, pH 8) for 10 min at 37°C. Thereafter cells were washed

three times with PBS, stained and examined under fluorescence microscope, by counting at least 800 cell/batches. The final viability data represent the mean of three determinations made in triplicate (on independent microbead batches) ± S.D. The evidence of the functions of the encapsulated Sertoli cells was determined by assessing the cell α-aromatase activity as previously described [46]. Briefly, 10^6 SC as monolayers or encapsulated in microbeads, were cultured for 3 days in the absence or in the presence of 1 µg/ml of follicular stimulating hormone (FSH) (Serono, Rome, Italy); thereafter, 0.2 µg/ml of testosterone enantate (SIT, Pavia, Italy) were added to the cells culture medium. After 8 h of treatment, the conditioned medium was withdrawn and assayed for 17-β-estradiol (E2) presence. E2 concentrations were determined by direct chemiluminescent technology (ADVIA Centaur, Estradiol-6 III, Bayer Diagnostics, Germany) (intra-assay CV<4.0%; inter-assay CV=6.0%). The reported data represent the mean of three determinations made in triplicate (on independent microbead batches) ± S.D.

In vivo biocompatibility of encapsulated SC

Under general anesthesia, induced by intra-peritoneal co-administration of 100 mg/Kg ketamine (Parke-Davis/Pfizer, Karlsruhe, Germany) and 15 mg/Kg xylazine, (Bayer, Leverkusen, Germany), microbeads were collected by a sterile transfer pipette and delivered into the peritoneal cavity of the recipient female NOD mice, weighing approximately 25 g. (Harlan, Italy) through a small abdominal incision. Each mouse received 10^6 SC encapsulated in alginate/agarose (1:1 blend, w/w) microbeads. Body weight of each recipient was monitored. At 4 months of transplant, the microcapsules were retrieved to evaluate their morphology, mechanical stability and biocompatibility. After animals' anesthesia, performed as above described, microbeads were retrieved by peritoneal washing with warm saline. General characteristics of the retrieved microcapsules were determined by examining extent of the fibrotic overgrowth under phase contrast microscopy, and morphological features such as microcapsules sphericity, surface smoothness and finally viability by double staining with

ethidium bromide and fluorescein diacetate.

2.4.1.2. Results

This study describes the development and optimization of a new method of preparation for polysaccharidic microbeads based on a microfluidic approach. As general approach, we employed a chip with a "Y" shaped microchannel configuration, for the formation of w/o multiphase flow regime. The w/o flow was constituted of a water dispersion of a polysaccharide into a continuous sun flower seed oil phase.
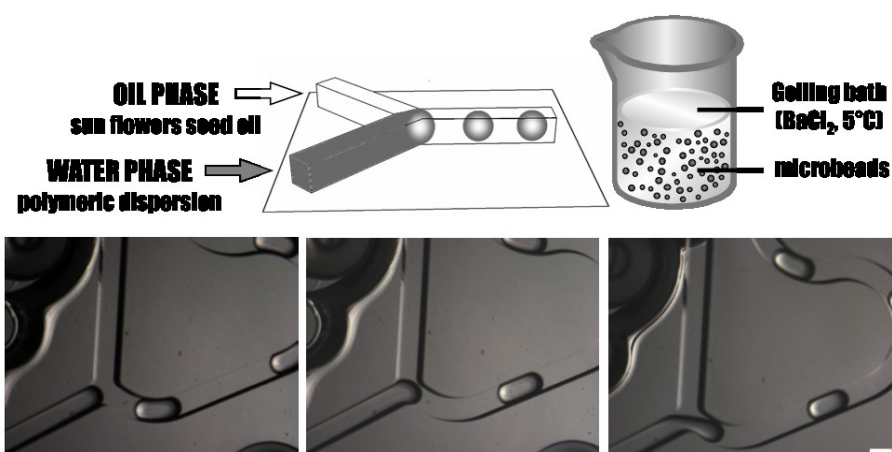

Fig. 23. Schematic representation of the microfluidic system setup for the preparation of polysaccharidic microbeads, including the drawing of the multiphase flow generator by "Y" junction squeezing mechanism (upper panel). Microphotographs of the multiphase flow formation, bar = 300 µm (lower panel).

Afterwards the generated microdroplets where conveniently converted into gelled microbeads by gelation procedures (see scheme in Fig. 23).

As first approach we tested the possibility to produce pure alginate microbeads by an "external gelation" procedure. By injecting the two immiscible phases in the microfluidic channels and by tuning their relative flow rates, a multiphase flow was easily obtained. Subsequently the formed alginate microdroplets were collected into a gelling $BaCl_2$ bath, allowing the gelation of the alginate droplets. As reported in Fig. 24, the obtained microbeads were unfortunately characterized by a very pronounced tail-shape (Fig. 24 A, B), even in the presence of a magnetic stirrer (Fig. 24 C, B).
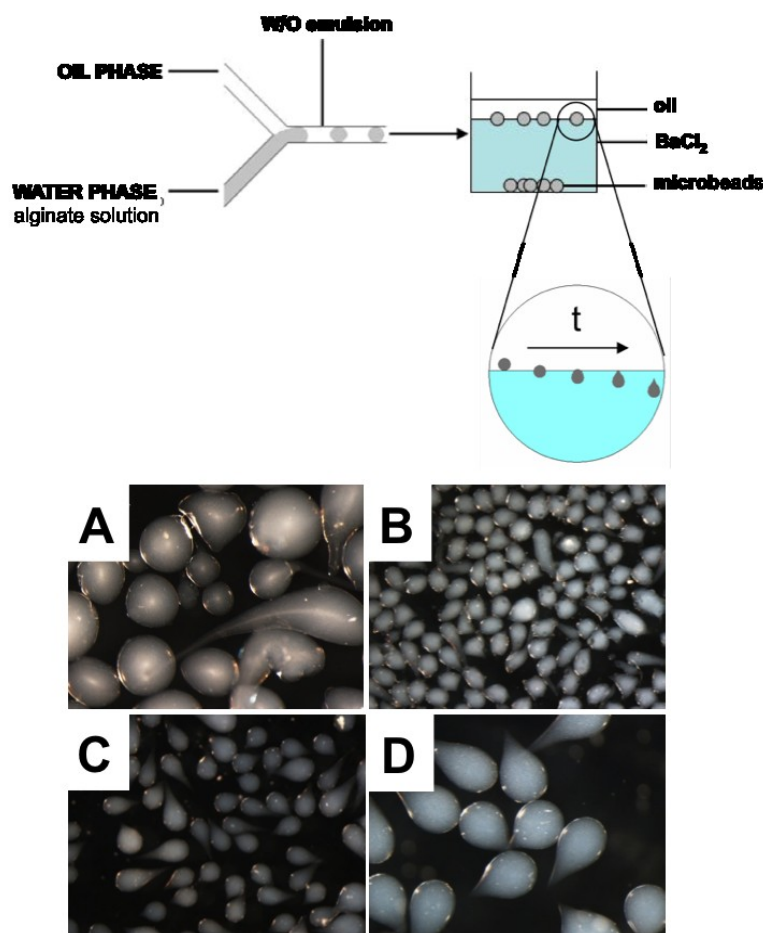
Fig. 24. Dark field stereophotomicrographs of Ba-alginate microbeads prepared by the 'external gelation' procedure, in the presence (A, B) or the absence (C, D) of a magnetic stirrer (250 rpm).

This particular shape was attributed to the slowly pass of the Na-alginate liquid droplets through the OP/gelling bath interface.

In order to possibly solve this main drawback, further experiments were conducted adding a thin, low viscous oil layer (OL) above the gelling $BaCl_2$ bath, to possibly facilitate the passage of the WP droplets through the interface (Fig. 24). As further improvement a small percentage (5–10%, w/w) of glycerol was added to the initial Na-alginate dispersion, in order to increase the density of the WP (Fig. 25).

As can be seen in the microphotographs shown in Fig. 24 A,B and 25 A,B, both approaches resulted in a significant reduction of the tails on the microbeads. Nevertheless the microbeads still presented a rather remarkable number of tails. In addition, as reported in Tables of Figs. 24 and 25, the

microbeads were polydispersed in terms of size (high S.D.).

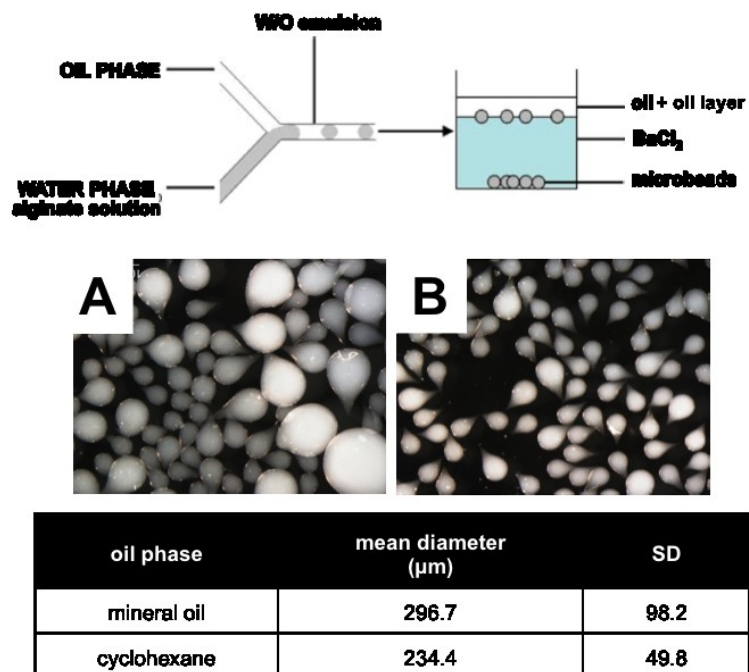| oil phase	mean diameter (µm)	SD
mineral oil	296.7	98.2
cyclohexane	234.4	49.8

Fig. 24. Dark field stereophotomicrographs of Ba-alginate microbeads prepared by the 'external gelation' procedure. Effect of the oil layer: mineral oil (A) and cyclohexane (B). In the table the dimensional characteristics are reported.

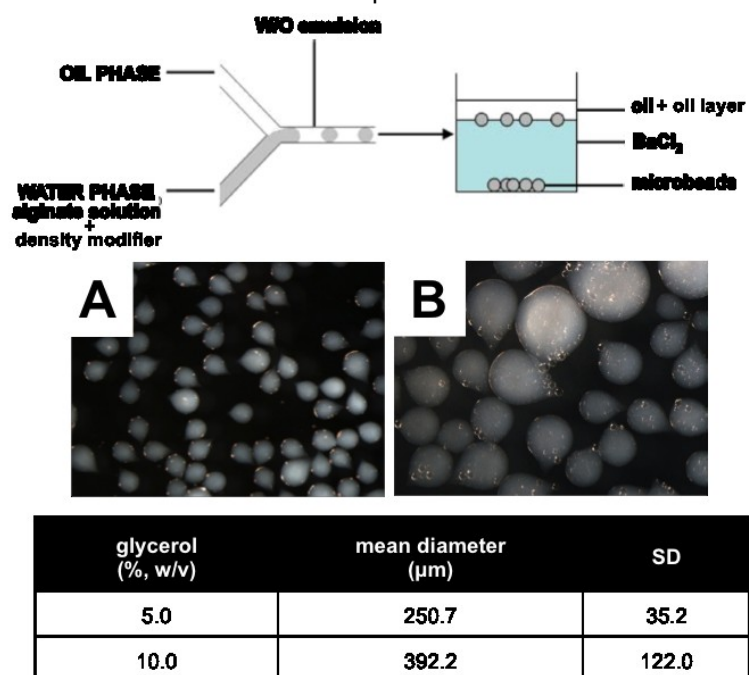| glycerol (%, w/v)	mean diameter (µm)	SD
5.0	250.7	35.2
10.0	392.2	122.0

Fig. 25. Dark field stereophotomicrographs of Ba-alginate microbeads prepared by the 'external gelation' procedure, in the presence of 5 (A) and 10 % (B) of glycerol. In the table the dimensional characteristics are reported.

Successively, the 'internal gelation' procedure was assessed to possibly

ameliorate the size and shape characteristics of the final Ba-alginate microbeads. The experiments were conducted by dispersing an insoluble or partially soluble barium salt. (BaCO$_3$, 5–10 mM) into the WP containing Na-alginate. The microdroplets gelation was achieved by gentle acidification with an oil soluble acid (acetic acid 0.15%, v/v) added to the OP. The lowering of the pH causes barium ion release and the consequent formation of Ba-alginate gel. From the analysis of the microphotographs reported in Fig. 26, it is evident that the content of BaCO$_3$ strongly influences the final characteristics of alginate microbeads. In fact, microbeads prepared with the lowest content of BaCO$_3$ (5.0 mM) (Fig. 26 A) are characterized by a high polydispersity, a strong tail-shape and by the presence of a remarkable number of coalescences.

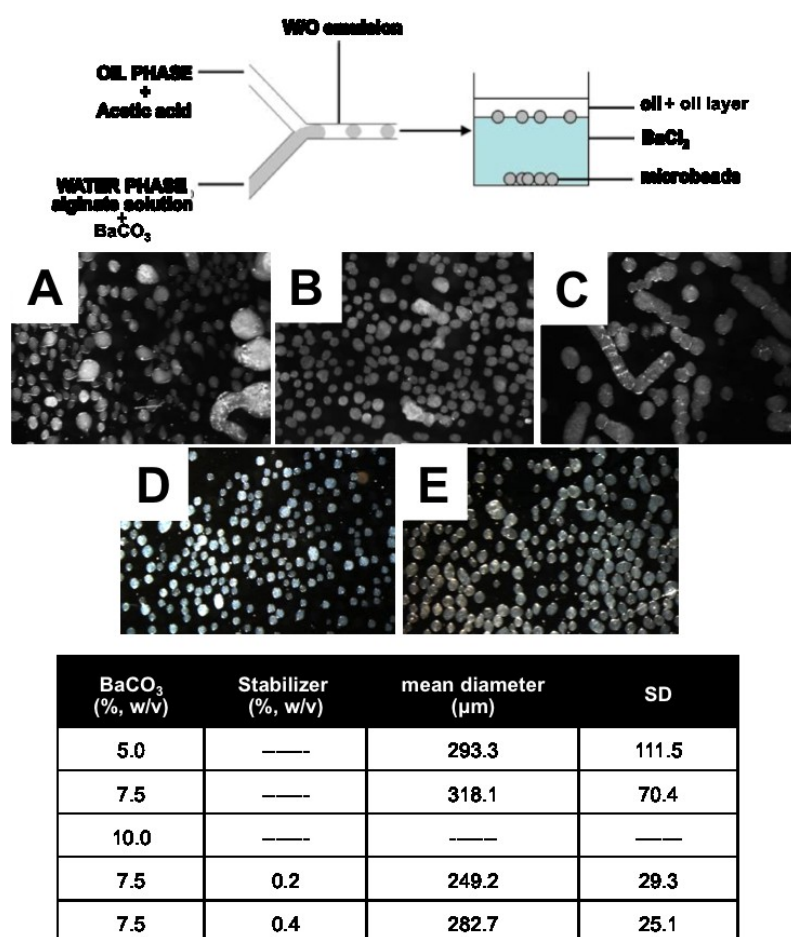| BaCO$_3$ (%, w/v)	Stabilizer (%, w/v)	mean diameter (µm)	SD
5.0	——	293.3	111.5
7.5	——	318.1	70.4
10.0	——	——	——
7.5	0.2	249.2	29.3
7.5	0.4	282.7	25.1

Fig. 26. Dark field stereophotomicrographs of Ba-alginate microbeads prepared by the 'internal gelation' procedure. Microbeads were prepared by dispersing 5 (A), 7.5 (B) or 10 mM (C) BaCO$_3$ or dispersing 7.5 mM of BaCO$_3$ in the WP in the presence of 0.2% (D) or 0.4% (w/v) (E) of span 80 as stabilizer. In the table the dimensional characteristics are reported.

On the other hand, microbeads prepared with the highest content of $BaCO_3$ (10.0 mM) are characterized by spherical shape, but an important number of coalescences are clearly detectable (chains of partially fused microbeads, Fig. 26 C).

Only with a precise content of $BaCO_3$ (7.5 mM), the produced microbeads present acceptable morphological characteristics (Fig. 25 B). The microbead morphology was greatly improved by adding to the OP a stabilizer (span 80) that deeply reduced the presence of coalescences, resulting in almost spherical microbeads (Fig. 26 D,E).

As further improvement of the quality of the produced alginate microbeads, a new gelation approach was tested and the subsequent experiments were conducted using alginate/agarose blend dispersions as water phases, with the purpose of starting the gelation process of the polymeric droplets when they are still resident into the chip microchannel. From the analysis of the microphotographs reported in Fig. 27 A-C, it is noticeable that the progressively increasing amounts of agarose (with the respect to alginate), results in an improvement of the final morphological characteristics of the obtained microbeads.

Microbeads constituted of small amounts of agarose (alginate/agarose from 9:1 to 4:1, w/w) still present (even if in a less pronounced way), the unwanted tail-shape. Only when the agarose content is increased to a ratio of 1:1 (alginate/agarose, w/w), the produced microbeads are characterized by a perfectly spherical shape, without signs of coalescence (Fig. 27 C). Interestingly, together with the amelioration of the microbeads morphology, a slight and progressive increase of the mean particle diameter, was observed, when agarose content was raised (see the size distribution analysis reported in Fig. 27 E). This behaviour was tentatively attributed to the different hardening process characteristic of agarose, in fact, agarose gelation does not involve in the shrink due to the complexation of divalent ions.
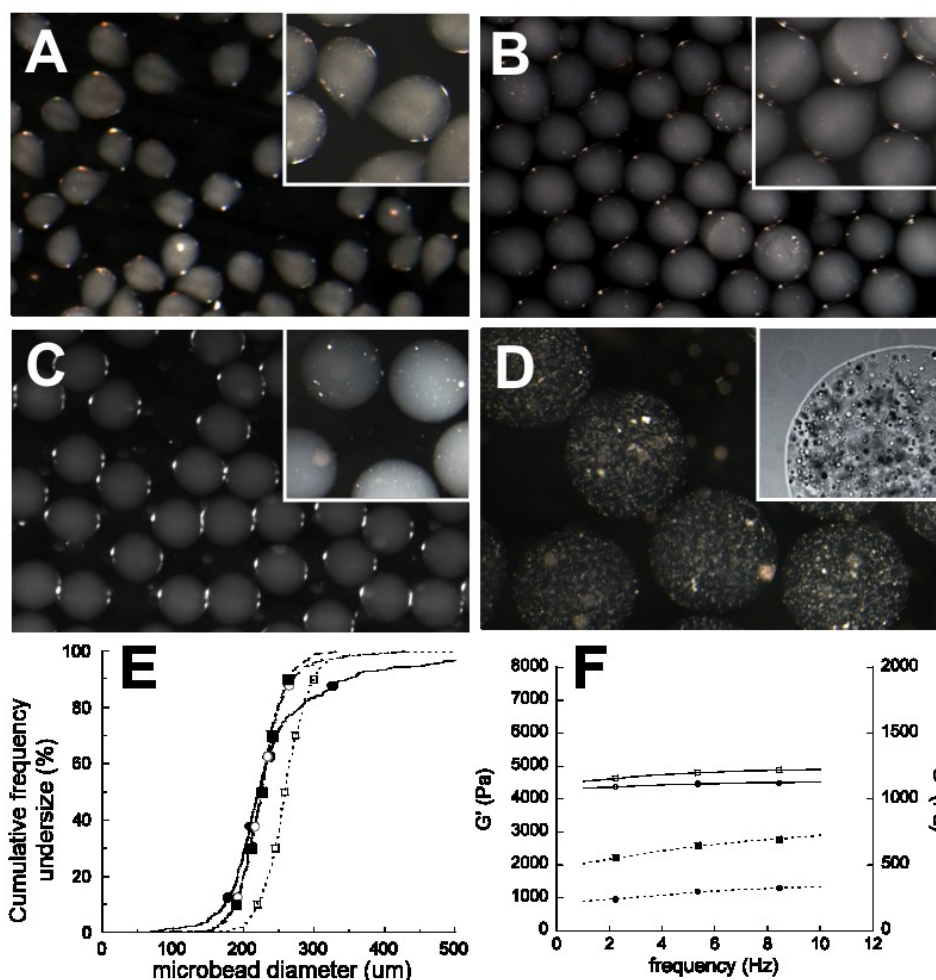
Fig. 27. Dark field stereophotomicrographs of polysaccharidic microbeads. Microbeads consisting of (A) 9:1, (B) 4:1, (C) 1:1, w/w alginate/agarose blends. Alginate/agarose (1:1 blend, w/w) microbeads containing SC (D). In the insets are reported dark field stereophotomicrographs showing, at higher magnification, the microbead surface and morphology. E: cumulative size distribution of microbeads prepared with 6:1 (filled circles), 4:1 (circles), 2:1 (filled squres) and 1:1 (squares) of alginate/agarose blends.
F: Frequency sweep tests showing the frequency dependence of the elastic G' (solid lines, open symbols) and loss G" (dotted lines, closed symbols) moduli of alginate/agarose gels. Gels were prepared using different weight ratios between alginate and agarose, namely: 9:1 (circles), 4:1 (squares) and 1:1 (diamonds). Data represent the average of three independent determinations. Bars correspond to 400 μm (A–C) and 150 mm (D).

In spite of these results indicating that only using a 1 to 1 weight ratio between alginate and agarose resulted in optimal microbeads (see above), we performed a rheological characterization, by oscillatory measurements, of gels constituted of alginate/agarose at different ratios (namely: 9:1, 4:1 and 1:1). Non-destructive oscillatory measurements were indeed performed in order to obtain information about the effect of the change of ratio between alginate and agarose.

Viscoelastic materials (such as alginate/agarose gels) show, after mechanical stress, contemporaneously viscous and elastic flow. In this respect, oscillation measurements furnish data regarding energy stored (storage modulus G'), dissipated energy (loss modulus G'').

Gel measurements were performed firstly by increasing stress from 0.1 to 100 Pa, working at constant frequency of 1 Hz. The test permitted to individuate the linear viscoelastic region in which it is possible to recognize the stress value useful to ensure instantaneous recovery after the removal of the applied force. Successively, oscillatory measurements were performed over a frequency range of 0.1 to 10 Pa and at constant stress, identified in the linear viscoelastic region.

As shown in Fig. 27 F, storage modulus (G') predominated in all gels demonstrating that these formulations were able to keep the furnished energy (applied stress) maintaining the primitive structure.

Particularly, increasing the agarose percentage content causes a progressive improvement of both G' and G''.

Once selected the optimal experimental setup and polymer concentration, resulting in microbeads with an excellent morphology and narrow size distribution (Fig. 27 C), we started a new series of experiments aimed at validating the entire experimental set up for the encapsulation of living eukaryotic cells, namely Sertoli cell. As reported in Fig. 27 D, the stereophotomicrograph clearly indicated that Sertoli cell were conveniently encapsulated into alginate/agarose microbeads, prepared with alginate/agarose (1/1 blend, w/w), with notable shape and surface, in term of microbead morphology.

Moreover, the fluorescence photomicrographs reported in Fig. 28 A-E demonstrated that SCs remain highly viable after encapsulation up to 16 days of cell culture. In Fig. 28 F is reported the entire viability profile that compare free and encapsulated SC.

These results showed that the encapsulated cells display viability strictly comparable to the free ones. In this respect, it is to be underlined that, although immortalized cell lines have provided invaluable information about

cell biology to researchers, primary cell culture offers a more relevant system for the study of cell function, disease states and patient therapy. However, working with primary cells in culture presents numerous challenges.
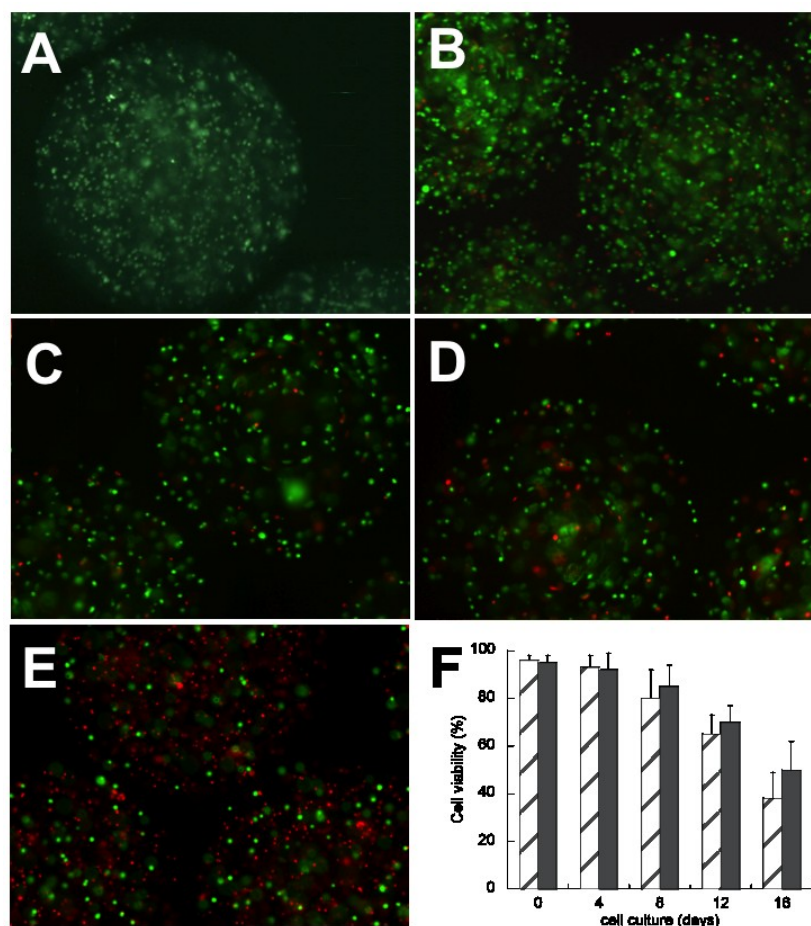

Fig. 28. Fluorescence micrographs showing the viability of SC encapsulated in alginate/agarose microbeads immediately after the preparation (A) and after 3 (B), 6 (C), 9 (D) and 16 (E) days of cell culture. SC encapsulating microbeads were prepared with alginate/agarose (1/1 blend, w/w), as described in the experimental section. In panel F is reported the comparative analysis of the viability of free (solid bars) and encapsulated (stripped bars) SC; data represent the mean of three determinations made in triplicate (on independent microbead batches) ± S.D. Bar = to 100 μm.

Primary cell cultures are sensitive to apoptosis due to contact inhibition, serum concentration, and the three dimensional (3D) environment, and many conditions for optimal growth and proliferation of primary cells remain unknown. Generally, primary cells can be maintained in culture for period ranging between 3-15 days, after that cells usually die.

To evaluate the functional capability of the encapsulated SC, the α-aromatase activity (in the presence or absence of FSH) was analysed. As

depicted in Fig. 29 A the α-aromatase activity, expressed in term of 17-β-estradiol biosynthesis, remain statistically unchanged in free and encapsulated SC both in presence (squares) or in absence (circles) of FSH, for the entire period of time analysed (6 days of cell culture).
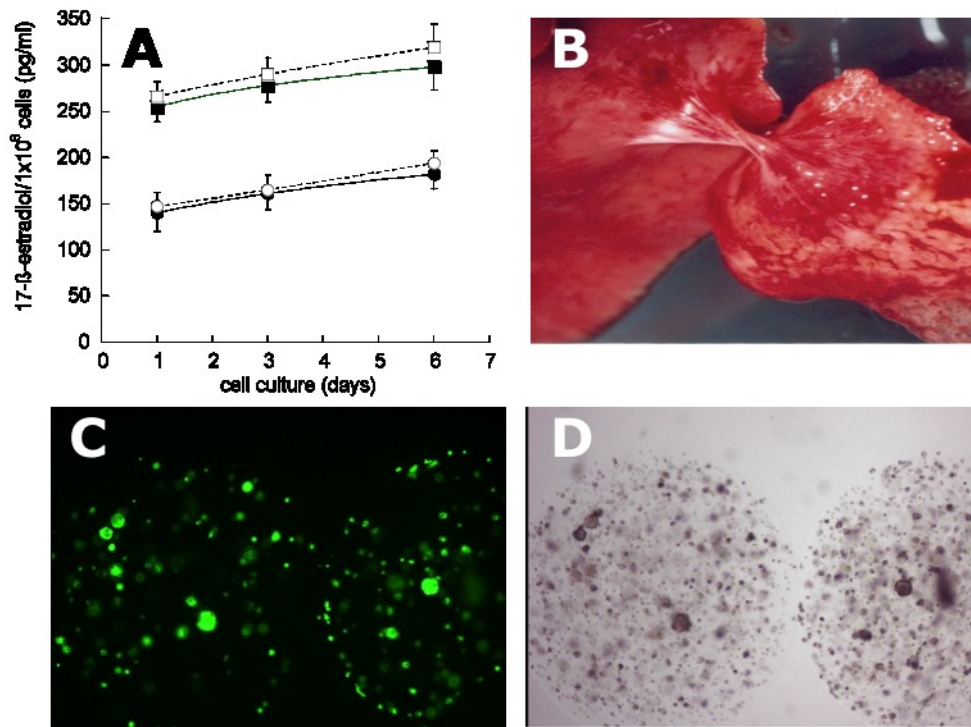

Fig. 29. Functional analysis (A) and biocompatibility (B-D) of alginate/agarose (1:1 blend, w/w) microbeads containing SC. As specific marker to evaluate the functional capacity of the encapsulated SC, the α-aromatase activity (expressed in term of 17-β-estradiol biosynthesis) was analysed (panel A). Open symbols, plain lines: free SC, closed symbols, dotted lines: SC encapsulated in alginate/agarose microbeads. α-aromatase activity was evaluated for the indicated length of time in the absence (circles) or in the presence of 1 µg/ml of FSH (squares). Data represent the mean of three determinations made in triplicate (on independent microbead batches) ± S.D. Examination of a typical batch of microbeads containing SC upon retrieval after 4 months from the peritoneal cavity (B), after double staining with ethidium bromide and fluorescein diacetate (C) bright field (D).

Finally, in order to evaluate the mechanical stability during the implantation procedure and the biocompatibility of alginate/agarose (1:1 blend, w/w) microbeads containing SC, the microbeads were transplanted in the peritoneal cavity of NOD mice as described in the experimental section. The obtained results, summarized in Fig. 29 B-D, demonstrated that the microbeads were mechanically stable as proved by the morphological intactness, with the majority of the microcapsules (over 85%) appearing free

of any fibrotic tissue overgrowth at 4 months from transplant (Fig. 29 C). In addition, the viability of SC encapsulated in alginate/agarose (1:1 blend, w/w) microbeads at 4 months of transplantation, was extraordinarily high.

2.4.1.3. Discussion

In conclusion, this paper confirms that microfluidic methods appear to be a promising procedure for the preparation of microparticles intended for cell encapsulation and tissue engineering applications.

In particular, the flow characteristics within microfluidic chip channels and the high dimension precision with which the chips are produced result in hydrogel based microparticles with highly controlled morphological and dimensional properties. In this respect, microfluidic techniques can be suitably used to obtain microparticles without common morphological defects often associated to other production methods. Batch emulsification or electrostatic technologies are indeed prone to the production of microparticles with presence of "tails", coalescences, surface irregularity together with large size distribution [51].

The reported data demonstrate that the conversion of liquid droplets into solid particles represents the critical point for the production of morphologically acceptable microbeads by microfluidic approach. In this respect, the use of alginate/agarose blends appears to be particularly appropriate for producing spherical, smooth monodisperse microbeads without interfering with cell viability and functions.

References

[1] Q. Chen, S.E: Harding, N.N. Ali et al. Biomaterials in cardiac tissue engineering: Ten years of research survey. Mat Scie Eng R 59, 1, 2008.

[2] G. Orive, S.K. Tam, J.L. Pedraz et al. Biocompatibility of alginate–poly-L-lysine microcapsules for cell therapy. Biomat, 27, 3691, 2006.

[3] U. Prusse, L Bilancetti, M. Bucko et al. Comparison of different technologies for alginate beads production. Chem Papers, 62(4), 364, 2008.

[4] M. J. Welsh, L. C. Tsui, T. F. Boat et al. Cystic fibrosis in The Metabolic and Molecular Bases of Inherited Disease, C. R. Scriver, A. L. Beaudet, W. S. Sly, and D. Valle, Eds., 3799, McGraw-Hill, New York, NY, USA, 1995.

[5] A. M. Jones, L. Martin, R. J. Bright-Thomas et al. Inflammatory markers in cystic fibrosis patients with transmissible Pseudomonas aeruginosa. Eur Respiratory Journal, 22(3), 503, 2003.

[6] T. L. Bonfield, J. R. Panuska, M. W. Konstan et al. Inflammatory cytokines in cystic fibrosis lungs. American J Resp Critical Care Med, 152(6), 2111, 1995.

[7] T. Lund and B. Østerud. The effect of TNF-α, PMA, and LPS on plasma and cell-associated IL-8 in human leukocytes. Thrombosis Research, 113(1), 75, 2004.

[8] V. Bezzerri, M. Borgatti, E. Nicolis et al. Transcription factor oligodeoxynucleotides to NF-κB inhibit transcription of IL-8 in bronchial cells. American J Resp Cell and Mol Biol, 39, 86, 2008.

[9] W. de Jager, H. Te Velthuis, B. J. Prakken et al. Simultaneous detection

of 15 human cytokines in a single sample of stimulated peripheral blood mononuclear cells. Clinical and Diagnostic LabImmunol, 10, 133, 2003.

[10] Y. Altschuler, C. Hodson, S. L. Milgram. The apical compartment: trafficking pathways, regulators and scaffolding proteins," Current Opinion in Cell Biology, 15(4), 423, 2003.

[11] B. A. Woodworth, E. Tamashiro, G. Bhargave et al. An in vitro model of Pseudomonas aeruginosa biofilms on viable airway epithelial cell monolayers. American Journal of Rhinology, 22(3), 235, 2008.

[12] S. Jaya, T. D. Durance, R. Wang. Effect of alginate-pectin composition on drug release characteristics of microcapsules. J Microencaps, 26(2), 143, 2009.

[13] A. Murua, G. Orive, R. M. Hernández et al. Xenogeneic transplantation of erythropoietin-secreting cells immobilized in microcapsules using transient immunosuppression," Journal of Controlled Release, 137(3), 174, 2009.

[14] S. Zheng, Z.X. Xiao, Y.L. Pan et al. Continuous release of interleukin 12 from microencapsulated engineered cells for colon cancer therapy. World Journal of Gastroenterology, 9(5), 951, 2003.

[15] P. deVos, M. Bucko, P. Gemeiner et al. Multiscale requirements for bioencapsulation in medicine and biotechnology, Biomaterials, 30(13), 2559, 2009.

[16] S. Mazzitelli, A. Tosi, C. Balestra et al. Production and characterization of alginate microcapsules produced by a vibrational encapsulation device. J Biomat Appl, 23(2), 123, 2008.

[17] J.J Minguell, A. Erices, P. Conget. Mesenchymal stem cells. Exp Biol

Med, 226, 507, 2001.

[18] J.E. Dennis, A. Merriam, A. Awadallah et al. A quadripotential mesenchymal progenitor cell isolated from the marrow of an adult mouse. J Bone Miner Res,14, 700, 1999.

[19] S.P. Bruder, N. Jaiswal, S.E. Haynesworth, sGrowth kinetics, selfrenewal, and the osteogenic potential of purified human mesenchymal stem cells during extensive sub-cultivation and following cryopreservation. J Cell Biochem, 64, 278, 1997.

[20] N. Jaiswal, S.E. Haynesworth, A.I. Capla et al. Osteogenic differentiation of purified, culture-expanded human mesenchymal stem cells in vitro. J Cell Biochem, 64, 295, 1997.

[21] G. Ferrari, G. Cusella-De Angelis, M. Coletta et al. Muscle regeneration by bone marrow-derived myogenic progenitors. Science, 279, 1528, 1998.

[22] E.J. Gang, J.A. Jeong, S.H. Hong et al. Skeletal myogenic differentiation of mesenchymal stem cells isolated from human umbilical cord blood. Stem Cells, 22, 617, 2004.

[23] Y.S Fu, Y.C. Cheng, M.Y. Lin et al. Conversion of human umbilical cord mesenchymal stem cells in Wharton's jelly to dopaminergic neurons in vitro: potential therapeutic application for parkinsonism. Stem Cells, 24, 115, 2006.

[24] R.G. Young, D.L. Butler, W. Weber et al. Use of mesenchymal stem cells in a collagen matrix for Achilles tendon repair. J Orthop Res, 16, 406, 1998.

[25] F.P. Barry, J.M. Murphy. Mesenchymal stem cells: clinical applications and biological characterization. Int J Biochem Cell Biol, 36, 568, 2004.

[26] S. Kern, H. Eichler, J. Stoeve et al. Comparative analysis of mesenchymal stem cells from bone marrow, umbilical cord blood, or adipose tissue. Stem Cells, 24, 1294, 2006.

[27] B.L. Yen, H.I Huang, C.C. Chien et al. Isolation of multipotent cells from human term placenta. Stem Cells, 23, 3, 2005.

[28] P. De Coppi, G. Bartsch, G., M.M. Siddiqui et al. Isolation of amniotic stem cell lines with potential for therapy. Nat Biotechnol, 25, 100, 2007.

[29] O.K Lee, T.K. Kuo, W.M. Chen. Isolation of multipotent mesenchymal stem cells from umbilical cord blood. Blood ,103, 1669, 2004.

[30] H.S. Wang, S.C. Hung, S.T. Peng et al. Mesenchymal stem cells in the Wharton's jelly of the human umbilical cord. Stem Cells, 22, 1330, 2004.

[31] T. Bakhshi, R.C. Zabriskie, S. Bodie et al. Mesenchymal stem cells from the Wharton's jelly of umbilical cord segments provide stromal support for the maintenance of cord blood hematopoietic stem cells during long-term ex vivo culture. Transfusion, 48(12), 2638, 2008.

[32] L.S. Ferreira, S. Gerechtd, J. Fullera et al. Bioactive hydrogel scaffolds for controllable vascular differentiation of human embryonic stem cells. Biomat, 28, 2706, 2007.

[33] H. Ma, S. Hung, S. Lin et al. Chondrogenesis of human mesenchymal stem cells encapsulated in alginate beads. J Biomed Mater Res A, 46, 273, 2000.

[34] S. Kestendjieva, D. Kyurkchiev, G. Tsvetkova et al. Characterization of mesenchymal stem cells isolated from the human umbilical cord. Cell Biol Int, 32, 724, 2008.

[35] F. Denizot, R.J. Lang. Rapid colorimetric assay for cell growth and survival. Modifications to the tetrazolium dye procedure giving improved sensitivity and reliability. Immunol Methods, 22, 271, 1986.

[36] A. Can, S. Karahuseyinoglu. Concise review: human umbilical cord stroma with regard to the source of fetus- derived stem cells. Stem Cells ,25, 2886, 2007.

[37] K.E. Mitchell, M.L Weiss, B.M. Mitchell et al. Matrix cells from Wharton's jelly form neurons and glia. Stem Cells, 21, 50, 2003.

[38] D.L. Troyer, M. Weiss. Concise review: Wharton's jelly- derived cells are a primitive stromal cell population. Stem Cells, 26, 591, 2008

[39] M. Dominici, K. Blanc, I. Mueller et al. Minimal criteria for defining multipotent mesenchymal stromal cells. The International Society for Cellular Therapy statement. Cytotherapy, 8, 315, 2006.

[40] L. Zhu, Y. Li, Q. Zhang. Fabrication of monodisperse, large-sized, functional biopolymeric microspheres using a low-cost and facile microfluidic device. Biomed Microdevices, 12, 169, 2010.

[41] C.N. Baroud, H. Willaime. Multiphase flows in microfluidics. Comptes Rendus Physique, 5, 547, 20014.

[42] T. Nisisako,T. Torii, T.Higuchi T. Characterization of spontaneous transformationbased droplet formation during microchannel emulsification. Chem Eng J, 101, 23, 2004.

[43] M. Seo, Z. Nie, S. Xu, M. Mok et al. Novel microreactors for functional polymer beads. Langmuir, 21, 11614, 2005.

[44] I. Cohen, H Li, J.L. Hougland et al.Using selective withdrawal to coat microparticles. Science, 292, 265, 2001.

[45] K.S. Huang, T.H. Lai,Y.C. Lin.Manipulating the generation of Ca–alginate microspheres using microfluidic channels as a carrier of gold nanoparticles. Lab Chip, 6, 954, 2006.

[46] G. Luca, M. Calvitti, C. Nastruzzi et al. Encapsulation, in vitro characterization, and in vivo biocompatibility of Sertoli cells in alginate-based microcapsules. Tissue En, 13(3), 641, 2007.

[47] G. Luca, C: Nastruzzi, M. Calvitti et al. Accelerated functional maturation of isolated neonatal porcine cell clusters: in vitro and in vivo results in NOD mice. Cell Transpl, 14, 249, 2005.

[48] R. Shamekh, S. Saporta, D.F. Cameron et al. Effects of Sertoli cell-conditioned medium on ventral midbrain neural stem cells: a preliminary report. Neurotox Res, 13, 241, 2008.

[49] R. Hemendinger, J. Wang, S. Malik et al. Sertoli cells improve survival of motor neurons in SOD1 transgenic mice, a model of amyotrophic lateral sclerosis. Exp Neurol, 196, 235, 2005.

[50] S. Sakai, I. Hashimoto, K. Kawakami K. Production of cell-enclosing hollow-core agarose microcapsules via jetting in water–immiscible liquid paraffin and formation of embryoid body-like spherical tissues from mouse ES cells enclosed within these microcapsules. Biotechnol Bioeng, 99, 235, 2008.

[51] S. Sakai, I. Hashimoto, K. Kawakami. Development of alginate–agarose subsievesize capsules for subsequent modification with a polyelectrolyte complex membrane. Biochem Eng J, 30, 76, 2006.

[35] S. Mazzitelli, A. Tosi, C. Balestra. Production and characterization of alginate microcapsules produced by a vibrational encapsulation device. J Biomat Appl, 23, 123, 2008.

[36] H. Auchincloss, D.H. Sachs. Xenogeneic transplantation. Annu Rev Immunol, 16, 433, 1998.

CHAPTER 3

Bioencapsulation for cell therapy:
engineered microparticles and fibrous multifunctional
scaffolds

This chapter is extracted from the articles:

1. *"Production and characterization of engineered alginate-based microparticles containing ECM powder for cell/tissue engineering applications*"

S. Mazzitelli, G. Luca, F. Mancuso, M. Calvitti, R. Calafiore, C. Nastruzzi, S. Johnson and S.F. Badylak, Acta Biomaterialia, 2011, 7 (3), 1050-1062.

2. "*Optimised production of multifunctional microfibres by microfluidic chip technology for tissue engineering applications"*

S. Mazzitelli, L. Capretto, D. Carugo, X. Zhang, R. Piva and C. Nastruzzi, Lab Chip, 2011, 11, 1776-1785.

3.1. Engineered microparticles

Despite of many favourable properties reported in Chapter 1 and 2, alginate-based scaffolds for cell delivery and tissue engineering applications present a number of limitations that require further improvement before they can routinely be used in clinical applications. Since alginate hydrogels are extremely different (from a molecular and chemical point of view) from the cell's microenvironment, which is largely composed of extracellular matrix (ECM), biochemical interactions between the cells and the polymer is often lacking.

ECM, which is usually isolated from a variety of natural sources, including dermis, submucosa of the small intestine and urinary bladder, has been proposed as a biologic scaffold from many research groups. It is known to play an important role in modulating cell adhesion, signalling, migration, proliferation and three-dimensional array [1].

On the other hand, ECM-based scaffolds do not offer the opportunity to create an immunoisolated environment required to avoid the immune system response. Furthermore, ECM scaffolds are inherently constrained by the material properties of the tissue from which they are derived, including shape, mechanical properties and oxygen diffusion. The material properties of ECM scaffolds can also be affected by the manufacturing process (i.e. mechanical decellularization vs. chemical decellularization), the age and health status of the animal from which the ECM is harvested, and inherent biological variability. There are limited ways in which the material and mechanical properties of ECM scaffolds can be manipulated to tailor the functional properties of the device for specific applications.

Highly purified and standardized scaffold materials (i.e. alginates) are an alternative to naturally derived ECM scaffolds, all marked by uniform and reproducible mechanical and material properties. However, as reported above, alginates lack the bioactivity and constructive host tissue response characteristics of ECM- derived scaffolds.

Therefore, combining alginates with ECM may capture the advantages of

both types of materials, i.e. mechanical and material properties, which can be manipulated with the "on-demand" gelling behaviour of alginates and bioactivity, which is provided by the ECM.

The idea of combining a polysaccharidic polymer with ECM derived materials such as collagen or gelatin in a microparticle-based device for cell entrapment has been partially investigated by other research groups. Tsai et al. [2], in a short communication, described the production of gel beads containing a soluble (purified and reconstituted) form of collagen in alginate, which in this respect does not offer a solid anchorage to the entrapped cells. In a second paper, Del Guerra and co-workers [3] exploited the possibility of cultivating bovine pancreatic islets into commercially available macroporous gelatin-based microcarriers (Culti-Spher- S) before encapsulation in alginate-based microcapsules. In this respect, it is important to underline that commercial products are not easily distinguished by composition: manufacturers only say that the microparticles are produced by cross-linked gelatin, without giving technical details about the cross-linking procedure or the cross-linker residues ultimately present. In addition, the authors stated that they encountered serious problems with the microcarrier loading procedure. In fact, only about 50% of the dispersed islet cells were embodied within the microcarriers. In addition, the islets within microcarriers-in-alginate-microcapsules released an amount of insulin which was only about 60% of that secreted by islets directly within alginate microcapsules.

In an attempt to reconstitute the cell environment within an immunoisolatory device for cell immobilization in a much more controlled, biocompatible and cell-friendly environment, we tested the feasibility of entrapping a powder form of ECM, isolated and purified from urinary bladder (urinary bladder matrix; UMB) [4], together with living Sertoli cells (SCs), in alginate-based microparticles. This is a relatively new approach, completely different, in terms of innovation, design and production strategy, from those above reported. SCs were selected as the cell model since they have been recognized as playing important roles at different levels, as described in Chapter 2.4.1.

The specific aims of the study were to demonstrate that the inclusion of a powdered form of UBM: (i) does not alter the morphological and dimensional characteristics of the fabricated micro- particles; and (ii) results in an optimal substrate for in vitro culture that predictably ameliorates the viability and function of the co- entrapped cells. Alginate microparticles were applied for SC encapsulation, while extracellular matrix (UBM) was embodied within these constructs to enhance cell survival and function.

3.1.1. Materials and methods

Isolation of SCs
SCs were isolated as previously described (Chapter 2.4.1.1). After isolation, purified SC monolayers were identified by anti-Mullerian inhibiting substance (MIS) immunostaining. Cell viability was assessed, before and after encapsulation, by double staining with PI and Calcein-AM according to the manufacturer's instructions.

UBM powder preparation
The preparation of UBM has been previously described [5]. In brief, porcine urinary bladders were harvested from 6-month old 108–118 kg pigs immediately following euthanasia. The excess connective tissue and residual urine were removed. The tunica serosa, tunica muscularis externa, tunica submucosa and the majority of the tunica muscularis mucosae were mechanically removed. The urothelial cells of the tunica mucosa were dissociated from the luminal surface by soaking the tissue in 1.0 N saline solution. The resulting material, which was composed of the basement membrane of the urothelial cells plus the subjacent lamina propria, was referred to as urinary bladder matrix (UBM). UBM sheets were placed in a solution containing 0.1 vol.% peracetic acid (Sigma), 4 vol.% ethanol (Sigma) and 95.9 vol.% sterile water for 2 h. Peracetic acid residue was then removed with two 15min phosphate- buffered saline (pH 7.4) washes, followed by two washes with sterile water for 15 min each. The decellularized UBM sheets were then lyophilized using an FTS Systems Bulk Freeze Dryer

Model 8-54 and comminuted to a particulate form using a Wiley Mini Mill.

Preparation of engineered alginate microparticles

The preparation of engineered alginate microparticles was performed with minor modification of previously reported method, by a gas-driven monojet device (Chapter 2.2). Depending on microparticle type, the gas-driven monojet device was fed with: (i) alginate dispersions in water (0.5–3.0%, w/v); (ii) alginate dispersions containing SC (4–12x10^6 cells ml$\square$1); (iii) alginate dispersions containing UBM powder (0.5–1.5%, w/v); and (iv) alginate dispersions containing SCs plus UBM powder (Fig.1).

The dimensional and morphological characterization of engineered alginate microparticles was performed as reported in Chapter 2.

The optimization of the preparation procedure of engineered alginate microparticles was evaluated by design of experiment (DoE) approach (Chapter 2.2.1.1), studying the effect and the influence of the different experimental parameters: "height", "gas" and "pump" (Table 1).

Reverse transcription–polymerase chain reaction (RT-PCR) analysis

Total RNA was isolated from SC by Invisorb Spin-cell RNA mini-kit (Invitek GmbH, Berlin, Germany). Reverse transcription (RT) was performed by RevertAid^{tm} H Minus First Strand cDNA Synthesis kit (Fermentas, Canada). Oligos sequences used are listed as forward then reverse, 5' to 3': β-actin 5'-ATGGTGGGTATGGGTCAGAA-3' and 5'-CTTCTCCATGTCGTCCCAGT-3' amplify a product of 123 bp; Mullerian Inhibiting Substance (MIS) 5'-GCGAACTTAGCGTGGACCTG-3' and 5'-CTTGGCAGTTGTTGGCTTGATATG-3' amplify a product of 75 bp; indoleamine 2,3 dioxygenase (IDO) 5'-ATGAAGGCGTTTGGGACACC-3' and 5'-GAGGAATCCAGCAGCAGAGC-3' amplify a product of 140 bp; Transforming Growth Factor β 2 (TGF β2) 5'- AATGTTGTTGCCCTCCTACG-3' and 5'-TGCTATGCTGG GTGTCAGAG-3' amplify a product of 140 bp; c-kit receptor also called Stem Cell Factor Receptor (c-kit) 5'-ACAAATCCATGCCCACACCCT-3' and 5'-TTAAGCCGTATGCAGTGGCCTC-3' amplify a product of 293 bp; Laminin 5'-CCGCCTTCTGGATGAACTG-3' and 5'-CCGCCACACTCTGTCTCG-3'

amplify a product of 114 bp; Laminin receptor 5'-ATGCCTGACCTCTACTTCTAC-3' and 5'-ACCTTCGGACCAATCTGC-3' amplify a product of 162 bp; Integrin α-6 5'-CGGCTGTGGCTGCTCTAC-3' and 5'-TCTCTGGTGTCCAAGTTGAAGG-3' amplify a product of 74 bp, Integrin β 1 5'- CAAGCGAGCCGAGGACTATC-3' and 5'-GCTGGTGTTGTGCTAATGTAAGG-3' amplify a product of 198 bp; Clusterin 5'-ATCTCGGACAAAGAGCTCCA-3' and 5'-TTGCGCTCTTCATTTGATTG-3' amplify a product of 128 bp; Transferrin 5'- CAGCAGAACACTGACGGAAA-3' and 5'-CTCCTCAGCAACACAGGTCA-3' amplify a product of 186 bp; c-kit ligand also called Stem Cell Factor (SCF) 5'-GATGCCTTCAAGGATTTGGA-3' and 5'-ATGGAATCTGAGGCCTTCCT-3' amplify a product of 182 bp; type IV Collagen 5'-CACACGCCTTCCCTCCTG-3' and 5'-GAACCACGACGCCTTTGC-3' amplify a product of 90 bp. RT-PCR analyses were performed in the Mx3000P® Instruments (Stratagene, CA) in a total volume of 20 μl reaction mixture following the manufacturer's recommendations, using the Brilliant® SYBR Green QPCR Master Mix 2x (Stratagene, CA) and 10 μM of each primer using the dissociation protocol. Negative controls contained water instead of first-strand cDNA. Each sample was normalized on the basis of its housekeeping gene (β-actin). The relative gene expression levels were normalized to a calibrator that was chosen to be the control sample (untreated). Final results, expressed as relative expression, were calculated by MxPro™ software (Stratagene, CA).

3.1.2. Results

Production of engineered alginate microparticles containing UBM powder and SC

Encapsulation scaffolds (i.e. microparticles) for cell transplantation protocols would require a number of specific requisites, such as a spherical shape, a dimensional range usually between 200 and 600 μm, good mechanical stability and a suitable extracellular microenvironment, with care being taken to ensure the viability of the embodied cell (eventually by also including extracellular adhesion molecules and growth factors) [6].

Keeping in mind these points, we started a series of experiments aimed at fabricating engineered alginate microparticles for tissue engineering applications, by the gas-driven monojet device, developed in our laboratory.

In Fig. 1, the general scheme depicting the preparation of alginate microparticles is reported. We designed engineered microparticles that simultaneously contained living cells (i.e. SCs) and an extracellular matrix component, namely a particulate ECM. This form of powdered ECM, consisting of UBM, could be combined advantageously with natural or synthetic polymers to create hybrid biomaterials [4].

Before the preparation of the engineered microparticles, the UBM-ECM powder, was characterized by stereomicroscopic and fluorescence microscopic analysis. The photomicrographs reported in Fig. 2 show the fibrous flakes aspect typical of the UBM powder, with a mean size usually comprised between 50 to 200 μm. It is noteworthy that UBM particles also when in comminuted form largely retain the ultrastructural, 3-D surface characteristics of the parent UBM sheets.

Therefore, suspensions made from the powdered form of lyophilized UBM into biopolymer dispersions can be successfully used in mixture with cells for the direct production of engineered alginate microparticles.
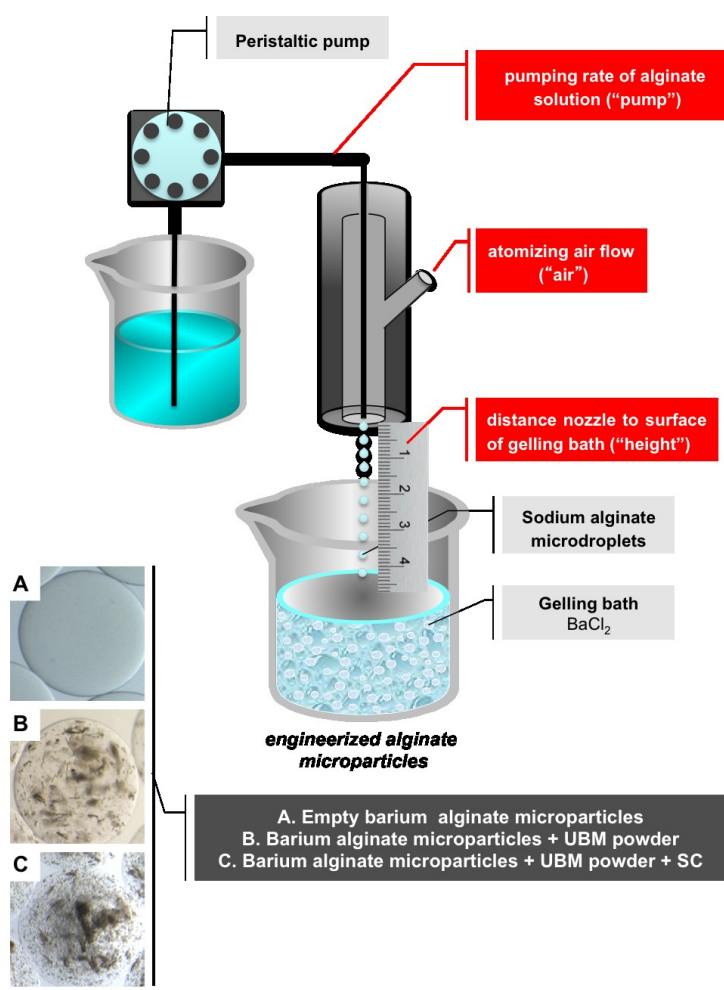
Fig. 1. General scheme depicting the preparation of barium alginate microparticles by a gas-driven monojet device. The insets present bright-field stereophotomicrographs of empty alginate microparticles (A), alginate microparticles containing UBM powder (B) and alginate microparticles containing UBM powder plus SCs (C); the bar corresponds to 260 μm. In the red boxes, the optimized experimental parameters considered for the microparticle preparation are indicated.

Alginate microparticles containing different amounts of UBM powders (Fig. 2 A-C) were produced and the effect of the presence of the powder was determined on microparticle morphology. Fig. 3 A-C shows that using UBM powder at 2.5-7.5 mg/mL (in alginate suspension) did not cause any appreciable alteration of the microparticle geometry. In addition the microparticle surface remains smooth without any signs of particle protrusion from the microparticle body.
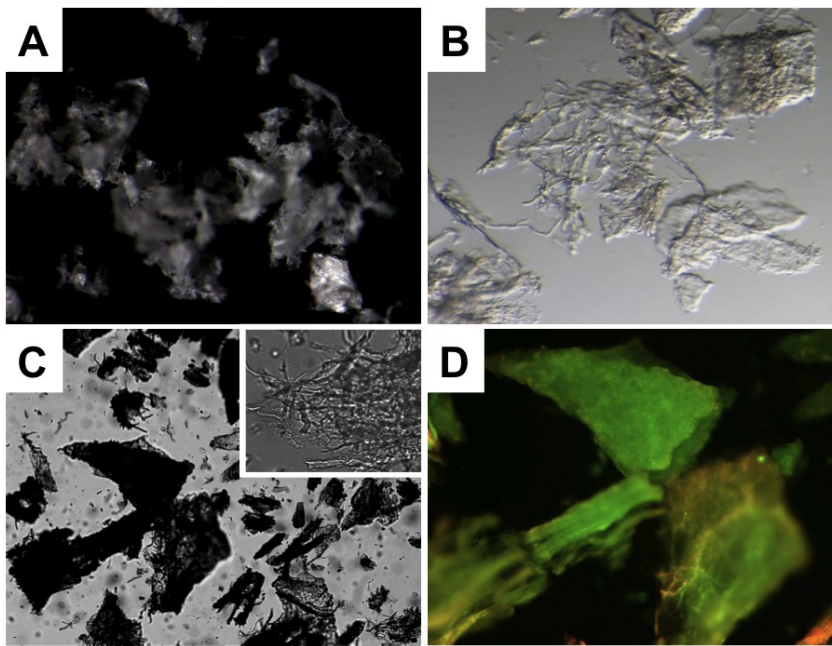
Fig. 2. Morphological characterization of UBM particles by stereomicroscopy: dark (A) and bright fields (B); by optical microscopy: bright field (C); and by fluorescence microscopy, after staining with fluorescein (D). The inset of panel C shows in detail the microfibrous structure typical of the UBM flakes. The bar corresponds to 50 lm for panels A–D and 10 μm for the inset of panel C, respectively.

Pre-pubertal Large-White piglets were used as SC animal donors. SC preparations were grown as monolayers (Fig. 3 D). After isolation, SC purity was assessed by immunostaining for MIS, as presented in Fig. 3 E. The presence of MIS has been detected in SCs of various mammals, including humans and immature mice. This cytoplasmic staining is essential to identify SC cells because, currently, there are no definitive function markers for this cell type [7]. In addition, viability of the final culture was excellent (>95%), as demonstrated by the fluorescence photomicrograph shown in Fig. 3 F.

For UBM powder, we tested the effects of different amounts of cells (4–12x10^6 cells ml$^-$1) on microparticle morphology. Fig. 3 G–I shows that in the presence of cells the geometry and surface of the microparticles remained unaltered.
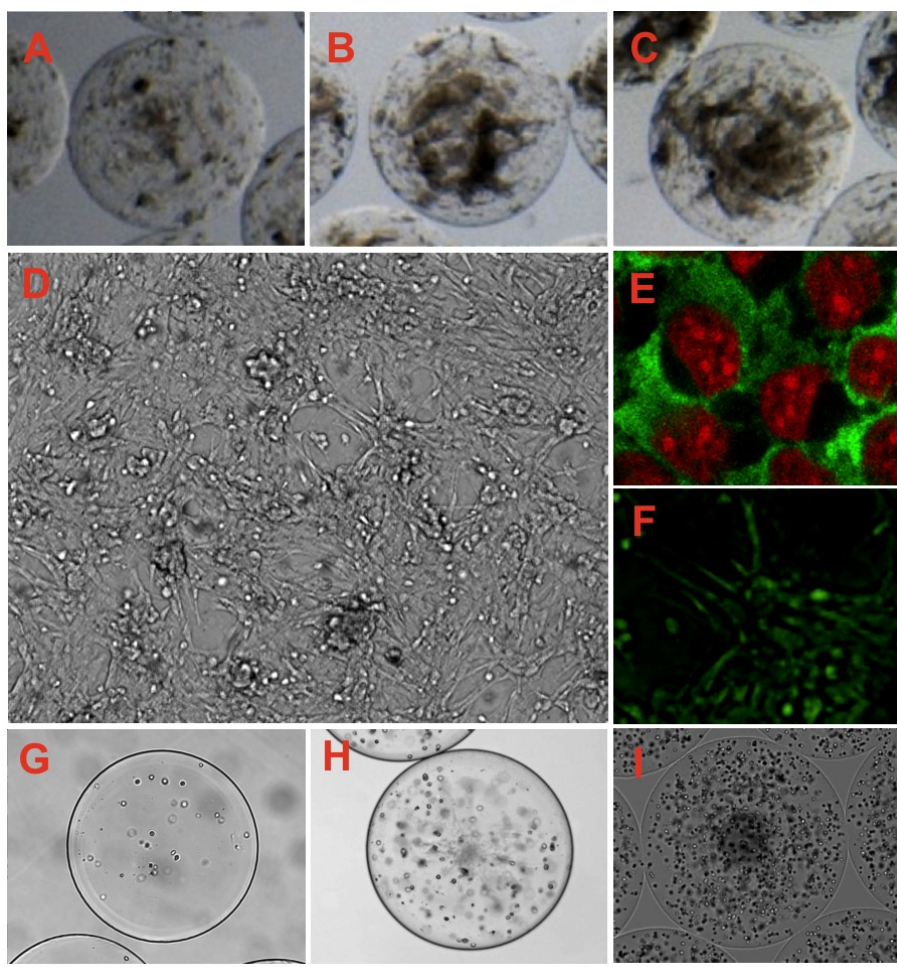
Fig. 3. Optical stereophotomicrographs of alginate microparticles containing UBM powder (A–C), prepared by a gas-driven monojet device. The microparticles contain 2.5, 5.0 and 7.5 mg of UBM powder per ml of alginate. Optical photomicrographs of SC monolayers: (D) before encapsulation; (E) SCs after immunostaining with specific antibody for MIS; and (F) the viability of SCs after double staining with Calcein-AM and propidium bromide. (G–I) Optical stereophotomicrographs of alginate microparticles containing SCs at (G) 4.0, (H) 8.0 and (I) 12.0×10^6 cells ml$^-$1. The bar corresponds to 180, 90, 10, 40 and 180 μm in panels A–C, D, E, F and G–I, respectively.

Finally, alginate microparticles containing both UBM powder and SCs were prepared (Fig. 4 A) and characterized for size distribution (Fig. 4 B). The photomicrographs presented in Fig. 4 clearly indicated that the combined presence of UBM and SCs, at the tested concentrations, did not cause any morphological alterations of the microparticles, which presented with smooth and regular surfaces. Likewise, as indicated in Fig. 4, SCs were uniformly distributed throughout the entire microparticle volume.
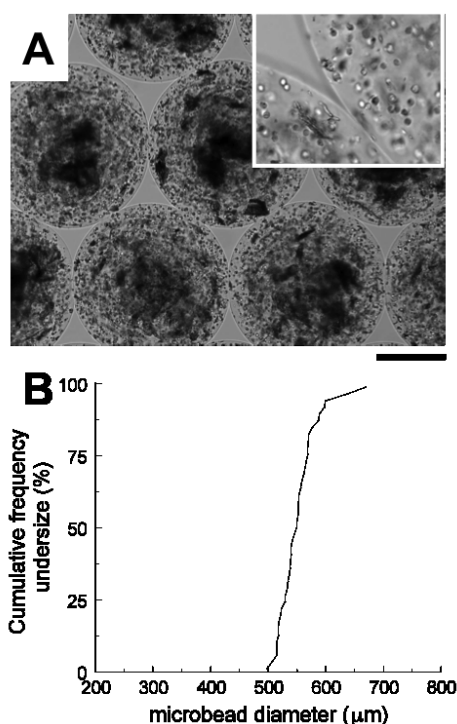
Fig. 4. Optical micrographs of alginate microparticles containing UBM powder plus SC (A). The inset presents an image at higher magnification showing the detail of the smooth microparticle surface. (B) Cumulative size distribution analysis of optical micrographs of alginate microparticles containing UBM powder plus SCs. The bar corresponds to 220 μm in A and 70 μm in the inset, respectively.

Nevertheless, in order to gather further information about the possible effects of UBM powder and SCs on microparticle production, a statistical experiment design was also planned.

Effects of the operating conditions on microparticle characteristics: DoE approach

Microparticle production was performed following the DoE approach (Chapter 2.2.1.1). The parameters "height", "gas" and "pump" (Table 1) were chosen as variables and tested at three levels, resulting in 27 possible combinations, to give a full factorial design. In our case, we selected fewer experiments by a randomized CCF design, which requires fewer trials (namely, 14). We also added three centre points in order to get estimation figures of the experimental error. In Table 2 the complete list of experiments for the CCF study is reported. In this way, we obtained a response surface modelling.

Table 1. Production of barium alginate microparticles by mono gas-jet device: investigated experimental parameters and their range of variation.

Parameter	Abbreviation	Meaning	Range
nozzle-to-gelling bath distance	height	the distance between the nozzle of the mono gas-jet device and the surface of aqueous barium chloride solution used to promote the ionotropic gelation of alginate	32.0-44.0 mm
atomizing gas	gas	the flow of atomizing gas causing the transformation of sodium alginate solution into microdroplets	3.8-5.8 L/min
feeding rate	pump	the pumping rate of alginate solution to the inlet of mono gas-jet device	0.38-0.52 mL/min

The multiple linear regression (MLR) equation (Eq. 1) for the responses of the chosen model is reported below:

$$y_i = Constant + A_1F + A_2P + A_3H + A_4F_2 + A_5P_2 + A_6H_2 + A_7FP + A_8FH + A_9PH$$

where *constant* is the mean of the seventeen runs and A_i the regression coefficients of the factors and their interactions.

The three-dimensional graphs of the investigated factors are presented in Fig. 5, which shows the influence of factors on "mean diameter" (panels A–C) and "SD" (panels D–F).

By examining the results presented in Table 3 and Fig. 5, the main finding was that a change in the factor "gas" from a low to a high level (from 3.5 to 4.5 L/min) resulted in a strong decrease of response "mean diameter", which decreased from over 600 to around 450 μm. In addition, the increase in "gas" was beneficial for the response "SD", which was progressively lowered.

The factor "pump" was associated with only marginal influence on the response "mean diameter", which declined slightly with increasing pump values. In contrast, this factor plays an important role in the microparticle size distribution, its high and low levels causing a marked increase in the response "SD".

Finally, the factor "height" appeared to exert minor effects on both responses, showing an effect at its upper level, on the microparticle size.

Table 2. Experimental design matrix and results of the DoE (design of experiments) approach for of engineered alginate microparticles containing ECM powder.

Run	Factors			Responses	
	Air (L/min)	Pump (mL/min)	Height (cm)	Mean Diameter (μm)	SD
#1	3.5	0.45	3.2	606.0	43.8
#2	4.5	0.45	3.2	459.0	17.2
#3	3.5	0.55	3.2	606.0	48.6
#4	4.5	0.55	3.2	455.0	23.7
#5	3.5	0.45	4.0	650.0	22.8
#6	4.5	0.45	4.0	454.0	18.5
#7	3.5	0.55	4.0	638.0	23.2
#8	4.5	0,55	4.0	442.0	36.2
#9	3.5	0.50	3.6	644.0	22.3
#10	4.5	0.50	3.6	438.0	23.3
#11	4.0	0.45	3.6	552.0	33.7
#12	4.0	0.55	3.6	488.0	39.8
#13	4.0	0.50	3.2	524.0	21.8
#14	4.0	0.50	4.0	538.0	36.3
#15	4.0	0.50	3.6	547.0	26.7
#16	4.0	0.50	3.6	551.0	33.8
#17	4.0	0.50	3.6	553.0	32.8

In order to assess the validity and the significance of the DoE model, an analysis of variance (ANOVA), was performed. This demonstrated that all the obtained experimental data fitted well the model, indicating its good reproducibility. In addition, in Table 3 are reported the results obtained for R^2 and Q^2, which respectively represent the percentage variation of the response explained by the model and that predicted by the model. The high values of both coefficients indicate that the model has good validity (R^2) and a significant power of prediction for new data (Q^2).
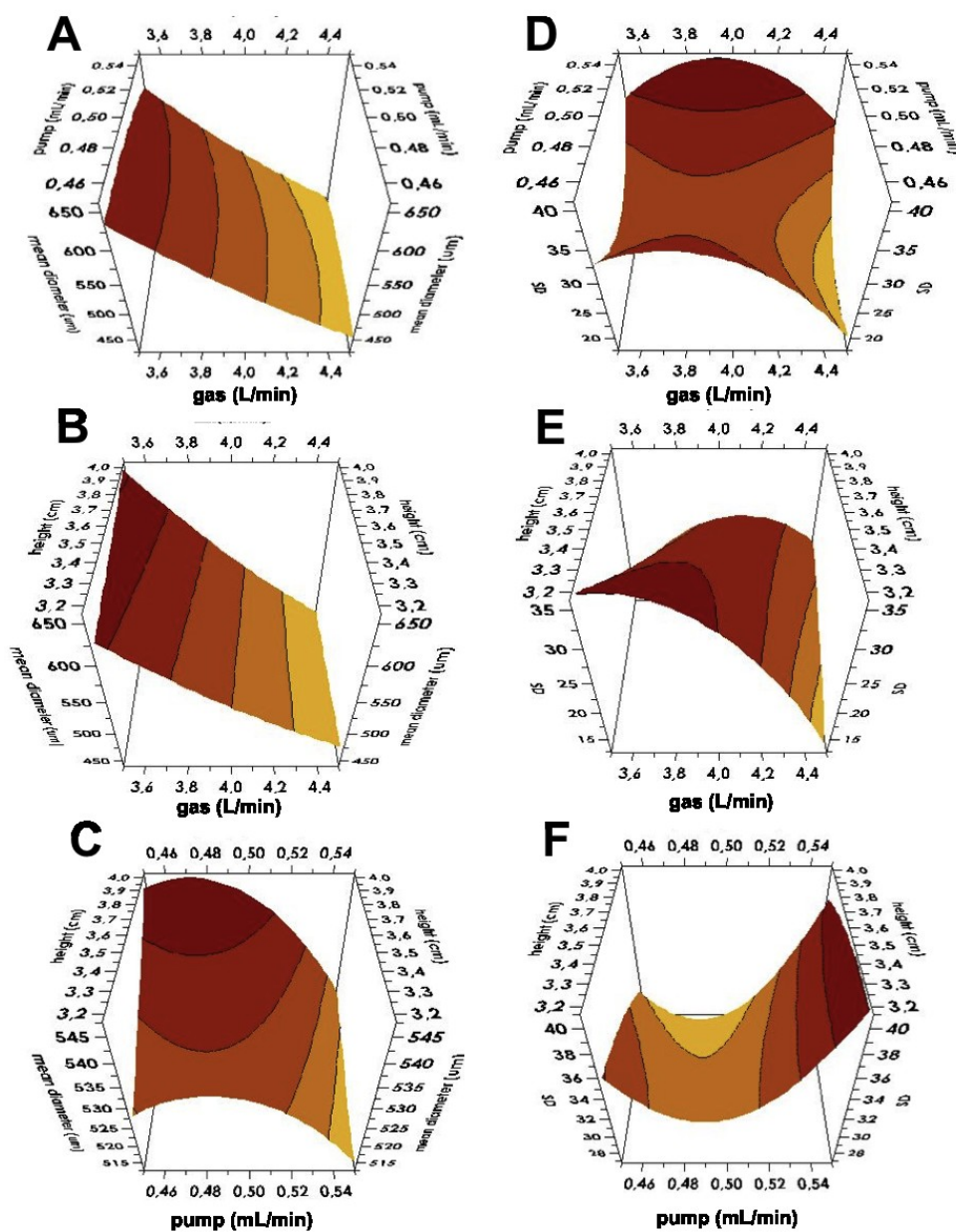
Fig. 5. DoE analysis for alginate microparticles containing UBM powder. Surface plots of the responses ''mean diameter'' (A–C) and ''standard deviation'' (D–F) for the interactions between gas and pump (A, D), gas and height (B, E), and pump and height (C, F). Factors, levels and responses employed for the DoE analysis are presented in Table 2.

Table 3. ANOVA analysis of variance of the model for DoE approach

	N	R^2	R^2Adj.	Q^2	Model validity	Reproducibility
Mean diameter	17	0.97	0.93	0.81	0.62	0.99
SD	17	0.76	0.41	0.61	0.81	0.72

N is the number of experiments; R^2 is the percent of the variation of the response explained by the model; R^2 Adj. is the fraction of the variation of the response explained by the model adjusted for the degree of freedom; Q^2 is the percent of the variation of the response predicted by the model.

Effect of UBM powder on the viability of SCs entrapped in engineered, alginate-based microparticles

The viability of SCs encapsulated in standard vs. engineered alginate microparticles containing UBM powder was investigated.

The fluorescent photomicrographs recorded immediately after the encapsulation (presented in Fig. 6 A and D) indicated that the cells were highly viable (>95%) for both standard and engineered microparticles (containing UBM). As indicated also by the bar plot presented in Fig. 6 G, after 24 h of cell culture, the viability of SCs remain very high (>85%). Significant differences between the viability of SCs encapsulated in standard vs. engineered microparticles became evident at day 7 (Fig. 6 B and E) and even more so at day 14 (Fig. 6 C and F) of encapsulation, assumed as day 0. The viability of SCs in standard vs. engineered microparticles is indeed significantly different being 65 vs. 79 and 45 vs. 65%, respectively, at days 7 and 14 ($p < 0.0001$).

These data clearly indicate that the viability of SCs encapsulated in engineered microparticles (containing UBM) increased. This effect was possibly due to the presence of individual UBM components in the same relative amounts existing in nature and in an ultrastructural milieu similar to that of native UBM. Likely, it is the diverse combination of both the structural and functional components present within UBM scaffolds that accounts for the success of UBM-based biomaterials. For instance, UBM has been shown to contain adhesion molecules such as fibronectin and laminin, the proteoglycan decorin and the glycoproteins biglycan and entactin [4].
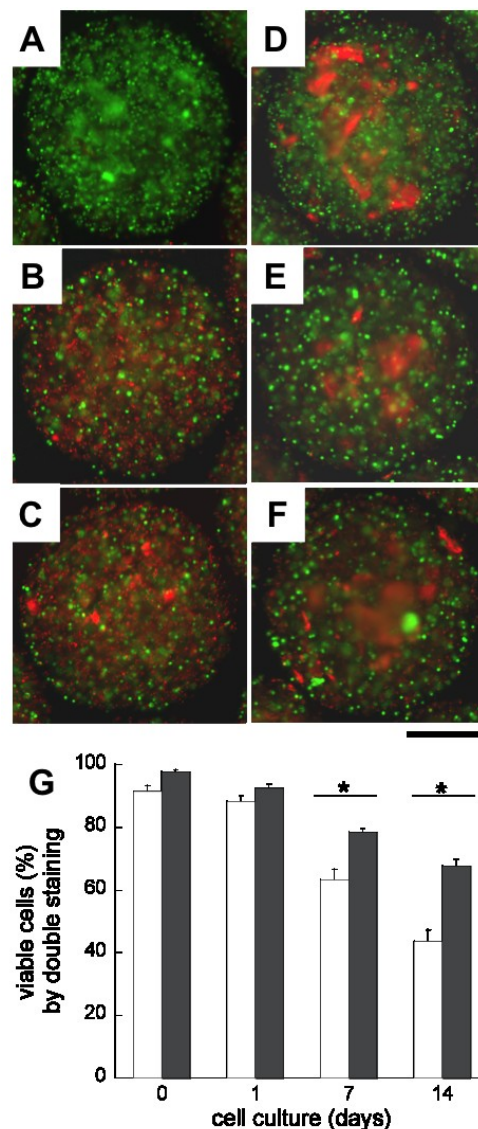
Fig. 6. Fluorescence micrographs of SCs encapsulated in alginate microparticles (A, B, C) and in alginate microparticles containing UBM powder (D, E, F) after a double-staining assay with Calcein-AM and propidium bromide, determined at days 0 (A, C), 7 (B, E) and 14 (C,F) of cell culture. The bar corresponds to 180 lm. The histogram plot of panel G reports the percentage of viable cells (by double staining) determined at days 0, 1, 7 and 14 of cell culture, for SCs encapsulated in alginate microparticles (open bars) and SCs encapsulated in alginate microparticles containing UBM powder (closed bars). Values are expressed as percentage of viable cells with respect to day 0 (rated to 100%), and represent the mean of five independent samples analysed in quadruplicate ±SD (*p < 0.0001).

Effect of UBM powder on the functions of SC entrapped in engineered

alginate microparticles.

In order to investigate whether the presence of UBM components, in powder form, in alginate microparticles could influence the cell function of the

embedded SCs, expression levels of a number of selected genes were analysed by quantitative real-time PCR. The gene expression of SCs encapsulated into plain alginate microcapsules was compared to SCs encapsulated into engineered microparticles (containing UBM) (Fig. 7).

To collect general evidence about the effect of UBM on SC function, different genes were studied, with special regard to those related to biomedical applications of SCs. Three different categories were considered, namely: (i) genes that support the maintenance of differentiated phenotype (MIS, IDO); (ii) genes related to cell growth and viability (TGF-β2, c-kit, clusterin, transferrin, SCF); and finally (iii) genes involved in the adhesion to extracellular matrix constituents (type IV collagen, laminin, laminin receptor, integrin β1, integrin α6).

The expression levels of the above-listed genes was quantified by real-time RT-PCR on reverse-transcribed mRNA isolated from SCs that were embedded in standard and engineered microparticles after 7 and 14 days of in vitro cell culture. The obtained result levels were normalized to mRNA levels of the reference gene β-actin.

Genes that support the maintenance of differentiated cell phenotypes

SC preparations were analysed for the expression of MIS. The presence of MIS has in fact been detected in SCs of various mammals, including humans. The obtained data indicated that MIS expression was not decreased by the presence of UBM (Fig. 7 A); this finding is particularly important since it clearly indicates that the embedding into alginate microparticles does not alter the typical SC phenotype and thus the differentiated status of cells. It should be remembered that MIS marker is currently the only marker used to identify SC cells because there are no other exclusive markers for this cell type [7].

To further characterize the effects of UBM on SC function, we analysed the expression of the IDO gene, since it represents a crucial enzyme. Recently, has been reported that isolated neonatal porcine SC, administered alone in highly biocompatible microcapsules, led to diabetes prevention (88% of cases) and reversion (81% of cases)   in overtly diabetic NOD (nonobese

diabetic) mice, with no need for additional beta cells or insulin therapy. The effect was associated with the restoration of systemic immune tolerance and detection of functional pancreatic islets that consisted of glucose-responsive and insulin-secreting cells. The curative effects by SCs were strictly dependent on efficient tryptophan metabolism in the xenografts, which is regulated by IDO activity [8]. For this reason, the level of IDO, which is an immune regulatory enzyme, was carefully considered.

Interestingly, IDO expression was remarkably up-regulated in SCs co-entrapped with UBM powder, which displayed a 5.5-fold increase (at day 14, Fig. 7 A) in IDO mRNA with respect to control SCs (encapsulated in plain alginate).

The positive effect of UBM on IDO suggests that SCs embedded in engineered alginate microparticles containing UBM could exert an increased ability to prevent/revert diabetes, at least in experimental animals. We plan extending the application of new SC-containing microparticles to other autoimmune disorders, e.g. experimental encephalomyelitis and cholitis, using rodent animal models.

Genes related to cell growth and viability. In addition to IDO, SCs secrete a number of proteins that are involved in the ability of SCs to inducing acquired tolerance to transplantation with no interference from the host's systemic immune surveillance system. Therefore we extended the study of the UBM activity on SC gene expression to TGF-β2 and c-kit (Fig. 7 B), clusterin and transferrin (Fig. 7 C) and SCF (Fig. 7 D). All are involved in the physiological proliferation and differentiation of germ cells [9,10] and influence the functional activity of SCs upon their transplantation. In particular, TGF-β2 was shown to modulate mesenchymal–epithelial interactions between peritubular cells and SCs [11]. The comparative mRNA expression levels for the above-reported secretion proteins was only marginally affected by the presence of UBM except for c-kit, which was slightly increased at both 7 and 14 days within engineered microparticles containing SCs.

Genes involved in the adhesion to extracellular matrix constituents. SCs are also known to produce ECM macromolecules. In vitro studies have

demonstrated that SCs synthesize laminin and type IV collagen, but not fibronectin [12]. In vivo, while the 1- and 3- laminin isoforms [13] and type IV collagen are immunolocalized in the basement membrane underlying the seminiferous tubular epithelium, upon direct contact with SCs, fibronectin is localized in the connective tissue external to the peritubular cells, and appears to be secreted by this cell type in a polarized manner. Stem cell factor receptor (c-kit or CD117) is secreted by fibroblasts, always localized in the connective tissue. Like many other ECM adhesion molecules, laminin binds to cell surface receptors of the integrin superfamily. There are an increasing number of laminin receptors, including the $\beta1$ subunit, that may be associated with $\alpha1$, $\alpha2$, $\alpha3$, $\alpha6$ or a7 and the $\beta4$ subunits, associated with either $\gamma5$ or $\gamma6$. Integrin receptors not only serve as structural receptors connecting the extracellular matrix to the cytoskeleton in order to attach the cell to their substrate, but also function as signalling receptors that lead to changes at the second messenger molecule level. Thus, the ability of ECM to influence growth, differentiation and other cell functions is likely related to its effects on signalling pathways inside the cells [14].

Interestingly, mRNA expression levels for type IV collagen (Fig. 7 D), laminin and laminin receptor (Fig. 7 E), and integrins $\alpha6$ and $\beta1$ (Fig. 7 F) were remarkably increased in SCs encapsulated in UBM, suggesting a role of the adhesion molecules present in the ECM powder form.
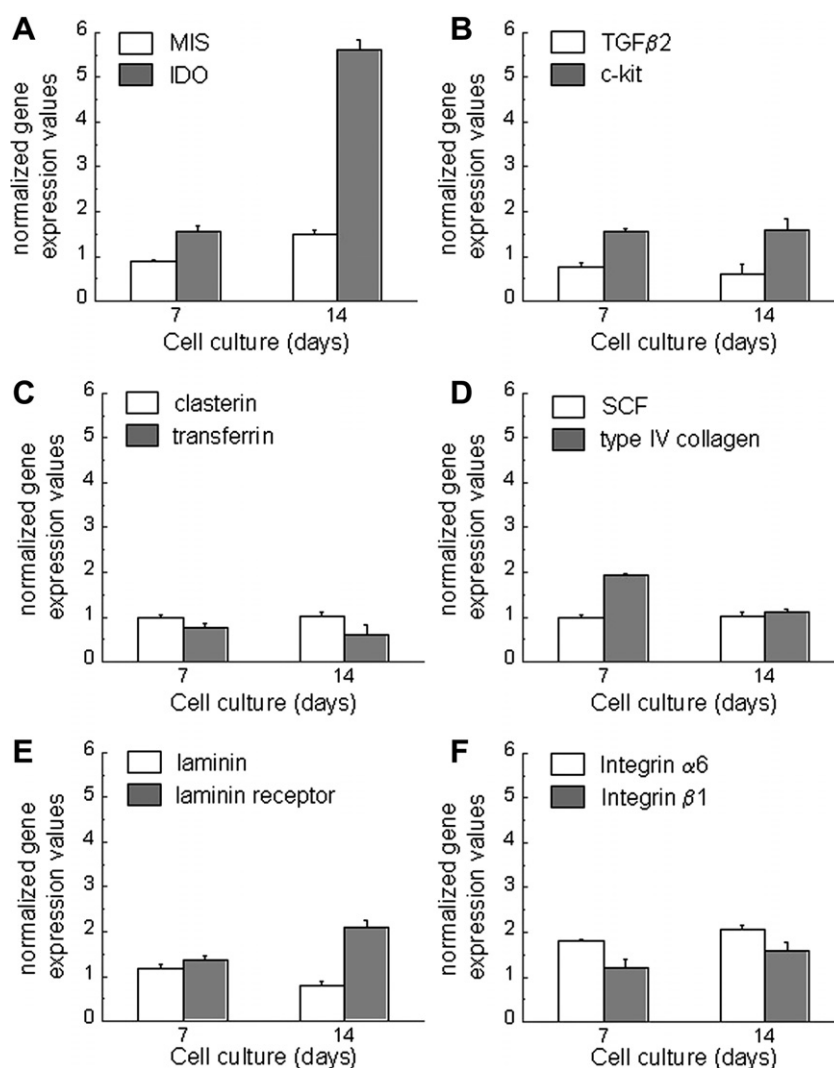
Fig. 7. Effect of UBM powder on mRNA expression levels of SCs entrapped in engineered alginate microparticles, as determined by real-time PCR. (A) MIS (open bar); IDO (closed bar); (B) TGF-β2 (open bar); c-kit proto-oncogene (closed bar); (C) clasterin (open bar); transferrin (closed bar); (D) SCR (open bar), type IV collagen (closed bar); (E) laminin (open bar), laminin receptor (closed bar); (F) integrin α6 (open bar), integrin β1 (closed bar). Data represent the mean of three determinations performed on three independent samples ±SD. The reported values were obtained by normalization, on the basis of the housekeeping gene (β-actin). The relative gene expression levels were normalized to a calibrator that was chosen to be the control samples (SCs encapsulated in alginate microbeads without UBM powder).

3.1.3. Discussion

This work confirms that the production of alginate microparticles, with highly controlled morphological and dimensional properties, by a gas-driven monojet device-based-procedure, is an important procedure for the

preparation of novel hybrid microparticles intended for cell encapsulation and tissue engineering applications.

In particular, we have demonstrated that the combined use of alginate and urinary bladder matrix resulted in a synergistic activity of both materials. While the engineered microparticles offer the mechanical and material properties of alginates, which can be varied through "on-demand" gelling procedures, UBM provides an array of bioactive functions that seem to improve the viability and function of the co-entrapped SCs.

UBM is constituted by an epithelial basement membrane on one surface and the connective tissue of the underlying tunica propria on the opposite surface [15]. This bimodal microstructure provides an ideal environment for the attachment and growth of cells. Moreover, UBM contains a variety of bioactive molecules, including cytokines and growth factors that act as potent modulators of cell behaviour. The list of growth factors is large, and includes vascular endothelial growth factor (VEGF), basic fibroblast growth factor (βFGF), epidermal growth factor (EGF), transforming growth factor beta (TGF-β), keratinocyte growth factor (KGF), hepatocyte growth factor (HGF) and platelet-derived growth factor (PDGF) [16].

In conclusion, the engineered microparticle concept presented here could be used to improve both the encapsulated cell survival and function of cells micro- and macro-encapsulated in devices fabricated for tissue engineering and cell transplantation purposes.

3.2. Fibrous multifunctional scaffolds

Scaffolds in a fibrous form could be an appealing alternative to spherical microparticles, representing an example of scaffold with controlled physical and architectural features for tissue engineering applications. This statement derives from the fact that they can enable the guided growth, alignment and migration of cells and they could find many potential applications as small vascular grafts [17], nerve conduits [18], artificial kidney tubules [19] as well as drug release vehicles [20].

Many technologies have been developed to create fibres with well-defined physical and architectural features including melt spinning [21] wet spinning [22] electrospinning [23] and microfluidics [24]. The latest technology developments have already shown the feasibility to produce monodispersed spheres [25] microcapsules (chapter 2) and colloidal crystals [26].

Microfluidics, due to the small channel dimensions typical of microchips and the efficient mixing, allows a precise control of the dimensional and morphological characteristics of the produced microfibers, providing new routes for in situ fabrication of micro/nanofibres. However, only a few reports are found in the literature describing the use of microfluidic devices for the production of polymeric microfibres. For instance, a recent report presented a method to produce poly(lactic-co-glycolic acid) (PLGA) microfibers within a microfluidic chip for the generation of 3D tissue engineering scaffolds [27]. Changing the flow rate of PLGA solution and of the sheath flow, it was possible to obtain microfibres with diameters ranging from 20 to 230 μm. Using a similar flow configuration (i.e., a coaxial flow channel) a novel cylindrical channel microdevice that generated coaxial flow without using a glass microcapillary or complicated silicon processing was recently developed by Kang and colleagues for the fabrication of microfibres [28]. Microfibres were fabricated without clogging the downstream channel, and the dimensions of the fibres were successfully controlled by regulating the flow rate through the channels. The generation of alginate microfibers with a roller-assisted microfluidic system was also reported [29]. This work used a

convenient microfluidic strategy with a simple and minimal-requirement design for the generation of uniformly sized alginate gel fibres that were collected with a rotor. In addition, Shin and colleagues reported the use of a poly (dimethylsiloxane) (PDMS) microfluidic device embedded capillary glass pipette as an apparatus for fibre generation [30]. Sodium alginate (sample flow) and $CaCl_2$ (sheath solution) were used, and the final fibre diameter was varied by changing both flow rates.

In addition, new technique for the control of inner and outer diameters of calcium-alginate hydrogel hollow microfibres, was also reported, using a coaxial triple cylinder. Aqueous solutions of dextran (core solution), sodium alginate (sample solution) and $CaCl_2$ (sheath solution) were extruded simultaneously from the inner, intermediate and outer cylinders, respectively [31].

While the control of dimensional characteristics are crucial for the possible implantation of such tissue engineering scaffolds, there are other important aspects to address for the final in vivo applications of fibrous, scaffolds, as cellular adhesion, proliferation and tissue formation are greatly influenced by the scaffolds' physical properties such as surface roughness, porosity, flexibility and three-dimensional geometries. As already discussed already for mircrocapsular scaffolds (Chapter 1 and Chapter 2) the surface roughness of the tissue engineering device can affect the scaffold in vivo effectiveness, since irregularities of biomaterial surface can promote cell adhesion of immune host cells, causing the so called cellular overgrowth and the decrease of diffusion rate.

The dimensional homogeneity of microfibres is also an important issue since the device thickness is crucial in controlling the rate of exchange of nutrient and bio-regulatory product (such as hormones and growth factor) in and out the tissue engineering device. Despite the important role played by morphological characteristic of the fibres on their in vivo applicability, the dimensional homogeneity and the surface smoothness of the produced scaffold are not evident from the previous mentioned papers. In order to address this issue, a simple but milder microfluidic production strategy, that

does not imply the use of either sheath flow or rotating roller, was applied for the generation of alginate based microfibres with different diameters and characterized by an uniform size and a smooth surface. Moreover in order to increase the encapsulated cell viability and to reduce of the foreign body response, engineered microfibres were considered.

Recent findings demonstrated that co-encapsulation of cells and drug delivery systems (DDS) offered a rational alternative to reduce the foreign body response to the encapsulating scaffold, favour retention of the cell viability, functional competence and therefore enhances the effectiveness of the tissue engineering construct [32]. Based on the promising results showed by this strategy, we used a microfluidic dispersing platform for the simultaneous immobilization, within the hydrogel matrix, of living cells together with other particulate DDS.

For the construction of microfluidic devices, glass was preferred to polymers such as PDMS and PMMA, since it offers good optical properties and the possibility to easily sterilize the devices, by autoclaving. Owing to its high biocompatibility and biodegradability we chose alginate as polymer for the production of scaffolds. Considering the different applications of biomaterial based-scaffolds in terms of implant site and animal size, it is important to have the possibility to finely regulate the size and mechanical properties of the device.

In this respect, aims of the present work were the production of alginate microfibres and the investigation of the effect of microfluidic chip geometry and experimental parameters, including polymer concentration and composition, on the morphological and functional characteristics of engineered microfibres for cell transplantation. Using microfluidic technique the production of engineered microfibres containing cells and drug delivery systems was performed while the fibre diameters and content (amount of cell and DDS) were controlled on demand.

3.2.1. Materials and methods

Production of glass microfluidic chips

A photolithography-wet etching procedure was used for the fabrication of glass microchips (Fig. 8 A) [33]. Briefly, the channel network was designed using AutoCAD software, and a film negative of the desired size was prepared by a commercial photo mask producer (J.D. Photo Tools, UK) to form the optical mask. Crown white glass (B-270) photolithographic plates (thickness of 1.5 mm) coated with a thin chromium metal mask layer plus an upper layer of positive photoresist (AZ1500), supplied by Telic (Telic, USA), were used for channel network fabrication. With UV exposure, the pattern of interconnecting channels was transferred from the optical mask to the photoresist layer which was then developed and removed, together with the chromium layer, to reveal the channel areas of glass to be etched. Once the pattern had been transferred, the glass plate was baked in oven overnight (~17 h) at 80°C to dry and harden the mask on glass. The channels were then etched using 1% hydrofluoric acid (Sigma-Aldrich, USA) buffered with 5% ammonium fluoride (Sigma-Aldrich, USA) solution at 65°C, under ultrasonic agitation (Ultrasonic Cleaner, VWR, UK). Before the bonding step the cross section profile of the etched microchannel was measured by a surface profiler (P-16+ stylus profiler, KLA Tencor, U.S.A.). Finally, the etched glass was thermally bonded (595 °C for 3 h) with a top plate of the same material into which outlet and inlet holes had been previously drilled to link the channels. TEFLON tubes (Upchurch Scientific, Oak Harbor, WA) with an inner diameter of 0.75 mm connected the microchip to a syringe. Teflon tube with different internal diameter vary from 210 to 700 µm were connected with the outlet. Fluidic reagents were introduced to the microfluidic network from glass gastight syringes (Hamilton, Reno, NV) by syringe pumps (model KD100, KD scientific Inc., Holliston, MA).
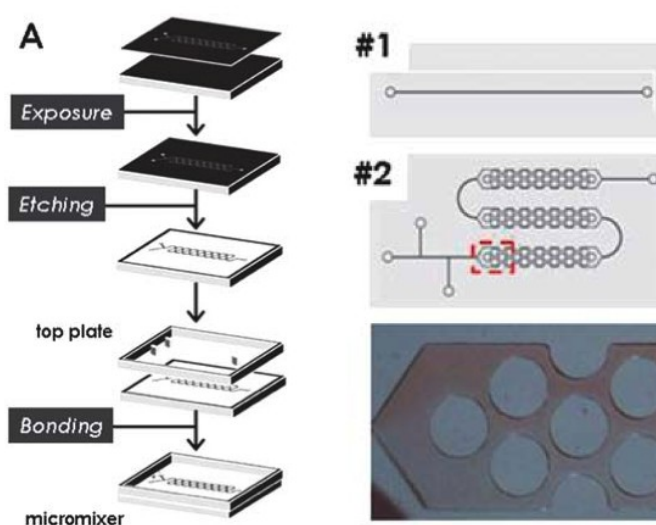
Fig. 8 Schematic representation of the fabrication procedure for glass microfluidic chips. Chip fabrication strategy and two microchip designs, Chips #1 and #2.

Production of drug delivery systems (DDS)

The materials used for the preparation of DDS included cellulose acetate (CA) CA-398/10-NF from EASTMAN (Tennessee USA), acrylic resin Eudragit® RS 100 (Eudragit RS) from Rohm Pharma GmbH (Germany), lipid mixture (glyceryl tristearate/glyceryl monostearate) from Fluka (Buchs, Switzerland) and Corn oil from Gattefossé (SaintPriest Cedex, France). For the preparation of coloured microparticles, oil red O and Sudan black from Fluka (Buchs, Switzerland) were used as dyes. CA microspheres (CAM) and Eudragit RS microspheres (ERSM), liposperes (LS) and corn oil based-emulsion (COBE) were prepared following the experimental procedures described in the supplementary information. CAM were prepared by solvent evaporation technique [34], ERSM by an in-liquid drying process from an oil-in-oil system [35], LS by melt dispersion technique and COBE by a microfluidic flow focusing technique [36,37]. Drug release experiments were performed as previously described [38]. Briefly, 20-25 mg of DDS were poured into a dialysis tube (molecular weight cut-off 10,000-12,000), then placed into 100 mL of isotonic borate buffer. Afterwards, samples were withdrawn at regular time intervals from the receiving buffer. The amount of release drug was determined by reverse-phase HPLC. Two cell types, namely Wharton's Jelly Mesenchymal Stem Cells (WJMSCs, isolated as

described in Chapter 2.3.1) and human myeloid leukemia K562, were used for the production of multifunctional alginate microfibre encapsulation.

Production of alginate microfibers

The polymer used was sodium alginate IE-1105 (viscosity, 20.0–40.0 cP; pH, 6.0–8.0, C = 1%, H_2O) (Inotech Biosystem International, Switzerland). For the gelation of polymer, barium chloride dehydrate (Sigma Aldrich, Germany) was employed. "Empty" and "multifunctional" (containing cells, DDS or both) barium alginate microfibres were produced with Chip #1 and Chip #2 (Fig. 1), respectively. Using Chip #1, a sodium alginate solution (1.5-2.5%, w/v), used as main constituent of the microfibres, was introduced into the inlet of the microchip at appropriate flow rates (see Table 4).

Table 4 Production of alginate microfibres by microfluidic chip technology: investigated experimental parameters and their range of variation.

Parameter	Abbreviation	Meaning	Range
outlet internal diameter	Outlet	The internal diameter of the outlet tube used to deliver the alginate solution into the gelling ionotropic bath	210-700 $\square$m
alginate concentration	Alg	The concentration of sodium alginate solution employed for the encapsulation procedure	1.5-2.5 %, w/v
$BaCl2$ concentration	barium	The concentration of the barium chloride solution employed for the microfibre gelation	0.5-3.0 %, w/v
pumping rate	pump	The pumping rate of alginate solution to the inlet of the microfluidic chip	15-35 $\square$L/min

Using Chip #2, a sodium alginate solution and two sodium alginate suspensions were delivered via the three inlets. The two suspensions contained different amounts (10-40 mg/mL) of either CAM, ERSM, LS, COBE or cell suspensions (2-9 x 10^6 cells/mL). The output from the outlet of the two chips was transferred via a Teflon microtube (with different diameters, see Table 4) into a $BaCl_2$ solution (0.5-3.0%, w/v) where the Na alginate flow stream was gelled to produce the final Ba-alginate consolidated microfibres. The produced microfibres were then examined by an optical stereomicroscope (Nikon SMZ 1500, Japan) with imaging analysis software (Eclipsenet   version   1.16.5,   Laboratory Imaging s.r.o. for Nikon

B.V.) to determine their dimensions. The mean diameter of microfibres (± SD) was obtained by taking 9 measurements along the (10 mm) length of the samples at equal interval. Each microfibre was measured in triplicate. For the determination of the gel strength, microfibres were prepared using Chip #1 equipped with a Teflon microtube (700 µm) and different $BaCl_2$ gelling solutions (0.5-3.0%, w/v). The strength of the microfibres was studied by measuring the mechanical resistances of hydrogels under compression with an Instron 1193 (Instron, Norwood, MA) mechanical testing machine. Freshly prepared microfibres were placed below the probe, which travelled toward the lower plane with a constant speed set as 0.5 mm/s. During probe displacement, the resistance of the samples to the compression was recorded at 50% compression and 75% compression. Ten microfibre samples of each batch were measured separately at room temperature.

Experimental design and statistical analysis were evaluated by design of experiment (DoE) approach (Chapter 2), studying the effect of the experimental parameters alginate (alg) and $BaCl_2$ (barium) concentrations, and pumping flow rate (pump), on the dimension and morphology of the microfibers. The Cell viability was assessed using a double staining method with propidium iodide (PI) and Calcein-AM26 before and after encapsulation in alginate microfibers (Chapter 2).

3.2.2. Results

Production of alginate microfibres based on an intuitive COST approach
It is understood that there are a number of operational parameters which affect the production of multifunctional alginate microfibres and their characteristics. The optimization of the operational conditions was achieved by either a classical intuitive approach "COST" (Changing One Separate factor a Time), or a "design of the experiments" (DoE) method. Initial experiments were carried out using Chip #1 (Fig. 8 A) with the general preparation procedure reported in Fig. 9 to evaluate the robustness of both preparation strategy and device selected for the generation of microfibres of

desired lengths (> 100 cm), with a controlled and homogeneous morphology (i.e. thickness).

An initial standard-line experiment, using mid-range variable values for a combination of safe physiological conditions and process control, was used to establish the reproducibility of the device and experimental conditions.

Microfibres obtained under different conditions (see Fig. 9) possessed a uniform shape (i.e. constant diameter through the entire microfibre length) and a highly smooth surface.
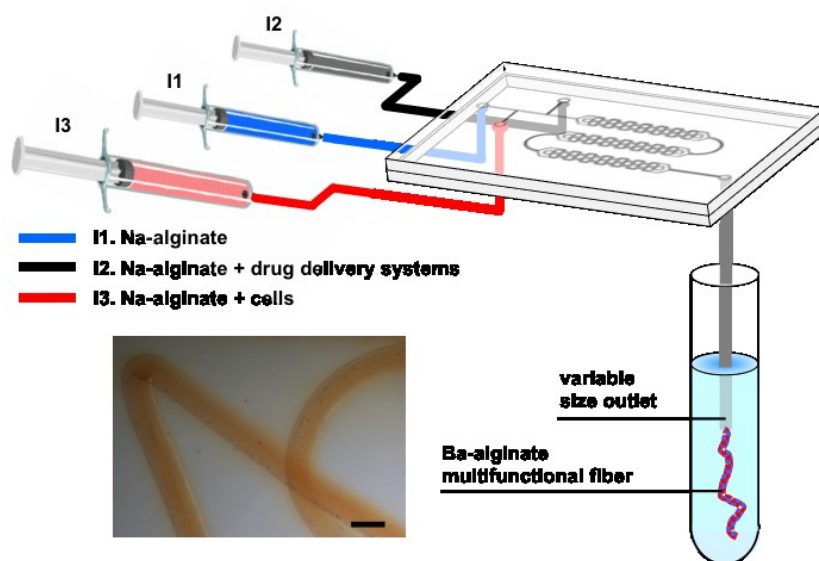

Fig. 9. Microfluidic set-up for producing multifunctional alginate microfibers and micrograph of the produced microfibers. Scale bar: 200 µm.

With respect to the microfibre surface characteristics (i.e. smoothness), as already mentioned, the surface properties of any implantable biomaterial have been recognized as key factors for its in vivo applicability and biocompatibility. The properties of a material surface, including the chemical composition, roughness and functional groups, play a significant role in determining the differential cell responses to the implants, including the host response and the inflammatory cell adhesion and infiltration.
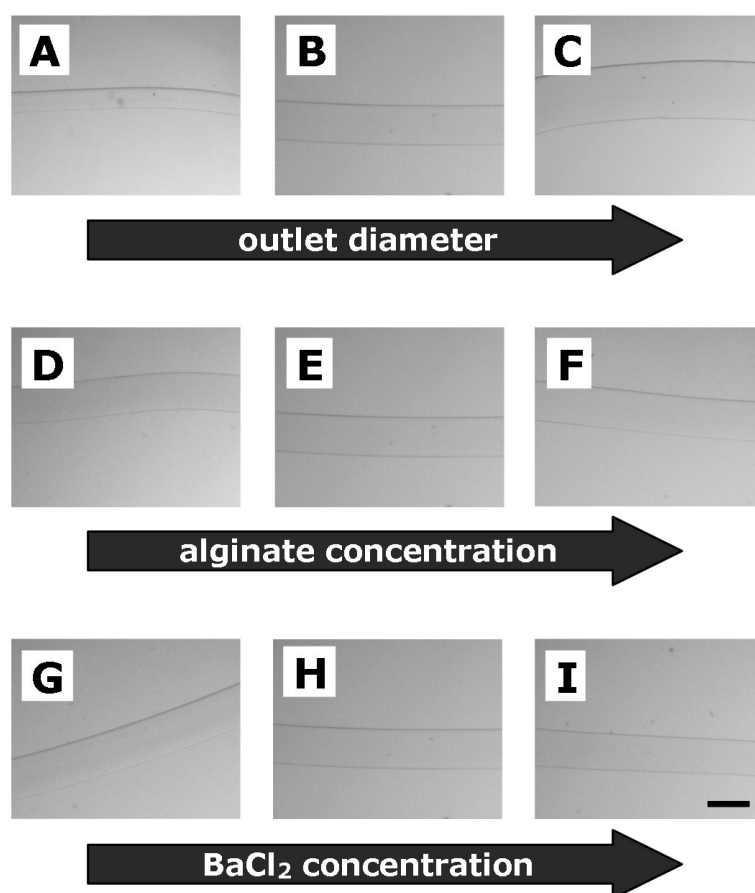
Fig. 10. Optical stereo photomicrographs of alginate microfibres, showing the effect of the experimental setup (following a COST approach) on microfibre dimension and morphology. Microfibres were produced by the single inlet linear microchip (#1). The investigated factors were: the diameter of the outlet tube (A-C) and the polymer concentration (D-E). The complete experimental conditions are reported in Table 5. Bar corresponds to 400 µm.

Native inflammatory responses often dominate the effects of biomaterials that are intended to guide tissue repair. These responses are characterized by invasion of macrophages, which initiate a host defence program involving production of oxygen radicals and matrix-degrading enzymes.

Therefore, to preserve scaffold functionality over weeks or months, it is of paramount importance to minimize the immune response activity over the tissue environment surrounding the implanted device.

Using different outlet tube dimensions (I.D. ranging from 210 to 700 µm), the corresponding diameter of the produced microfibre, spanned from 180 to 500 µm (Fig. 10 A-C), demonstrating the capability of this system for microfibre size control. It was found that by varying the diameter of the outlet tube,

thinner or thicker microfibres could also be easily produced (data not shown). Microfibres were designed for cell encapsulation, where the size of cells or cell clusters (i.e. pancreatic islets) usually exceeds one hundred microns, the microfibres with greater diameters (>200 μm) were desired. If the fibre diameters were too small, the number of partially protruding cell/cells cluster could proportionally increase, which could also increase the probability of inflammatory response after in vivo transplantation. When changing alginate concentrations (Fig. 10 G-I), the microfibre dimension varied correspondingly, spanning from 368 to 398 μm, though the effect was not as significant as that on mechanical proprieties.

Finally, different $BaCl_2$ concentrations were also considered for the initial experiments designed by intuitive COST approach.

This choice was made since the structural and mechanical properties of ionically cross-linked alginate hydrogels largely depend on the ionic strength of the gelation medium or the ion source. When selecting a hydrogel network for a given application (e.g. tissue engineering), it is necessary to tune its properties such as gel strength, handling, surface smoothness and cell viability, through the formulation parameters. For these reasons, different $BaCl_2$ concentrations were considered, ranging from 0.5 to 3.0% (w/v).

The results are displayed in Fig. 11. As it can be seen from the plot and microphotographs (Fig. 11 A), the diameter of the obtained microfibres decreased significantly and progressively from 500 μm to 350 μm, when $BaCl_2$ concentrations increased. $BaCl_2$ influenced also significantly the mechanical properties of the microfibres Fig. 11 B shows the mechanical resistance of alginate microfibres determined at 50% and 75% compression.
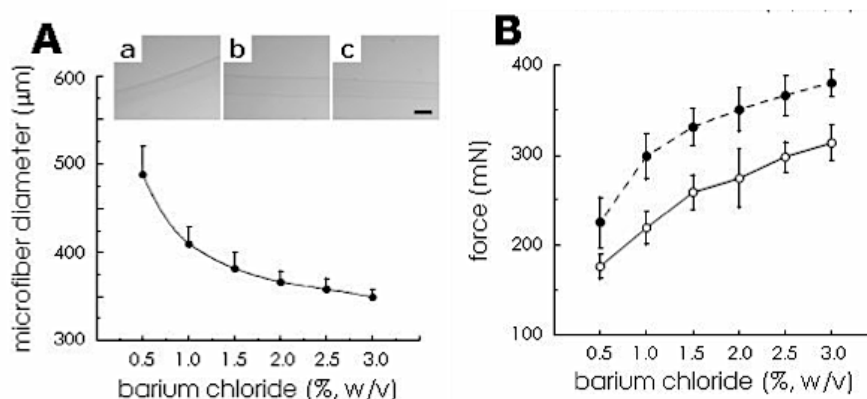
Fig. 11. Effect of barium chloride (expressed as percentage, w/v of $BaCl_2$, in the gelling bath) on the dimension (diameter) (A) and on the mechanical resistance (B) of alginate microfibres; 50% compression (open circles), 75% compression (closed circles). Ten microfibre samples of each batch were measured separately. Data represent the mean ± SD. Microfibres were produced using Chip #1 with an alginate concentration of 2 % (w/v). The insets of panel A report the optical stereo photomicrographs of microfibres obtained using 1.0 (a), 1.5 (a) and 2.0 %, w/v $BaCl_2$ (c). Bar corresponds to 370 μm.

Table 5 summarises the effect of a number of selected experimental parameters, including outlet internal diameter, alginate and barium chloride concentrations, and pumping flow rate of alginate solution on the final microfibre mean diameter. The experiments were performed using the intuitive COST approach.

Table 5 Production of alginate based microfibres by Chip #1: experimental parameters used for the COST approach.

Run	Outlet diameter	Alginate concentration (%, w/v)	$BaCl_2$ concentration (%, w/v)	Mean diameter
A	212	2.0	1.5	180 (12)
B	400	2.0	1.5	398 (12)
C	700	2.0	1.5	510 (35)
D	400	1.5	1.5	368 (22)
E	400	2.5	1.5	386 (19)
F	400	2.0	1.0	408 (24)
G	400	2.0	2.0	366 (14)

It is generally understood that concentrations of alginate and barium solutions are closely related to the cross linking extent and thus the porosity and mechanical strength of microfibres produced. These effects were examined by varying the concentration of alginate in the

range of 1.5-2.5% (w/v) and barium chloride between 1.0% and 2.0% (w/v). When the concentrations of alginate and barium chloride solutions were selected below 1.5 and 1.0 %, respectively, the resulting microfibres exhibited an insufficient mechanical strength when handling with standard procedures (e.g. by tweezers). On the other hand, when the alginate was employed at concentrations above 3%, the solution became very viscous causing difficulties to flow through the microchip channels. It was also observed that using a gelling bath containing barium chloride at concentrations above 2.5% caused severe viability impairment to the eventually present cells.

Applications of DoE approach

The DoE analysis was employed for the optimization of microfibre production based on results of COST approach.

Three experimental parameters were selected as key factors, namely, "alg" (i.e., alginate concentration), "barium" (i.e., $BaCl_2$ concentration) and "pump" (i.e., flow rate) which were tested at three levels (Table 6) resulting in 27 possible combinations in a full factorial design. By using a randomized central composite face-centred design (CCF), we selected 14 experiments with two center points in order to have an estimation of the experimental error.

The results of these experiments are reported in Fig. 11 as three-dimensional graphs showing the responses of both microfibre diameter and relative standard deviation to the three key factors. The surface plots show the inverse relationship between microfibre diameters and both $BaCl_2$ concentrations and pumping rate. Conversely, the diameter of the produced microfibre increased when the alginate concentration was increased.

However, the diameter reaches its maximum for an alginate concentration of 2.2 % (w/v). A further increase in alginate concentration caused the diameter of the microfibre to decrease. The results provided clear guidelines for selecting appropriate experimental conditions in order to obtain microfibres with desired dimensions and mechanical and biological properties.

Table 6. Production of alginate based microfibres by Chip #1: experimental design matrix and results of the DoE (design of experiments) approach[a].

Run	Factors			Responses	
	Alg (%, w/v)	$BaCl_2$ (%, w/v)	Pump (mL/min)	Mean Diameter (μm)	SD
#1	1.5	1.0	15	372	30
#2	2.5	1.0	15	368	9
#3	1.5	2.0	15	350	25
#4	2.5	2.0	15	359	15
#5	1.5	1.0	35	399	11
#6	2.5	1.0	35	372	32
#7	1.5	2.0	35	368	16
#8	2.5	2.0	35	367	20
#9	1.5	1.5	25	368	22
#10	2.5	1.5	25	386	19
#11	2.0	1.0	25	409	16
#12	2.0	2.0	25	363	12
#13	2.0	1.5	15	379	18
#14	2.0	1.5	35	402	13
#15	2.0	1.5	25	398	12
#16	2.0	1.5	25	396	13
#17	2.0	1.5	25	400	15

[a] For all the reported experiments a 400 mm I.D. outlet tube was used.

After investigating the factors and their interactions on the responses, the validity and the significance of the model was estimated by analysis of variance (ANOVA) (data not shown).

All the data obtained fitted well with the model, suggesting a good reproducibility of the studied model. We got a large regression coefficient R^2 that resulted in a necessary condition for a validity model with a significant power of prediction Q^2 .
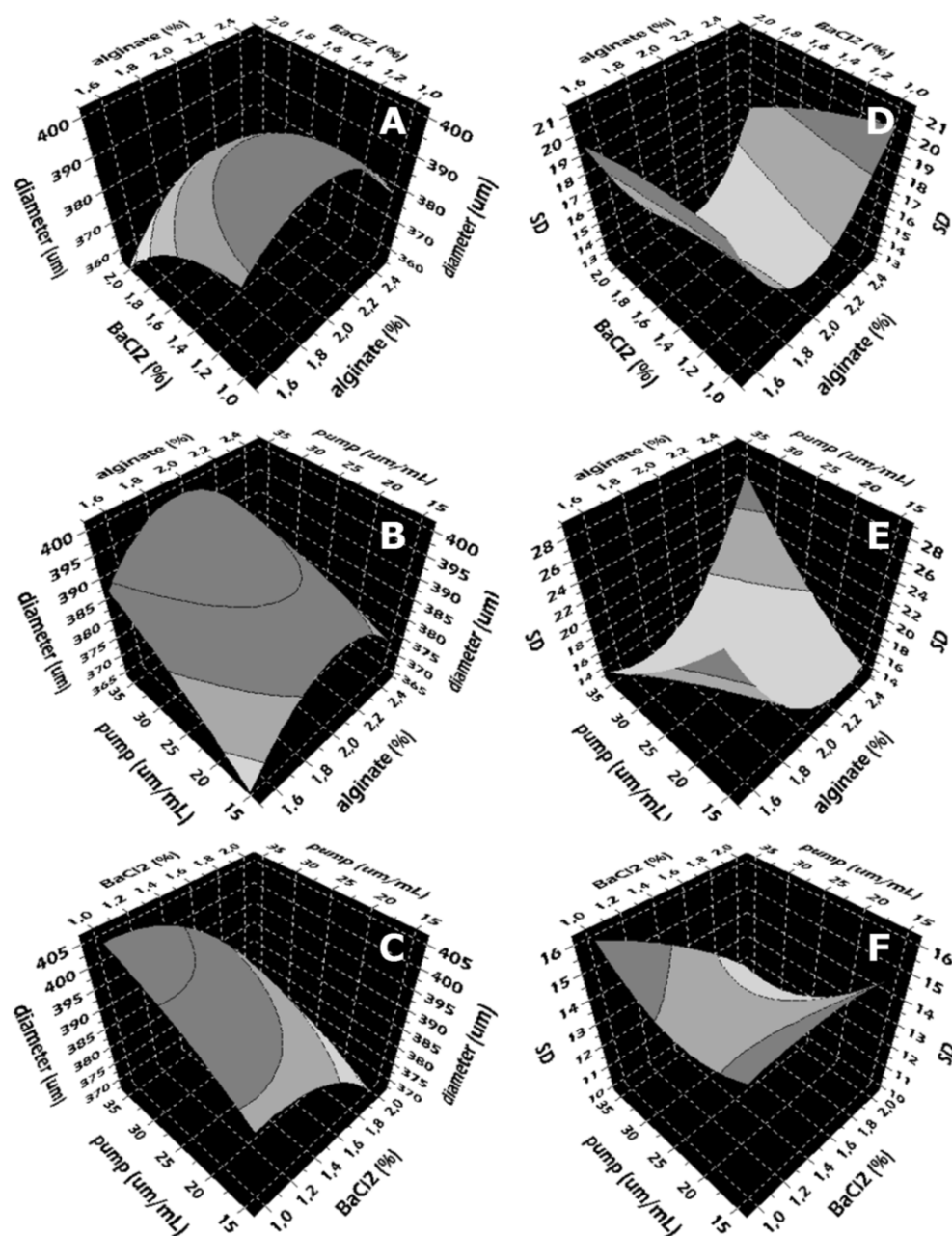
Fig. 11. DoE analysis of the alginate microfibre production. Surface plots of the responses "diameter (A-C)" and "SD" (D-F) for the interactions between "alg" and "BaCl$_2$" (A, D); "pump" and "alg" (B, E); "pump" and "BaCl$_2$" (C, F). Factors, levels and responses employed for the DoE analysis are reported in Table 6.

Production of multifunctional alginate microfibres by single channel chip

In the first set of experiments, Chip #1 was used to produce microfibres, containing different DDS or cells. The DDS included into the alginate microfibres were produced and characterized in our laboratory, namely: CAM, ERSM, LS and COBE. The experimental procedures for the

preparation of the different DDS were reported in figures 12-15. In addition, different cell types were also embedded into the microfibres, they include the human myeloid leukemia K562 (representing a stable cell line growing in suspension) and the Wharton's Jelly Mesenchymal Stem Cells (WJMSC) (representing a primary cell population isolated from the umbilical cord). Fig. 16 shows the optical photomicrographs of some examples of the produced alginate microfibres containing ERMS (A-C) or WJMSCs (D-E). In order to quantitatively evaluate the influence of the presence of DDS or cells, multifunctional microfibres were produced including variable amounts of dispersed phase. It is important to underline that, when using the single inlet chip, the homogeneous dispersion of the particulate phase (DDS or cells) within the alginate solution was accomplished by vortexing, prior to the injection into the microfluidic device. This procedure was crucial to obtain an even dispersion of particles into the final microfibre hydrogel matrix.
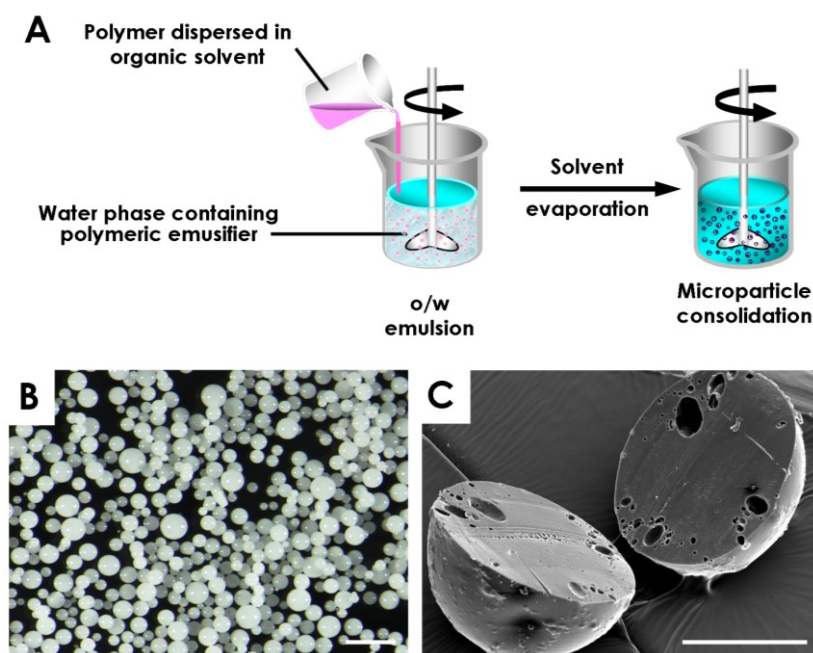
Fig. 12. Schematic representation of the solvent evaporation technique used for cellulose acetate microspheres (CAM) production. Optical stereo photomicrograph (B) and SEM image (C) of the produced CAM. Scale bars correspond to 100 (B) and 40 (C) μm. Typically, 1 to 2 g of polymer (cellulose acetate (CA) CA-398/10-NF from EASTMAN, Tennessee USA) were dissolved in 5 mL of CH_2Cl_2. The organic solution was emulsified with an aqueous phase containing hydrolysed poly(vinyl alcohol) (PVA) (Airvol 205, Air Products Corp., PA, USA) as stabilizer. The obtained emulsion was maintained under continuous stirring with a four-blade turbine impeller at 350 rpm. At different time intervals, samples were observed microscopically throughout complete evaporation of CH_2Cl_2, usually occurring in 3–5 h. Once the consolidation of CAM was complete, microspheres were isolated by filtration and extensively washed.

Different final ratios (w/v), between DDS and alginate, were tested, namely: 10 (Fig. 16 A), 20 (Fig. 16 B) or 40 mg mL^{-}1 (Fig. 16 C). Whilst, cells were added to the alginate at the ratios of 2 (Fig. 16 D) 6 (Fig. 16 E) or 9x10^6 cells per mL (Fig. 16 F).

In all cases, the inclusion of the DDS, in form of either rigid polymeric microspheres (CAM and ERSM), soft liposheres (LS) or liquid droplets (COBE) had no significant effect on the morphology, including surface characteristics, and homogeneity of microfibres.
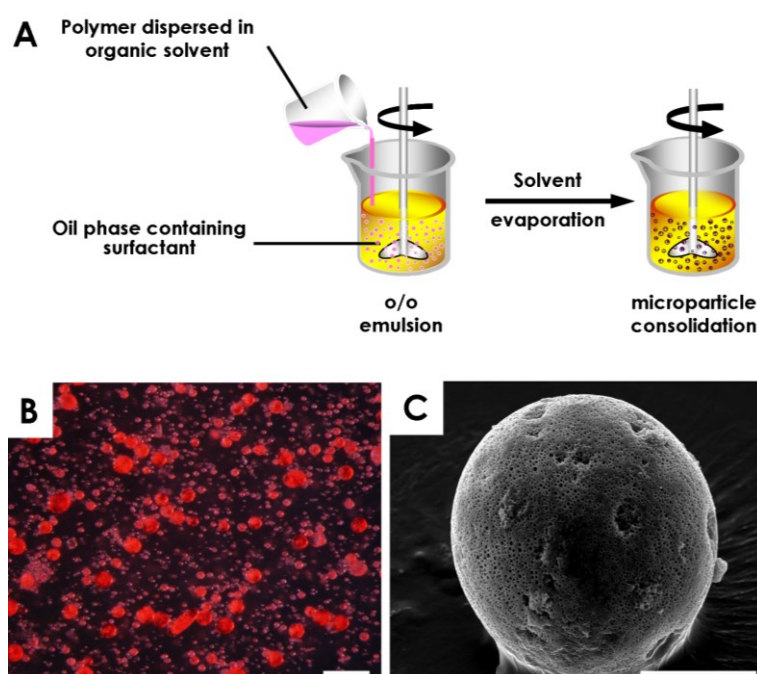
Fig. 13. Schematic representation of the "in-liquid drying process from an oil-in-oil system" technique used for Eudragit RS microspheres (ERSM) production. Optical stereo photomicrograph (B) and SEM image (C) of the produced ERSM. Scale bars correspond to 150 (B) and 40 (C) μ m. Typically, 500 mg of polymer (acrylic resin Eudragit® RS 100) were dissolved in 15 ml of CH_2Cl_2. The solution was then poured into 100 ml of light mineral oil: d=0.84 g/ml (Sigma Chemical Co., St. Louis, Missouri, USA) containing 0.5% (w/v) soybean lecithin as emulsifier. The mixture was stirred at 350 r.p.m. by a four blade turbine impeller. The system was then heated at 35°C, in order to evaporate CH_2Cl_2. After 5 hours, the microspheres were isolated by filtration, and extensively washed with n-hexane to remove residues of mineral oil.
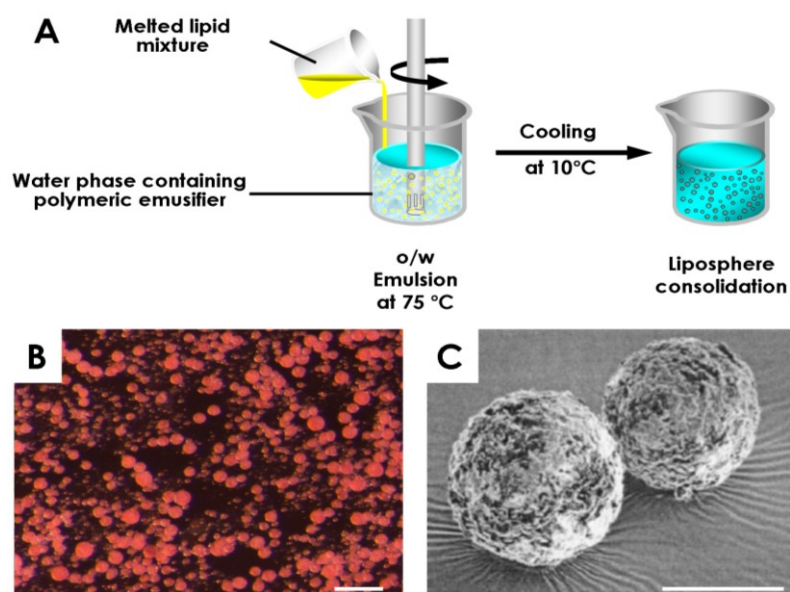
Fig. 14. Schematic representation of the melt dispersion techniques used for liposphere (LS) production. Optical stereo photomicrograph (B) and SEM image (C) of the produced LS. Scale bars correspond to 100 (B) and 20 (C) μm. A lipid mixture constituted of glyceryl tristearate/glyceryl monostearate from Fluka (Buchs, Switzerland) was melted at 70–75°C and then emulsified into 15 mL of an external aqueous phase containing 2% (w/v) of PVA as the dispersing agent. The emulsion was stirred at 8000 rpm using an IKA T25 Ultra-turrax (IKA Labortechnik, Germany) for 2 min. Once the agitation was stopped, the milky emulsion was rapidly cooled to about 10°C by immersing in a cool water bath. The obtained LS were isolated by centrifugation (10 min at 5200×g) and the pellet was washed three times with water and finally dried under vacuum. For the preparation of coloured LS, the dye oil red O from Aldrich (Germany), was used.
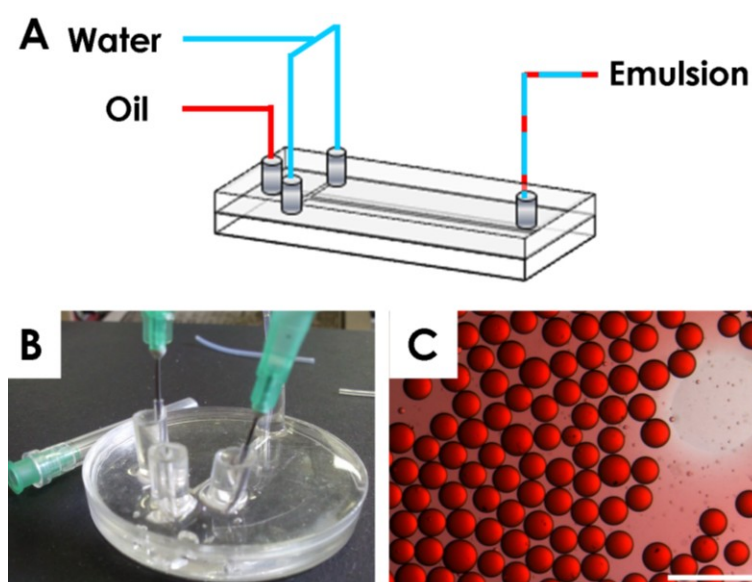

Fig. 15. Schematic representation of the microfluidic flow focusing technique used for the production of corn oil based-emulsion (COBE). Photographs of microfluidic chip (B) and of produced COBE (C). Scale bar corresponds to 250 μm. The used microfluidic chip was constituted of polydimethylsiloxane (PDMS) and contains channels with a square section of 200×200 μm. Both dispersed and continuous phases were injected into the microfluidic chip by a syringe pump (KDS Model 100 Series,   Kd   Scientific).   The   microchip   was

connected to syringes through fluorinated ethylene propylene FEP tubes. Corn oil (Gattefossé, SaintPriest Cedex, France) was used as oil internal phase and slowly injected into the central inlet of the flow focusing geometry. The second immiscible liquid (water) was injected into the two lateral inlets as continuous phase. Corn oil was forced into the water phase at the junction of the focusing channel, forming a multiphasic flow (droplets) represented by a o/w emulsion. For the preparation of coloured COBE, the dye oil red O from Aldrich (Germany), was used.

Moreover, microfibres maintained a highly uniform diameter distribution throughout the entire fibre length; finally the results indicated that the presence of either DDS (Fig. 16 A–C) or cells (Fig. 16 D–F) did not affect the ionic gelation molecular mechanism accounting for microfibre formation. These results suggest that various DDS can be easily loaded during the alginate microfibres fabrication and that the resulting engineered fibres can be utilized for the delivery of drugs. In addition, DDS can be included into the microfibres to produce multifunctional scaffolds in order to enhance and/or prolong the viability, function and/or differentiation of the embedded cells. To this aim, different drug classes can be usefully selected, such as: differentiating and/or antioxidant vitamins, steroidal hormones and nonsteroidal anti-inflammatory drugs (NSAIDs).
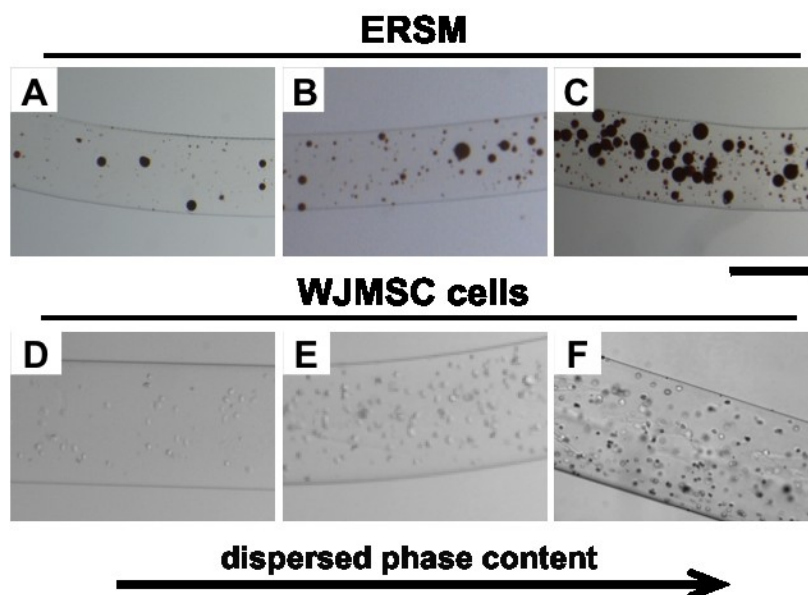

Fig. 16. Optical stereo photomicrographs of typical alginate microfibres, produced by Chip #1, containing DDS (A–C) or cells (D–F). The fibres contained different amounts of: ERSM (A–C) or WJMSC cells (D–F). The dispersed phases were added to the alginate solution giving final ratios of 10 (A) 20 (B) or 40 mg mL^{-}1 (C) for ERSM or 2 (D) 6 (E) or 9×10^{6} cells per mL (F) in the case of cells. Bar corresponds to 200 μm.

As an example, Fig. 17 shows the drug release profiles from vitamin D3 from CAM (Fig. 17 A), vitamin C from ERSM, progesterone from LS and flurbiprofen from COBE (Fig. 17 B). Notably, no significant differences were found when the release profiles of tested drugs were comparatively measured from DDS embedded in microfibres of different diameters (Fig. 18). This result was attributed by the fact that alginate gel is constituted mainly by water (98% by weight) and the pores of the polymer network, forming the hydrophilic gel, are comparatively very large with respect to the drug molecular volume. In this respect, it is noteworthy to remember that the molecular weight cut-off of barium alginate gels is above 80 kDa, well exceeding all the molecular weights of all the tested drugs.
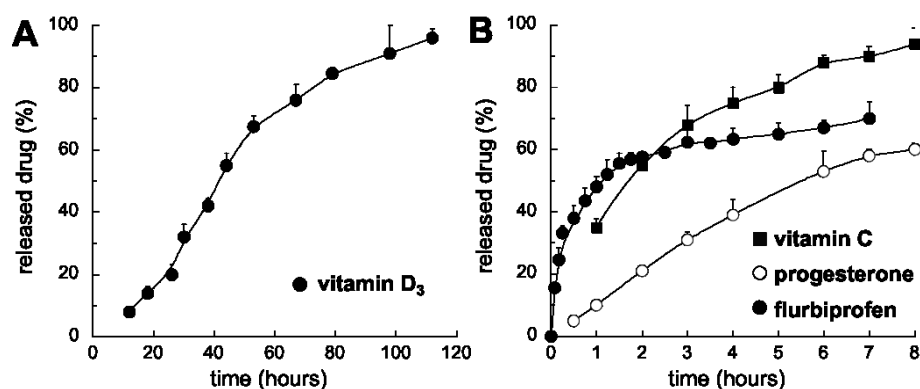

Fig.17. Drug release profiles from different DDS. A: release of vitamin D3 from CAM, B: release of vitamin C from ERSM (filled squares), progesterone from LS (open circles) and flurbiprofen from COBE (filled circles). Data represent the average of four independent experiments±SD.
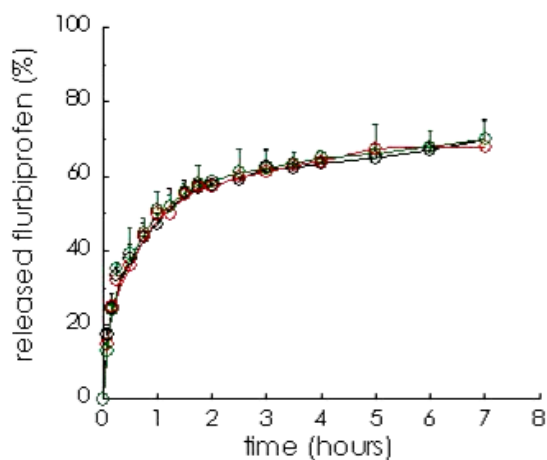

Fig. 18. Flurbiprofen release from COBE embedded into alginate microfibres with a mean diameter of 180 (green symbols), 398 (black symbols) and 510 μm (red symbols). Data represent the average of four independent experiments ± SD.

Production of multifunctional alginate microfibres by multiple inlet chip

As the next step, we aimed to produce microfibres containing desired amounts of DDS/cells in an ''on-demand'' adjustable manner. The first microfluidic device considered was constituted of two inlets and a straight channel (as shown in Fig. 19). Unfortunately, as clearly appreciable from the optical stereo photomicrographs of the produced microfibres (see Fig. 19 B and C), the use of such chips resulted in an undesirable uneven distribution of the particulate phase along the fibre minor axis. The particulate phase segregated along one side of the microfiber corresponding to the inlet position (relatively to the main chip channel), from which it was injected. This result was assigned to the fact that the dispersion of particulate matter, in laminar fluid flow conditions, typical of microfluidic devices, is only scarcely affected by passive molecular diffusion.
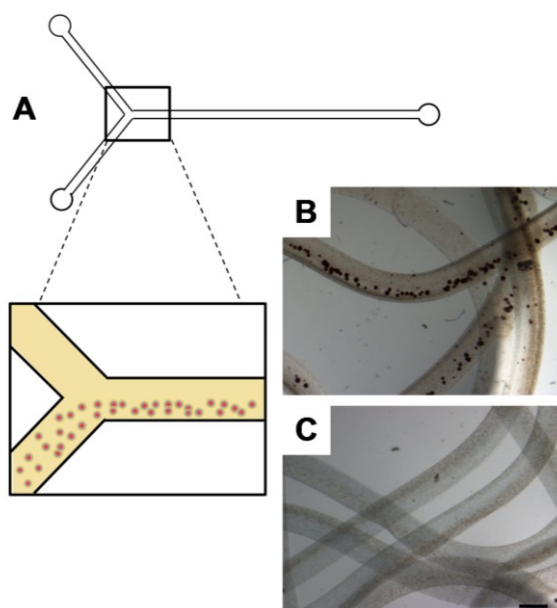

Fig. 19. Schematic representation of the microfluidic device with two inlets and a single straight channel used for the production of multifunctional alginate microfibres containing DDS or cells. The inset shows the mechanism of segregation of the particulate matter within the chip channel. Optical stereo photomicrographs showing alginate microfibres containing CAM (B) or K562 cells (C). Microfibres were produced by two independent syringe pumps, one pumping alginate solution (Pump #1), the other pumping alginate solution containing microparticles (80 mg/mL) or cells (18×10^6 mg/mL) (Pump #2). Microfibres were prepared with a Pump #1/Pump #2 rate ratio of 50/200 µl/min. Bar corresponds to 400 µm.

The use of particulate elements (DDS, cells or both) that are characterized by low diffusion coefficients, together with the high viscosity of the carrier

flow (alginate solution), resulted in a poor dispersion of the particulate phase (segregation), within the microfibre structure. Therefore, in order to possibly overcome this issue, a microchip design that produces transverse transport inside the microfluidic device was considered, for an effective dispersion of the particulate phase.

The design of Chip #2 provided for three dispersing chambers, each of them containing cylindrical-type pillar obstructions. Pillars were regularly alternated along the dispersing chamber axes; each row of obstacles is laterally offset with respect to the previous row above it. Pillars have a diameter of 750 mm; the centre-to-centre spacing between pillars and the relative shift between adjacent pillar rows are equal to 900 and 450 mm, respectively (see Fig. 20). In addition, Chip #2 has three inlets that allow varying "on demand" the content of the dispersed phase within the microfibre, by adjusting the flow rates of independent pumps, delivering either plain alginate or alginate containing particulate matter, through three independent feeding channels. Specifically, using the microfluidic set-up shown in Fig. 9, different alginate solution/suspensions were pumped into the chip through three separate inlets, namely: (a) plain alginate through inlet 1 (I1), (b) alginate containing DDS through inlet 2 (I2) and (c) alginate containing living cells through Inlet 3 (I3).

After flow through the array of micropillars present in the dispersing chambers, the alginate suspension was driven, through a variable size outlet, into a gelling bath, constituted of a barium chloride solution. The Ba^{2+} ions rapidly diffuse into the alginate suspensions causing the almost instantaneous ionic crosslinking, forming the typical egg box structure.
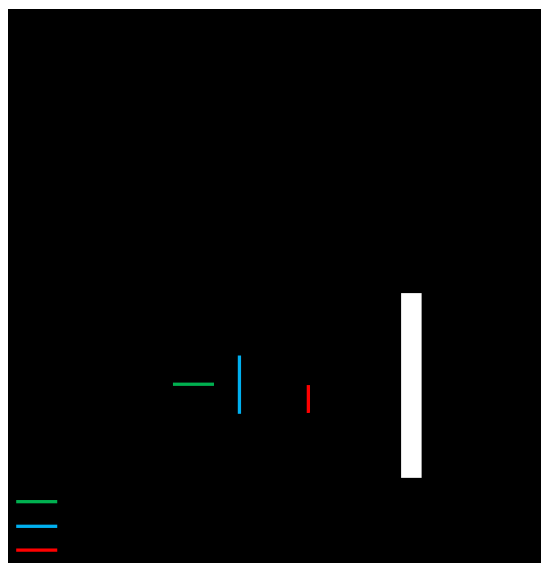
Fig. 20. Schematic representation of the microfluidic Chip #2. Inset reports the characteristic dimensions of the particulate dispersing chamber with pillar obstructions.

Fig. 21 shows the photomicrographs of microfibres produced with Chip #2, at selected pump #1/pump #2 flow rate ratios: 50/ 50 (Fig. 21 A and D), 50/100 (Fig. 21 B and E), and 50/200 mL min⁻1 (Fig. 21 C and F). The microfibres produced with Chip #2 confirmed the good morphological properties in terms of shape, dimension and surface characteristics. These features remained stable under all conditions tested. It is important to note that comparing the microfibres produced by Chip #1 (Fig. 16) and Chip #2 (Fig. 21), there was no evident difference in DDS/cells distribution within the microfibre matrix. For instance, the microfibres always presented a homogeneous dispersion of the DDS and cells. This result indicates that the dispersion strategy implemented in Chip #2 was capable to produce a dispersion extent comparable with the "off-chip" vortexing, employed as the preliminary dispersion step, for the production of microfibres by Chip #1. This feature was further confirmed by the observation that, although the particulate elements were introduced as a suspension, via one of the lateral inlets, the DDS/cells were distributed evenly across the microfibres (Fig. 21). Moreover, photomicrographs reported in Fig. 22 illustrate alginate microfibres simultaneously containing K562 cells and CAM (Fig. 22 A), ERSM (Fig. 22 B) or LS (Fig. 22 C).
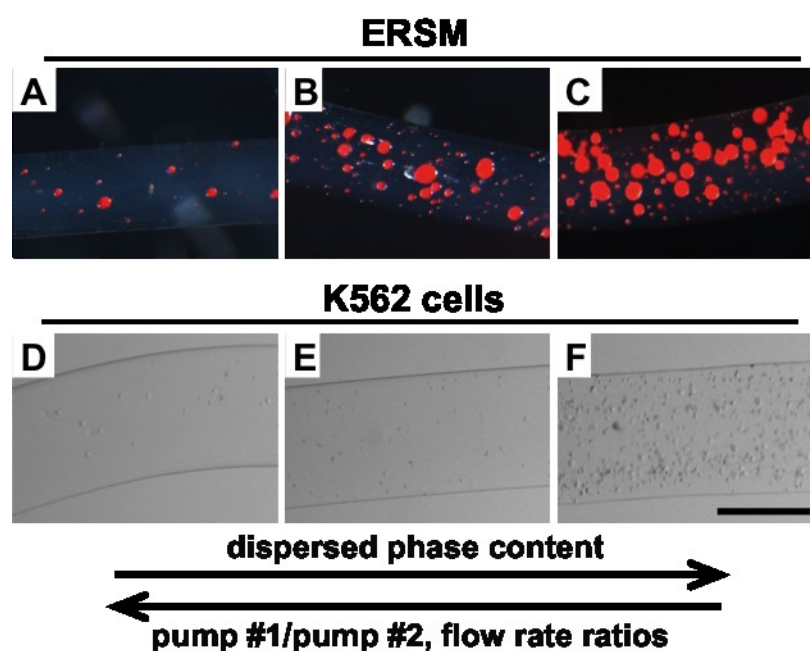
Fig. 21. Dark field (A–C) and bright field (D–E) optical stereo photomicrographs of alginate microfibres, containing different amounts of ERSM (A–C) and K562 cells (D–F). Microfibres were produced by the triple inlet pillar Chip #2 and two independent syringe pumps, one pumping alginate solution (Pump #1), the other pumping alginate containing microparticles (80 mg mL⁻1) or cells (18x10^6 mg mL1) (Pump #2). Microfibres were prepared at different pumping rates, Pump #1/ Pump #2: 50/50 (A and D), 50/100 (B and E) or 50/200 mL min⁻1 (C and F). Bar corresponds to 200 μm.

The cylindrical-type pillar obstruction geometry of Chip #2 resulted in a marked improvement of the dispersion, by the size- dependent hydrodynamic behaviour of the suspended particles in the constructed microgeometry.

Particles were observed to attain different y-positions within the dispersing chamber feeding channels (with y being the direction perpendicular to the main flow direction), depending on the spatial location of the injection site, injection flow rate and particle size. It should be noted that particulate matter suspensions in alginate were characterized by a relatively wide range of dimensions, with DDS and cells having a diameter ranging between 20–130 and 10–20 μm, respectively.

However, given the low-Reynolds regime, the radial position at the injection site was maintained along the channel. Lift- generated radial migration of particle/cells within confined microdomains was indeed observed only at Re > 1.32. Given the specific design of Chip #2, where pillars were considerably shifted at subsequent rows and the   fluid flow was divided into two main

streams by the first obstacle, the radial position and size of the suspended particulate played a significant contribution to the flow behaviour of DDS and cells. In this regard, particles entering the dispersing chamber within peripheral flow streams were observed to be confined in the near-wall region, while particles having a central y-position at the chamber inlet interacted with the first pillar and were observed to partition according to the flow distribution, similarly to what shown for particles flowing at branching microchannels. In addition, both particle size and inter-particle interactions were observed to alter the particle spatial distribution, improving the dispersion outcome.

With respect to their dimensions, particles had two different flow behaviours. Those above the critical diameter were moved by hydrodynamic lateral drag (i.e. bumped) into adjacent streamlines at subsequent rows of micropillars. Larger particles moved through different flow streams and their y-position, at the dispersing chamber outlet, differed from the corresponding position at the dispersing chamber inlet.
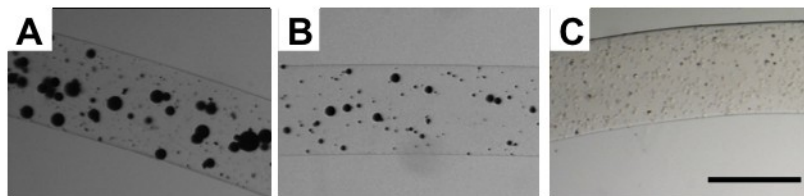

Fig. 22. Optical stereo photomicrographs of multifunctional alginate microfibres, containing K562 cells and different DDS. Microfibres were produced by the Chip #2 and three independent syringe pumps. Pump #1: alginate solution; pump #2: alginate containing K562 (18×10^6 mg mL^{-1}) and pump #3: alginate containing different DDS (80 mg mL^{-1}), namely: CAM (A), ERSM (B) and LS (C). Microfibres were prepared at pumping rates pump #1/pump/#2/pump #3: 50/50/50 mL min^{-1} (D). Bar corresponds to 400 μm.

In contrast, small particles were observed to behave in a "zigzag mode", maintaining a y-position at the chamber outlet similar to their location at the chamber inlet. These variabilities in particle flow behaviour contributed to enhance the dispersion of the injected suspension.

Effect of embedding into alginate microfibres on cell viability

Immortalized cell lines have been largely used as model cells for bioencapsulation and biomaterial seeding. In this respect, the effect of

embedding into alginate microfibres on the cell viability was firstly evaluated on human myeloid leukemia K562. The performed experiment demonstrated that K562 cells can be efficiently encapsulated in alginate microfibres with no significant changes in the cell viability, when analysed after 10 days of in vitro cell culture, thereby facilitating consideration of these encapsulated cells for in vitro studies (see the viability kinetics reported in Fig.23).

Nevertheless, primary cell culture offers a more relevant system for the study of cell function, disease states and patient therapy. This aspect is particularly important for tissue engineering and cell transplantation applications, though working with primary cells in culture presents numerous challenges such as including the requirement for unique cell supplements and growth conditions.
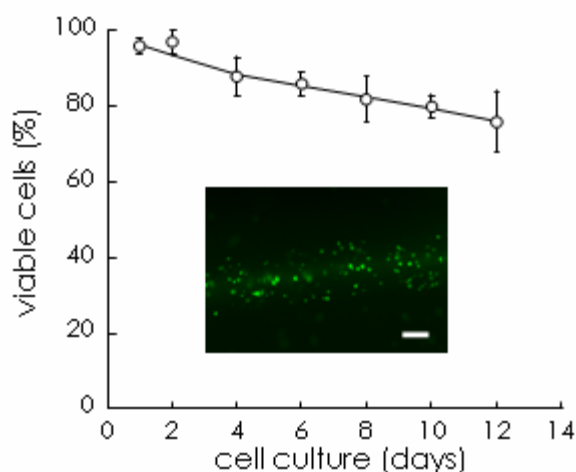

Fig. 23. Graph reporting the percentage of viable K562 cells determined by double staining, after different length of time of *in vitro* cell culture. Values are expressed as percentages of viable cells respect to total entrapped cells and represent the mean of three independent samples analysed in quadruplicate ± SD. In the inset is reported a fluorescence microphotograph of multifunctional alginate microfibres containing K562 cells. Microfibres were produced by Chip #2. Fluorescence photomicrograph was taken after double staining with Calcein-AM and propidium iodide, after 4 days of cell culture. Bar corresponds to 200 µm.

In spite of these possible drawbacks, in this study, the microfibre preparation protocol developed was evaluated with human primary mesenchymal stem cells that represent a much more challenging and informative model. We prepared microfibres containing WJMSC and the cells embedded in microfibres were double-stained (following different times of in vitro cell growth) with calcein-AM (a marker of living cells; fluorescent signal was monitored using 485 nm excitation   wavelength and 530 nm emission

wavelength) and with PI (a marker of cell death; excitation, 535 nm; emission, >610 nm).

The fluorescence photomicrograph recorded immediately after the microfibre preparation (time 0, Fig. 24 A) shows that the cells maintained a very high viability (>95%), indicating that the presented preparation strategy is highly biological compatible and suitable for the encapsulation of primary cells. After 3 and 7 days of cell culture (Fig. 24 B and 24 C), the viability of WJMSC remained high (85% and 62%, respectively). It was observed that the viability decreased below 50% after 12 days (Fig. 24 D) from the preparation. The entire viability kinetics, reported in Fig. 24 E, is comparable to most primary cell types when seeded/embedded in biomaterials scaffolds.
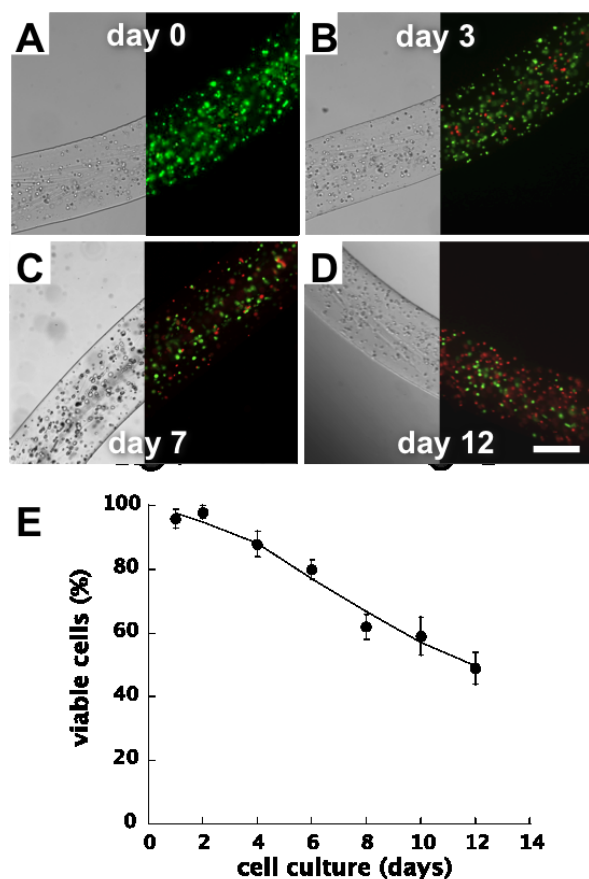

Fig. 24. Optical bright field and fluorescence microphotographs of multifunctional alginate microfibres, containing WJMSCs, produced by Chip #2. Fluorescence photomicrographs were taken after double staining with calcein-AM and propidium iodide, at day 0 (A), 3 (B), 7 (C) and 12 (D) of cell culture. Bar corresponds to 250 μm. (E): graph reporting the percentage of viable WJMSCs determined, by double staining, after different lengths of time of in vitro cell culture. Values are expressed as percentages of viable cells with respect to total entrapped cells and represent the mean of three independent samples analysed in quadruplicate $\pm$SD.

3.2.3. Discussion

A simple, cost-effective, well-controlled and biological compatible process has been developed for the production of uniform alginate microfibres, with controlled size and content, possibly capable of scaling up, working towards FDA approval. The effect of different experimental parameters such as the total flow rate, sodium alginate and barium ion concentrations were investigated and their effects on the morphological and dimensional characteristics of the produced microfibres were statistically evaluated.

We demonstrated that the fibre diameter is controllable with the highly uniform diameter distribution along the entire fibre length. The key advantages of the microfluidic fibre generation system are the versatility of size, little limitation in fibre length and possible incorporation of DDS and living cells. The process has been indeed used to produce multifunctional microfibres based on a wide range of DDS, especially designed to control the release of the entrapped molecules.

In conclusion, it is worth highlighting that a fibre shaped carrier offers an important advantage over spherical shaped carriers since fibre can be easily located and removed from patients when either adverse effects are observed or after the cessation of function.

Moreover, the proposed DDS co-encapsulation may pose a significant impact on the way that cells respond to the external signals, thus providing potentials to better understand and regulate cell differentiation, more co-ordinately and in a precisely defined 3D configuration.

3.3.References

[1] S.F. Badylak, D.O. Freytes, T.W. Gilbert. Extracellular matrix as a biological scaffold material: structure and function. Acta Biomat, 5, 11, 2009.

[2] S. Tsai, M. Jeng, R. Tsay, Y. Wang. Gel beads composed of collagen reconstituted in alginate
Biotech Tech, 12, 21, 1998.

[3] S. Del Guerra, C. Bracci, K. Nilsson et al. Entrapment of dispersed pancreatic islet cells in Cultispher-S macroporous gelatin microcarriers: preparation, in vitro characterization, and microencapsulation. Biotech Bioeng, 75, 741, 2001.

[4] T.W. Gilbert, S. Wognum, E.M. Joyce et al. Collagen fiber alignment and biaxial mechanical behaviour of porcine urinary bladder derived extracellular matrix. Biomaterials, 29(36), 4775, 2008.

[5] J.L Ray, R. Leach, J.M. Herbert. Isolation of vascular smooth muscle cells from a single murine aorta. Methods Cell Sci, 23(4), 185, 2001.

[6] P. De Vos, M.M. Faas, B. Strand et al. Alginate-based microcapsules for immunoisolation of pancreatic islets. Biomat 27 (32), 5603, 2006.

[7] D.F. Cameron, J.J. Hushen, T. Dejarlais et al. A unique cytoplasmic marker for extratesticular Sertoli cells. Cell Transplant, 11, 507, 2002.

[8] F. Fallarino, G. Luca, M. Calvitti et al. Therapy of experimental type 1 diabetes by isolated Sertoli cell xenografts alone. J Exp Med, 206(11), 2326, 2009.

[9] L. Gnessi, A. Fabbri, G. Spera. Gonadal peptides as mediators of

development and functional control of the testis: an integrated system with hormones and local environment. Endocr Rev, 18, 541, 1997.

[10] P. Rossi, C. Sette, S. Dolci et al. R. Role of c-kit in mammalian spermatogenesis. J Endocrinol Invest, 23, 609, 2000.

[11] L. Konrad, M. Albrecht, H. Renneberg et al. Transforming growth factor β2 mediates mesenchymal–epithelial interactions of testicular somatic cells. Endocrinology, 141,3679, 2000.

[12] M. Dym. Basement membrane regulation of Sertoli cells. Endocr Rev, 15, 102, 1994.

[13] I. Virtanen, J. Lohi, T. Tani et al. Distinct changes in the laminin composition of basement membranes in human seminiferous tubules during development ad degeneration. Am J Pathol, 150, 1421, 1997.

[14] A. Taranta, A. Teti, M. Stefanini et al. Immediate cell signal induced by laminin in rat Sertoli cells. Matrix Biol,19, 11, 2000.

[15] Badylak SF. Extracellular matrix as a scaffold for tissue engineering in veterinary medicine: applications to soft tissue healing. Clin Tech Equin Practice, 3(2), 173, 2004.

[16] S.F. Badylak. The extracellular matrix as a biologic scaffold material. Biomaterials, 8, 3587, 2007.

[17] J.M Caves, V.A. Kumar, A.W. Martinez et al. The use of microfiber composites of elastin-like protein matrix reinforced with synthetic collagen in the design of vascular grafts. Biomat, 31, 2010.

[18] S. Madduri, M. Papaloïzos, B. Gander et al. Trophically and

topographically functionalized silk fibroin nerve conduits for guided peripheral nerve regeneration. Biomat, 31, 2323, 2010.

[19] K.M. Schumacher, S.C. Phua, A. Schumacher et al. Controlled formation of biological tubule systems in extracellular matrix gels in vitro. Kidney Intern, 73, 1187, 2008.

[20] Q. Wang, X. Hub, Y. Du et al. 2010. Alginate/starch blend fibers and their properties for drug controlled release. Carbohyd Polym, 82: 842-847.

[21] Y.H. Lee, J.H. Lee, I.G.An et al. Electrospun dual-porosity structure and biodegradation morphology of Montmorillonite reinforced PLLA nanocomposite scaffolds. Biomat, 26, 3165, 2005.

[22] E. Chevalier, D. Chulia, C. Pouget et al. Fabrication of Porous Substrates: A Review of Processes Using Pore Forming Agents in the Biomaterial Field. J Pharm Sci, 97, 1135, 2008.

[23] K. F. Leong, C. M. Cheah, C. K. Chua. Solid freeform fabrication of three-dimensional scaffolds for engineering replacement tissues and organs. Biomat, 24, 2363, 2003.

[24] A.L. Thangawng, P.B. Howell, J. J. Richards et al. A simple sheath-flow microfluidic device for micro/nanomanufacturing: fabrication of hydrodynamically shaped polymer fibers. Lab Chip, 9, 3126, 2009.

[25] D. N. Breslauer, S.J. Muller, L.P. Lee. Generation of monodisperse silk microspheres prepared with microfluidics. Biomacromol, 11, 643, 2010.

[26] T. Kanai, D. Lee, H.C. Shum et al. Fabrication of tunable spherical colloidal crystals immobilized in soft hydrogels. Small, 6, 807, 2010.

[27] C.M. Hwang, A. Khademhosseini, Y. Park et al. Microfluidic chip-based fabrication of PLGA microfiber scaffolds for tissue engineering Langmuir, 24, 6845, 2008.

[28] E. Kang, S. Shin, K. H. Lee et al. Novel PDMS cylindrical channels that generate coaxial flow, and application to fabrication of microfibers and particles. Lab Chip, 10, 185, 2010.

[29] S. Shin, J. Park, J. Lee et al. "On the Fly" continuous generation of alginate fibers using a microfluidic device. Langmuir, 23, 9104, 2007.

[30] T. Takei, N. Kishihara, S. Sakai et al. Novel technique to control inner and outer diameter of calcium-alginate hydrogel hollow microfibers, and immobilization of mammalian cells. Biochem Eng J, 49, 143, 2010.

[31] J. T. Wilson, E. L. Chaikof. Challenges and emerging technologies in the immunoisolation of cells and tissues. Adv Drug Del Rev, 60, 124, 2008.

[32] G. Luca, G. Basta, R. Calafiore, et al. Multifunctional microcapsules for pancreatic islet cell entrapment: design, preparation and in vitro characterization. Biomat, 24, 3101, 2003.

[33] X. Zhang, P. Jones, S. Haswell. Attachment and detachment of living cells on modified microchannel surfaces in a microfluidic-based lab-on-a-chip system. Chem Eng J, 135, S82, 2008.

[34] G. Fundueanu, M. Constantin, E. Esposito et al. Cellulose acetate butyrate microcapsules containing dextran ion-exchange resins as self-propelled drug release system. Biomat, 26, 4337, 2005.

[35] R. Cortesi, E. Esposito, C. Nastruzzi et al. Eur J Pharm Sci, 6, S64, 1998.

[36] A. Tosi, S. Mazzitelli, L. Capretto et al. Optimization of lipospheres production by factorial design and their performances on a dielectrophoretic lab-on-a-chip platform. Colloids Surf A, 340, 77, 2009.

[37] L. Capretto, S. Focaroli, X. L. Zhang et al. Production of low cost microfluidic chips by a "shrinking" approach: Applications to emulsion and microparticle production. J Control Rel, 148, e26, 2010.

[38] C. Nastruzzi, E. Esposito, R. Cortesi et al. Kinetics of bromocriptine release local anaesthetics from microspheres: comparative analysis between different in vitro models. J Microencap, 11, 565, 1993.

CHAPTER 4

4.1. Conclusions

Hydrogel encapsulation of mammalian cells is finding increasing applications in biomedical applications (i.e. cell therapy and tissue engineering). The protection of transplanted cells from the surrounding host environment is indeed crucial to the potential in vivo use of cell-based scaffolds for controlled delivery of therapeutics to specific physiological sites.

The key to the success of this technology is the development of microcapsules with number of fundamental characteristics including: the manufacturing process, material biocompatibility, mechanical properties and adequate permeability for the controlled transport of biological molecules trough the hydrogels.

The production of microcapsular scaffolds typically starts with the generation of a controlled-size droplet, followed by a gelation process resulting in solid microcapsule structure. Firstly, new encapsulation devices and procedures were designed and tested, along side with the optimization of a commercially available encapsulator for large scale productions. Specifically, the novel technique, based a coaxial bead generator with unique and peculiar features named "*gas driven mono-jet device*", demonstrated its great applicability and flexibility for alginate microbead preparation

Aside these traditional technologies, innovative techniques based on the use of microfluidic platforms have been developed in order to obtain hydrogel based microparticles with highly controlled morphological and dimensional properties. Noteworthy, the obtained results demonstrated that all the encapsulation procedures, optimized by a statistical approach, do not interfere with cell performances, whereas in some cases an improvement of specific cell functionalities was observed (i.e. the osteogenic differentation of encapsulated WJMSCs).

Despite the great potential of immunoisolating microcapsules as cell-delivery vehicles, for their in vivo application several challenges still exist, including the problem of reaching an optimum balance between the mechanical strength of the device and the long-term viability as well as the lacking of cell adhesion and homing exhibited by many hydrogels.

Given these cons, new approaches to modify the conventional alginate hydrogel were developed resulting in hybrid hydrogel able to the control the cell fate in a more effective way. The hybrid hydrogels were processed in form of engineered microparticles or multifunctional microfibres.

Since the survival of certain cells requires attachment to the ECM (i.e. Sertoli cells) a powered form of ECM was included in the alginate forming engineered microcapsules, to improve cell viability and functions.

With respect to microfibres, a simple and cost-effective microfluidic platform was used to produce multifunctional microfibres based on a wide range of drug delivery systems, especially designed to the controlled release of the entrapped therapeutics. The aforementioned approach, referred as "multifunctional", was successfully used to release differentiating and/or antioxidant vitamins, steroidal hormones and non steroidal anti-inflammatory drugs in order to prevent acute inflammation or to ameliorate the performances of the entrapped cells.

Further studies are obviously necessary to progress towards routine clinical applications, including a detailed analysis, at molecular level, of the complex events occurring after the in vivo cell transplantations and an accurate evaluation of the processes underlying the interactions of the scaffold and host immune systems.

Taken together, the presented results represent a strong starting point for the effective application of hybrid immunoisolation systems towards the development of embedding techniques meeting GMP regulations, finally resulting in the gain of medical approval and bridging the bench to bedside.